UNIVERSITA DEGLI STUDI DI MILANO
FACOLTA DI MEDICINA E CHIRURGIA

DOTTORATO DI RICERCA IN FISIOLOGIA

SETTORE SCIENTIFICO DISCIPLINARE BIO---09

CICLO XXVI°

Tesi di Dottorato di Ricerca

Proteins modifications fostered by the pro-oxidant environment of Parkinson's and Alzheimer's diseases cerebrospinal fluid: the ceruloplasmin case

Dottorando:
Dott. Marco Barbariga
Matricola:
R09210

Tutor:
Dott. Massimo Alessio

Relatore:
Prof. Antonio Malgaroli

Coordinatore:
Prof. Michele Mazzanti

Anno Accademico 2012-2013

"You can't look too far ahead. Do that and you'll lose sight of what you're doing and stumble. I'm not saying you should focus solely on the details right in front of you, mind you. You've got to look ahead a bit or else you'll bump into something. You've got to conform to the proper order and at the same time keep an eye out for what's ahead. That's critical, no matter what you're doing."

— Haruki Murakami, *Kafka on the Shore*

Contents

Common abbreviations

CSF: CerebroSpinal Fluid

CNS: Central Nervous System

CP: Choroid Plexus

CPECs: Choroid Plexus Epithelial Cells

BBB: Blood-Brain Barrier

BCSFB: Blood-CSF Barrier

SVZ: Sub-Ventricular Zone

TJ: Tight Junctions

Cp: Ceruloplasmin

Tf: Transferrin

TfRs: Transferrins Receptors

DMT1: Divalent Metal transporter 1

AD: Alzheimer's disease

PD: Parkinson's disease

MMSE: Mini Mental State Eamination

WD: Wilson's Disease

MD: Menkes Disease

ROS: Reactive Oxygen Species

RNS: Reactive Nitrogen Species

AGEs: Advanced Glycation End-Products

NFT: Neuro-Fibrillary Tangles

App: Amyloid Precursor Protein

ApoE: Apolipoprotien E

Aβ: Amyloid Beta

LBs: Lewy Bodies

α-syn: Alpha Synuclein

DA: Dopamine

Asp: Aspartic Acid

Asn: Asparagine

isoAsp: IsoAspartic Acid

NGR: Asparagine-Glycine-Arginine motif

DGR: Aspartic acid-Glycine-Arginine motif

IsoDGR: isoAspartic acid-Glycine-Arginine motif

PIMT: Protein-l-isoaspartyl/d-aspartyl Methyltransferase

CD13: Aminopeptidase N

RGD: Arginine-Glycine-Aspartic acid motif

FN: Fibronectin

1 Abstract

In the last decades the role of metals in neurodegenerative diseases assumed a great importance, in particular regarding copper and iron. Ceruloplasmin (Cp), an enzyme present in the plasma secreted by the liver and in the cerebrospinal fluid (CSF) as product of the epithelial cells composing the blood-CSF barrier, may play a crucial function in the metabolism of copper and iron in the central nervous system (CNS), being Cp able to transport copper and to oxidize toxic ferrous iron; Cp's ferroxidasic function is essential for iron export outside cells of the CNS, thus protecting tissues from oxidative damage. Investigating Cp patterns using two-dimensional electrophoresis (2D-E), we found that in Parkinson's (PD) and Alzheimer's (AD) diseases the Cp profile proved to be more acidic than that found in healthy controls and patients affected by other neurological pathologies, suggesting a possible use of Cp 2D-E profile as a pathological marker. *In vitro* oxidation of Cp generated a 2D-E shift resembling that observed in patients, indicating that Cp oxidation contributes to the electrophoretic profile seen in PD and AD; Cp oxidation caused a decrease of ferroxidase activity, promoting intracellular iron retention in cultured neurons.

Among all the possible Cp's amino acidic modifications induced or accelerated by oxidation, the deamidation of asparagine appears attractive, being this reaction related to protein aging, dis-function, degradation and/or aggregation, all phenomena observed for several proteins in AD and PD. In particular our attention has been focused on the asparagine present at the level of the two Asp-Gly-Arg (NGR) motifs present on the Cp sequence; the first, ^{568}NGR, is exposed on the surface and in direct contact with the environment while the second ^{962}NGR, is hidden within the tertiary structure of the protein. The function of NGR-motif has been recently discovered: deamidation of the asparagine at this level results in the formation of *iso*DGR-motif that can bind integrins containing RGD-binding site. This open a new interesting research field on latent integrin-recognition-sites, which can be activated in physiological or pathological conditions.

We observed that the Cp exposed ^{568}NGR site can deamidate under conditions mimicking accelerated asparagine aging, while the hidden ^{962}NGR-site can deamidate exclusively when aging occurs under oxidative conditions; this result suggest that oxidation-induced structural changes foster deamidation at this site. NGR-deamidation in Cp was associated with gain of integrin binding function, intracellular signalling and cell pro-adhesive activity**.** Moreover,

deamidated-Cp intracellular signals in epithelial and neural stem cells caused cell proliferation arrest.

In addition, also the *ex-vivo* aging in the CSF from Alzheimer and Parkinson disease patients, but not in control or peripheral neuropathies CSF, induced Cp structural changes, deamidation with gain of integrin-binding function, carbonylation and ferroxidase-activity reduction. These results indicate that in the pathological CSF are present compounds (small molecules or proteins) able to induce oxidative modifications on other proteins. In particular, the modifications observed in Cp aged in pathological CSF may be the consequence of oxidation resulting from the high H_2O_2 concentration we detected in the AD's and PD's CSF.

Concluding, the CSF of AD and PD patients favors Cp deamidation at NGR-sites with gain-of-function in cell adhesion and loss of ferroxidase activity, raising Cp deamidation as an additional contributor to neurodegenerative diseases characterized by oxidation.

2 Introduction

2.1 The CSF environment, a regulator of central nervous system development, nutrition and functioning

2.1.1 The CSF: flow and composition

The cerebrospinal fluid (CSF) is a nutrient-rich liquid that permeates the brain and the spinal cord, filling the ventricles and the spinal channel. The major site of CSF formation is the epithelial cells layer of the choroid plexus (75% of the total volume of CSF produced), but there is also an extra-choroidal secretion, which may result from ion transport by brain capillaries. The CSF volume, estimated to be about 150 ml in adults, is distributed between 125 ml in cranial and spinal subarachnoid spaces and 25 ml in the ventricles; CSF secretion in adults varies between 400 to 600 ml per day, such that the liquid and the salts components of CSF are replaced three or four times each day. Interestingly, during the aging, cerebral atrophy cause a relative increase of the CSF compartment compared to the brain parenchyma, bringing a reduction of CSF turnover after the age of about 70 years [9]. This mechanism causes an impairment in the scavenging of metabolites, neurotransmitters catabolites and aberrant proteins (like beta-amyloid) letting them to accumulate in specific regions of the central nervous system [9].

The CSF circulation is a dynamic phenomenon, propelled by three main forces: arterial pulsations in the choroid plexus (corresponding to the systolic pulse wave in choroidal arteries), hydrostatic pressure gradient, and ciliary motion of the ependymal cells lining the ventricles [3]. CSF flows from the sites of secretion to the sites of absorption according to a unidirectional rostrocaudal flow in ventricular cavities and a multi-directional flow in subarachnoid spaces: the fluid produced in the lateral ventricles passes through the foramina of Monro into the third ventricle, travels in the aqueduct of Sylvius and then into the fourth ventricle. From here, CSF passes through the foramen of Magendie to the cisterna magna and then circulates into the cerebral and spinal subarachnoid spaces (Figure 2.1.1). At the level of foramina between the ventricles obstructions can occur (for example by inflammation or thrombosis), causing the ventricle upstream from the obstruction to enlarge, producing obstructive hydrocephalus. In the cranial subarachnoid space, CSF circulates to the villous sites of absorption (spinal arachnoid villi) or caudally to the spinal subarachnoid space (Figure 2.1.1): arachnoid villi are finger-like endothelium protrusions of the arachnoid outer-layer through the *dura mater* in the lumen of venous sinuses [10], that adsorb the CSF with a dynamic process which adapts the filtration rate to CSF pressure. Their absorption of CSF is described to be like a valve-like process, permitting the one-way flow of CSF from the subarachnoid spaces into the venous sinuses.

CSF absorption does not occur until CSF pressure exceeds the pressure within the sinuses. Once this threshold is reached, the rate of absorption is proportional to the difference between CSF and sinus pressures. The interplay absorption by the arachnoid villi and the selective removal of molecules by the choroid plexus means that there can be a concentration gradient for molecules reaching the interstitial fluid of the brain to diffuse into the CSF. Regarding its biological function, for a long time the cerebrospinal fluid was considered only a “hydro-mechanical damper” that protects the central nervous system from injuries. This function is true, but is not the only one: from the purely mechanical point of view, for example, being the skull a rigid structure, an increase in brain volume (such as those that occur from vasodilation) could cause marked rises in intracranial pressure; the fluid in the CSF system, whose volume can be modulated, limits such changes in pressure. Similarly, if the brain is dehydrated, the CSF acts as a source of fluid to rehydrate it. Early work on the CSF focused primarily on the importance of this pressure homeostasis in the developing brain [11]: too little pressure decreases brain size, while too much pressure leads to impaired neural stem cell division and hydrocephalus. Nowadays, molecular biology shown that CSF plays an essential role also in homeostasis of the interstitial fluid of the brain parenchyma and in the regulation

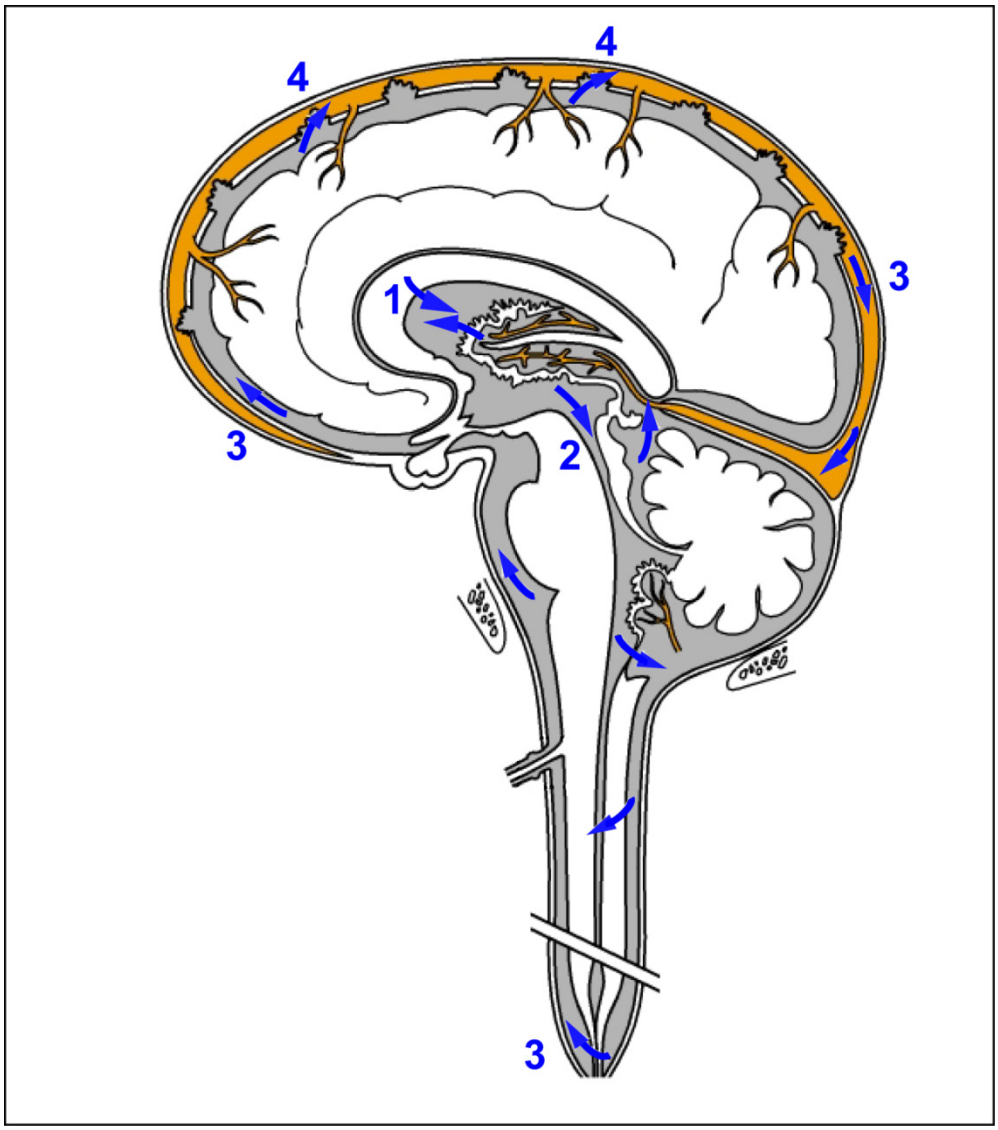

Figure 2.1.1: The description of the CSF pathway. The CSF is produced by the choroid plexus (1) from where it moves from the lateral ventricles to the third and fourth ventricles (2). Then it flows across the surface of the brain and down the spinal canal (3). CSF is finally reabsorbed by the arachnoid granulations (4) back in to the blood stream. (Image adapted from [1]).

of the neuronal activity, and disorders of these CSF hydrodynamics and composition are responsible for the major alterations of cerebral physiology observed in hydrocephalus and dementia, reflecting the importance of exchanges between CSF and the neuronal environment. CSF role in these mechanisms comprise the regulation of electrolyte balance, circulation of active molecules, elimination of catabolites (wastes of brain metabolism, peroxidation products and glycosylated proteins) and transport of the choroidal plexus secretions (hormones, growth factors, inflammatory molecules) to their sites of action. This mode of distribution by CSF circulation modulates the activity of certain regions of the brain by impregnation [12]. Furthermore, the bulk flow of CSF along the optic and olfactory nerves drains through lymphatic tissue, letting the antigenic material in the CSF to produce a systemic immune reaction.

As described above, the CSF system is the major source of entry into the brain for a number of substances, and several constituents are maintained at different concentrations in CSF from those in plasma: some substances enter the CSF via the blood-CSF barrier and others enter via the blood-brain barrier. Besides, neo-synthesized molecules are produced by specialized cells population of the CNS, like astrocytes, glial cells and epithelial cells of the choroid plexus.

CSF is composed by 99% water, provided primarily by Aquaporin-1 channels located on the apical membrane of the epithelial cells in the ventricles, but it is also a rich source of proteins, ions, lipids, hormones, cholesterol, glucose, and many other molecules and metabolites. Recent works have turned to investigate the biological functions of known CSF-resident factors. Many of these CSF-distributed factors, being the fluid in intimate contact with the thalamus, hypothalamus and pineal gland, have been speculated to influence a wide range of behaviors including sleep and appetite, circadian rhythms and loco motor activity. Many studies have taken advantage of advances in proteomic tools including mass spectrometry to better characterize these proteins that compose the CSF proteome [13]. These studies have demonstrated that the CSF proteome consists of hundreds of proteins of the extracellular matrix, ion carriers, regulators of osmotic pressure, hormone-binding proteins, growth-factors,

regulators of lipid metabolism and various enzymes and regulators. The CSF is home of hundreds of proteins and signaling activities, providing an elaborate range of biological functions for this complex fluid [14]. Although the factors responsible for the favorable effects of embryonic and adult CSF are only beginning to be uncovered, the range of factors already known to be active in CSF during embryonic brain development includes fibroblast growth factors (FGFs), insulin-like growth factors (IGFs), sonic hedgehog (Shh), retinoic acid, melatonin, bone morphogenic proteins (BMPs), Wingless-related integration site (Wnt), and others [15-17]. Melatonin, a hormone that regulates circadian rhythms, is released by the pineal gland into the CSF: melatonin is a potent free radical scavenger and antioxidant, and acts as a neuroprotective agent that decreases oxidative stress removing reactive oxygen species from the CNS [18].

Igfs (Igf1 and Igf2) are a class of growth factors present prevalently in the embryonic CSF, regulating prenatal growth and body size and stimulating cell proliferation [19]. Depending on cellular context, Igf1 can also regulate neuronal differentiation, glial development, and cell size [20]. The effects of CSF Igf2 are also age-dependent [3]: CSF-Igf2 levels in rodents are modest at the earliest stages of neurogenesis, peak near the end of neurogenesis, and decrease post-natally, suggesting that Igf2 may regulate specific aspects of neurogenesis. In adulthood, it is thought that Igf2 levels in the CNS remain relatively stable [21], but evidences suggests that Igf2 may be an important regulatory molecule released in a penetrating model of traumatic brain injury [22].

Retinoic acid, a hormone signal derived from vitamin A, is produced by the choroid plexus epithelial cells [23] and by the meninges [24], providing long-range signaling activity for the developing brain [25]. Interestingly, while choroid plexus derived retinoic acid is secreted directly into ventricular CSF, meningeal sources of retinoic acid may reach the neuro-epithelial cells via the lateral ventricular CSF as well as by crossing the cerebral mantle.

Last, Wnt signaling plays a key role in regulating early development of the CNS [26].

The CSF has also attracted interest in the field of brain injury, possessing neurogenic and neuroprotective factors believed to have therapeutic effects following brain injury. The choroid plexus-CSF system can be disrupted in a wide range of CNS injuries, from hydrocephalus to age-associated neurologic diseases [23], and a plethora of growth factors are up-regulated in the brain and CSF following injury; these include, together with the already mentioned Igf1 and Igf2 [22, 27], FGF [28], nerve growth factor (NGF) [29] and transforming growth factor beta (TGF-β) [30].

Resuming, it appears that the key mechanism for promoting neural repair following brain injury is through the endogenous up-regulation of neurotropic factors important in neurogenesis and neuronal survival. The CSF may act as a vehicle for transmission and transport of important nutrients and growth factors to sites of brain injury and to the whole CNS to contributing to the mainteinance of the homeostasis, to promote neuroprotection and neurogenesis and to remove toxic products generated by injuries.

This huge amount of features that characterize the CSF and the continue discoveries of its new functions open very large perspectives about the treatment of neurological diseases intervening directly *via* CSF. The possibility of administering a cocktail of neurogenic and neuro-protective factors to the CNS through this fluid provides an intriguing, non-invasive method that is particularly exciting from the therapeutic point of view [31]. A recent study showed that media conditioned with choroid plexus secretome supports neural stem cell proliferation compared to media conditioned with cortical tissue [23]. Alternatively, suggested other ways for the treatment of neurological disorders have been made, manipulating endogenous choroid plexus or implanting it intra-ventricularly or at the site of brain damage, providing essential neurogenic growth factors and other proteins necessary to enhance CSF homeostasis.

Concluding, CSF components, which can potentially be dispersed over large areas, may be more significant and pervasive regulators of brain development, neural stem cell renewal, disease, neurodegeneration, aging, behavior, and other states of consciousness than previously thought: in the mature brain, cells with access to the ventricles may respond to factors released into the CSF followed by all these both physiological and pathological processes.

2.1.2 The Blood-CSF barrier

The discovery of cellular barriers between the blood circulation and the CNS dates in the 1880s, when Paul

Ehrlich discovered that certain dyes, injected into the vascular system, were not taken up by the brain and spinal cord [32]. Ehrlich explained this phenomenon as a lack of affinity of the nervous system for these dyes, but Edwin E. Goldmann a few years later showed that the same dyes, injected into the cerebrospinal fluid, stained nervous tissue but not any other tissue [33], suggesting that differential staining was not due to a different affinity to these dyes, but to something within CNS that prevented their access to the blood circulation, and *vice versa*.

Nowadays, researchers identified at least four different barriers that separate the brain from other organs: the blood-brain barrier (BBB) at the level of the cerebral blood vessels endothelium, the embryonic CSF-brain barrier, created by separation of the ventricular system from the extracellular fluid of the brain [34], the arachnoid *mater* in the subarachnoid space between the *pia* and the *dura mater* and the blood-CSF barrier, at the level of the choroid plexus epithelial cells (CPECs).

Choroid plexus is a villous structure that floats on the ventricular surface into the lumen of the lateral, third and fourth ventricles (Figure 2.1.2), where it produces the CSF and form a unique interface between the peripheral blood and the liquor. CP plays key roles in many processes, maintaining the biochemical and cellular status of the central nervous system under both normal and pathological conditions.

During mouse embryogenesis, the choroid plexus is clearly visible already at E12.5; in the human embryo, the choroid plexus begins to develop at approximately 44 days post-ovulation in the fourth and lateral ventricles and is easily visible already after 9 weeks of gestation, filling a large part of the lateral ventricle and spanning the length of the fourth ventricle [35]. Albeit CPs of the lateral, third and fourth ventricles exhibit embryological, anatomical and functional differences [36], in adulthood these regions are almost similar: the adult CP structure is characterized by a monolayer of epithelial cells derived from the ependymal cells, interconnected by apical tight junctions that line the wall of the brain ventricles. Under this monolayer of epithelial cells lays a stroma perfused with an extensive capillary network (CP receives 10 times fold higher blood flow compared to the brain parenchyma [37]), fibroblasts and immune cells such as dendritic cells and macrophages (Figure 2.1.2). The glomerular-type capillaries [38] within the choroid plexus parenchyma differ from those of the brain, having an attenuated endothelium that allows free movement of molecules across the cells through fenestrations and intercellular gaps [39] similar to the endothelium of kidney and intestine. Is therefore evident that, within the CP, the barrier function is localized in the epithelium, where tight junctions between the epithelial cells, channels and active transporters confer to the tissue its permeability and secretory selectivity [40]. The CP epithelial cells are cuboidal-shaped cells that display a polarized morphology, with a basolateral membrane facing the CP stoma, an apical surface in contact with the brain ventricles and lateral membranes between adjacent epithelial cells; their high secretory activity is reflected by the intracellular presence of a large central spherical nucleus, a big Golgi apparatus and an high density of ribosomes and mitochondria, that provide the necessary energy (ATP) to feed the CSF production and the neurochemical homeostasis functions [41, 42]. The basal lamina of these cells shows a convoluted shape that increases the surface area between the epithelia and the interstitial fluid, so as to maximize the exchange of molecules between these two compartments. Their apical membrane instead expand its surface area sending out numerous finger-like villi and cilia [43]; so although, being the surface area apparently small referred to the whole CNS volume, it is not negligible [44]. On the apical membrane, a few macrophage-like cells (Kolmer cells) adhere tightly to the ciliated border of the CP epithelium [45]. Looking at the most apical portion of the lateral membranes, the presence of parallel strands of tight junctions (TJ) inhibits the para-cellular passage of blood derived cells and proteins [40]. The TJ composition between the epithelial cells of the CP are different from those connecting the endothelial cells of the blood–brain barrier: in addition to being on the apical part of the lateral membranes, CP tight junctions show a relatively short zonula occludens and a different composition, being formed by claudin-1 claudin-2, claudin-11, and occludin [46], causing the CP barrier to be leakier compared to the one forming the blood brain barrier.

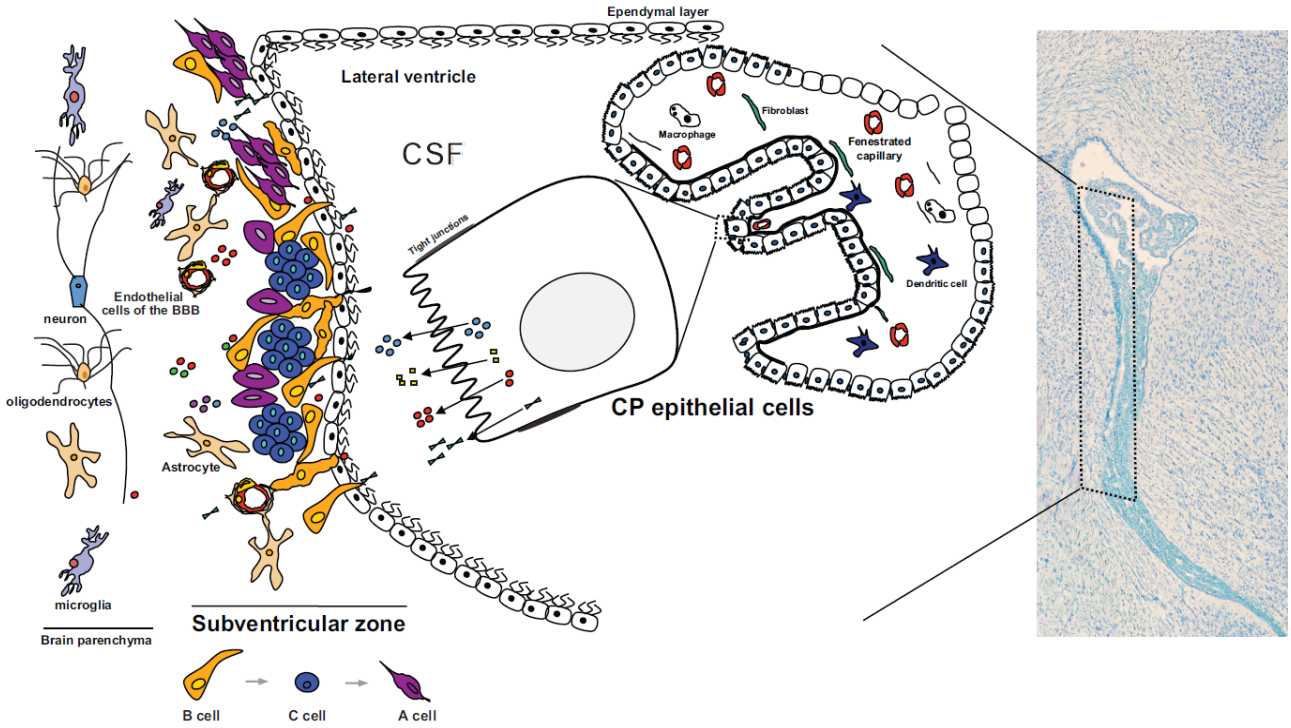

Figure 2.1.2: influences the SVZ neuronal progenitor cells differentiation. Facing the SVZ, the CP and hence its secreted proteins, rapidly enter in contact with the cells of the SVZ; in particular, type B stem cells are in direct contact with CSF, projecting a cilium toward the ventricle. These cells, present in the adult SVZ, under differentiative stimuli generate type C cells that in turn give rise to neuroblasts (from [5]).

Besides TJ restrict permeability across the choroid plexus epithelium, these cells also perform absorptive endocytosis and express a broad range of transporters for water molecules and ions, small peptides and polypeptides [47-50], allowing the passage of nutrients into the CSF and the removal of toxic agents out of the CNS. Together with these specific transport mechanisms, the capacity of these cells to synthetize and secrete a plethora of different proteins complete their CSF production process. In this view, the CP has an important autocrine, paracrine and endocrine effect on CNS by producing CSF and polypeptides and distributing them from the ventricles within the whole brain and the spinal cord: the expression of receptors (both in the apical and basolateral sides) for molecules such as neurotransmitters, cytokines and toxins that regulate the CP transcriptome and secretome [23, 51, 52] confirms that the modulation of these "active barrier functions" are essential for the health of the central nervous system.

In addition to this primary function in secreting the CSF (that will be discussed in detail in chapter 2.1.3) choroid plexus epithelial cells cover many other roles: in the last years the interest has been directed to the understanding of CP function within the neuroimmune system [43]. T cell migration into the CNS *via* the choroid plexus was provided by a recent study demonstrating that Th17 cells may penetrate the BCSFB via binding to CCL20 receptor produced by choroid plexus epithelial but not endothelial cells in rodents and man, using then specifically the choroid plexus as CNS entry site [53]. Choroidal epithelial cells also constitutively express MHC class I and, in some species such as mice, MHC class II molecules that are inducible by infectious agents [54, 55], making these cells also to be included in the family of the antigen-presenting cells. Secondly, Ling and colleagues described monocyte recruitment through the choroidal vessels and subsequent migration across the choroid plexus epithelium [56]. Interestingly, choroid plexus epithelial cells constitutively express at low levels the adhesion molecules ICAM-1 and VCAM-1 polarized to their apical surface [57], and both adhesion molecules can be up-regulated during inflammation, mediating adhesion of immune cells in vitro [58]; however, several studies failed to detect expression of E-/P-selectin, ICAM-1 and VCAM-1 at the level of the basolateral membrane of the CP endothelial cells [58], making them to not be directly accessible for leukocytes migrating from the blood into the CSF compartment across the BCSFB. Nevertheless, a demonstrated enhanced leukocyte counts in the CSF

during inflammation and multiple sclerosis [57, 59] suggest an active recruitment into this compartment. The mechanism of immune cells extravasation across the CP is not clear: circulating immune cells would need to first migrate across the fenestrated choroid plexus capillaries, enter the parenchyma and then penetrate the layer of choroid plexus epithelial cells, either by passing through the parallel TJ strands or by passing through the choroid plexus epithelial cells at a trans-cellular level. All these data indicate that these cells may serve as an immune-surveillance barrier of the CNS, in synergy with other cells present in the parenchyma and on the apical surface of the CP, including the Kolmer cells, that normally act as phagocytic scavenger cells, displaying antigen inducible class I and II MHC molecules and proliferating when stimulated with toxins [56]. Choroid plexus then seems to have a crucial role in the intrinsic surveillance system defending against blood-born or CSF-generated antigens and pathogens.

Lying within the central ventricular system, the CP is also in an ideal position for the monitoring of the CSF's presence of toxic compounds or damaging cellular invasions; furthermore, it protects the brain against acute neurotoxic insults, using a complex detoxification system [60] that include a full set of metabolizing enzymes like glutathione and metallothioneins (that potently sequester toxic agents circulating in the CSF) protective enzymes such as superoxide dismutase, glutathione-s-transferase, and glutathione peroxidase/reductase, providing a complete system which protects against free-radical oxidative stress [61].

Neurorprotection is, so, a trivial function that is paralleled with neurogenesis regulation [62], suggesting both a constitutive and an emergency role in cellular repair and replacement in the CNS: CP epithelial cells actively produce mitogens such as amphiregulin for regulating stem cell proliferation and neurogenesis [63, 64], and conditioned media from CP also enhanced neurite outgrowth and dopamine uptake on cultured neuroblastoma cells and on embryonic mesencephalic tissue, respectively. Yamamoto and colleagues showed that the CP modulates neurite outgrowth in the developing cerebellum [65]. The ability of CP epithelium to provide a scaffold for the extension of neurites is consistent with its known production of extracellular matrices including laminin and fibronectin [66]. The neurotrophic activity of CP acts also on the fast-proliferating cells (type A cells) of the sub-ventricular zone (SVZ), that are, in the ventricles, in direct contact with the CP secretion (Figure 2.1.2). These cells, migrating along the rostral migratory stream (RMS) anteriorly toward the olfactory bulbs, differentiate into GABAergic interneurons [67]; the SVZ also gives rise to oligodendrocyte progenitors, although in lower number [68]. Moreover, this proliferative function is accomplished also by CP–resident stem cells, since proliferative markers clearly show their presence in the CP. These choroidal stem cells proliferate in response to trauma: Li and colleagues [62] demonstrated that CP cells proliferate and differentiate after stroke in adult rats, and transplant studies demonstrated that, when grafted into damaged regions of the CNS, CP cells have the ability to differentiate [69]. Additionally, CP stem cells isolated and maintained in vitro, exerts potent neuroprotective effects [70] and similar benefits have been observed in vivo too.

The evidence that this small and complex organ play a primary role in the development and homeostasis of the CNS is demonstrated by the observation that its subtle physiological and pathological changes can have wide range consequences [71, 72]. The altered function of the CP may be implied in several diseases characterized by secretory cell dysfunction: in fact, since the CP epithelial cells are equipped with transporters for several proteins and metabolites, pathological damage to the CP itself will alter the CSF composition and the ventricular volume, as in the case of hydrocephalus [23]. For example, Miyan and colleagues [73] observed that hydrocephalus in rats impairs cortical development.

In humans, the height of CP epithelial cells decreases by about 10% during aging [54], with decreased CSF production (about 45% in animal models [72]), diminished enzymatic and metabolic activity, reduced clearance of toxins and loss of polypeptide synthesis [74]. As said in the previous chapter, due to this decreased secretion and the simultaneously increased CSF volume caused by brain atrophy, CSF turnover takes significantly longer in elder people [9], causing an inadequate distribution of nutritive substance: these alterations may impact in all the cells in direct contact with the CSF, like the SVZ stem cells population. Degenerative pathologies, such as Alzheimer disease, manifest themselves as exacerbations of these changes: epithelial cell atrophy is greater, with cell height decreased up to 22% compared to age-matched controls [54]. We can

then speculate that it's possible that continued loss of normal choroidal function leads to additional cellular stress and contributes to the cognitive and motor decline in specific neurological disorders: indeed is proven that in AD, amyloid-beta clearance impairment contribute to the progress of the pathology [72, 75].

2.1.3 The CSF production by choroid plexus epithelial cells

In contrast to the CP's relatively small volume, the rate of the CSF production is relatively high, suggesting the vital importance of a refreshing system and a flow of fresh fluid for the removal of the brain metabolism products. The structure of the CP is, indeed, very well adapted for the secretive activity [76]: its excellent blood supply, an extensive array of adrenergic, cholinergic, peptidergic and serotoninergic nerve fibers that modulate the CSF production by the epithelium [77, 78] and a complex set of transporters and ion channels, distributed unequally between apical and basolateral membrane, are essential features of this tissue [79]. The net force of fluid secretion across the epithelial monolayer is an active, unidirectional flux of ions from one side of the epithelial layer to the opposite side, which creates an osmotic gradient accompanied by the movement of water: this force cause the molecules secreted by the CP to be conveyed to the brain parenchyma via volume transmission, convective distribution and intra-parenchymal diffusion/receptor-mediated retrograde transport [80]. There are major differences between transport by the BCSFB and by the BBB: in terms of O_2, CO_2, glucose and amino acid entry into the brain, the BBB predominates, but for some other compounds like Ca^{2+} the BCSFB is the major site of entry. The first step of the cerebral fluid secretion consists of passive filtration of plasma from choroidal capillaries to the choroidal interstitial compartment, according to a pressure gradient; the second is the active transport from the interstitial compartment to the ventricular lumen across the choroidal epithelium, involving specific enzymes and membrane ion carrier proteins. Before discussing about the complex intra-cellular transport of ions and substances, a little mention has to be made about the paracellular passage of molecules: as discussed above, CP tight junctions are looser compared to those of other barriers, like the BBB. In fact, hydrophilic solutes like Na^+ and small proteins can gain access to the ventricles by a slow leakage through these tight junctions: promoting this passage is the presence of Claudin 2, a TJ permeability enhancer, which specifically transfers solutes across the epithelium without entering the cells through the formation of channels [81].

Numerous active transporters, together with ions and water channels, participate to the intra-cellular transport of molecules from blood to CSF (Figure 2.1.3): starting with the baso-lateral membrane, plasma-derived Na^+, Cl^- and HCO_3^- which are unable to diffuse through the cell membrane, enter the cells with a carrier-mediated transport: at the level of this membrane in fact, Na^+/H^+, Cl^-/HCO_3^- and sodium dependent Cl^-/HCO_3^- exchangers are expressed, aside from Na^+-HCO_3^- co-transporter. Na^+ enters the cell prevalently down a chemical gradient in exchange for H^+, while Cl^- influx into the epithelium is via a Cl^-/HCO_3^- exchanger, favored by the exit from the cell of HCO_3^- [82]. This ion exchange maintained by the presence, in the CP cells cytoplasm, of the carbonic anhydrase enzyme, which catalyzes the formation of H^+ and HCO_3^- from water and CO_2, letting them to be available and exchanged for Cl^- and Na^+ [83]. In addition, a small amount of HCO_3^- can leak out of the cell down the concentration gradient, through Na^+-HCO_3^- co-transporters located at the apical side. Overall, the net effect of the carbonic anhydrase is an intracellular accumulation of Na^+ and Cl^- which triggers the CSF secretion [84]. On the apical surface, since Cl^- and HCO_3^- levels inside the cells are above the electrochemical equilibrium, these ions diffuse down gradients through specific apical channels and through other carriers. The most important is the Na^+/K^+ ATPase pump that, on the contrary to others epithelia, is found on the apical brush membrane and not the basal membrane [83]. This enzyme uses the energy derived from the ATP hydrolysis to pump $2K^+$ in the cell and $3Na^+$ out of the cell in the CSF, against their concentration gradients. This action, which provides the electrochemical gradient for basolateral Na^+ entry into the epithelium, leads to the accumulation of K^+ within the cells, which is subsequently excreted from the apical membrane through the Na^+-$2Cl^-$-K^+ co-transporter and the K^+ channels [85] or, in minor amount, from the basolateral membrane via K^+-Cl^- co-transporter [86]. Cl^- efflux from the epithelium to the CSF is primarily via Cl^- channel or co-transporters, which are either of the K^+-Cl^- or Na^+-$2Cl^-$-K^+ type [87]. The last one generates ion transport in both directions and has a crucial role in the regulation of

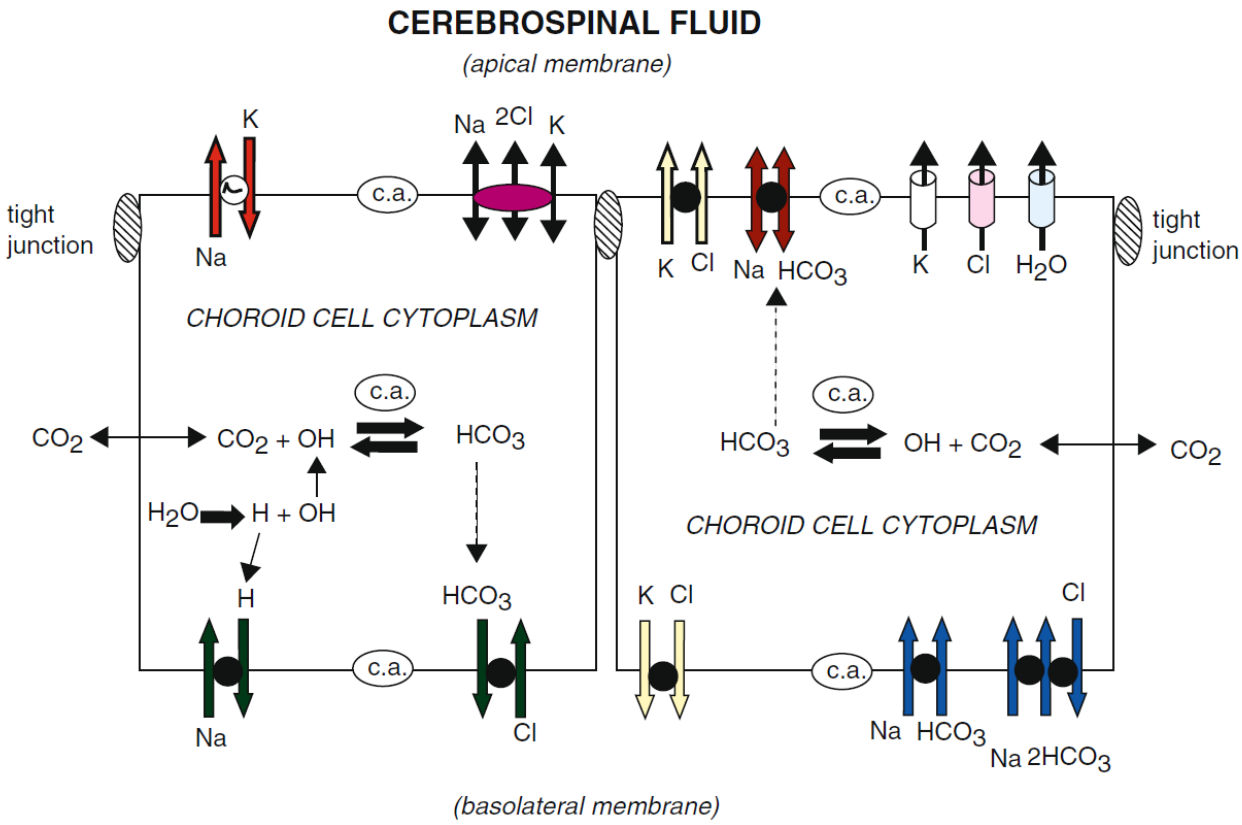

Figure 2.1.3: schematic representation of ions transport across choroid plexus epithelial cells (from [3]).

CSF secretion and composition. Summarizing, the net effect of all these ion movements is the unidirectional flux of Na^+, HCO_3^- and Cl^- (NaCl and $NaHCO_3$) from basolateral to apical space [76], generating an osmotic gradient that cause the diffusion of water, which can pass in the CSF trans-cellularly or also through the apical aquaporine-1 channel [83].

CP is the main site of entry of Ca^{2+}, being its influx rate ten-fold higher than the blood-brain barrier value: CP shows an active transport system, moving Ca^{2+} against unfavorable electrochemical gradients.

Not only ions, but also nutrients and other molecules can be transported from blood to CSF by choroid epithelial cells, and their secretion is finely regulated: recent studies indeed shown that CP expresses different hormone receptors, mediating the secretive activity of the CP itself and affecting both the local metabolism and the CSF composition [61].

Glucose and others sugars, that are necessary for the brain activity, are subjected to a powerful homeostatic mechanism, that maintain their concentration constant and different from that in the plasma, resulting in the equilibrium between influx and efflux: basolateral membrane of CP is very permeable to sugars, favoring the influx of glucose, but concentrative active transport across the CP [88] is responsible of significant efflux from the CSF to the plasma, causing the concentration of glucose in the CSF to be steadily lower than in plasma [88]. Also the concentration of free amino acids in CSF is much lower than in plasma, with the CSF/plasma ratio between 0.29 and 0.38 [89]; in the brain interstitial space, the concentration of free amino acids is for more lower, almost 1/3 of the CSF concentration [90]. Except glutamate, aspartate, glycine and glutamine, that are synthesized by the brain, the low concentration of other amino acids in the CSF is again the result of active efflux from the CSF by the secondary active transport across the CP, like in the case of sugars.

Finally, as said in paragraph 2.1.2, the choroid plexus also may be involved in the transport of hormones into the CSF or be the source of those hormones [91].

Although the secretion of substances out of the CNS is carried out mainly by the arachnoid villi, also CP disposes of unneeded molecules by diffusion across pores or putative pinocytosis of large proteins [92], with diffusion to the basolateral membrane and then

to the blood [93]. This mechanism, which works against an unfavorable CSF to blood gradient, is responsible of the removal of weak organic acids from the CSF.
In conclusion, choroid plexus use the energy released by ATP hydrolysis to generate unidirectional flux of ions across the epithelial monolayer, which then drives trans-epithelial movement of water by osmosis. Moreover, regulating the passage of specific nutrients/hormones/molecules with dedicated inducible carriers, CP modulates and influences the osmosis and the activity of the whole central nervous system.

2.1.4 Copper and iron metabolism in the CNS

Copper and iron are essential cofactors for specific proteins, catalyzing electron transfer reactions and mediating inorganic ions binding used as substrates for these reactions [94]. Due to the loss of function of the iron- and copper-dependent proteins, an altered homeostasis of Cu and Fe results in metabolic abnormalities that can involve the whole organism, from the blood to the central nervous system [95].
Copper homeostasis plays an important role in normal function and development of the central nervous system: in fact, copper concentration in the brain is one of the highest, second only to the liver, and is high in particular in the basal ganglia, cerebellum, cortex, lateral Amygdala and hippocampus. These copper concentrations most likely reflect the higher metabolic demands for copper in these regions. The metabolic demands for copper in the CNS change during brain development, and also copper concentration in the CNS increases with age [96] and in patients affected by several neurological disorders [97]. Copper, present in all major cell compartments in the CNS, take part in cellular respiration, defense from dangerous radicals and specialized processes such as production of peptides and hormones [98]. Moreover, copper is released at the synapse of some neurons [99] suppressing long-term potentiation in the hippocampus [100].
This metal is readily available in the diet and, following absorption through the stomach and duodenum, is released from the enterocyte and travels, bound mainly to albumin, in the portal blood to the liver. Biliary excretion is the only physiological mechanism of copper elimination, and at steady state the amount of copper excreted into the bile is equivalent to that absorbed from the intestine [101].
Unlike Fe, there are no physiological intracellular storage systems of Cu, and body levels are therefore maintained by balancing dietary absorption, distribution and biliary excretion. Newly acquired Cu is rapidly addressed to a number of Cu-dependent enzymes through the action of several intracellular chaperone proteins [102]: in the liver a major proportion of the Cu is loaded onto Ceruloplasmin (Cp).
Copper concentration in CSF was estimated to be approximately 20 mg/l, considerably lower than copper concentration in serum (more or less 1 g/l [103]), so the blood brain barrier effectively limits copper's access to the brain. Comparison of the initial rates of copper transport, which demonstrated that the entry of copper into cells of the choroid plexus was faster than the copper entry into the brain parenchyma, suggest that copper efflux from the epithelial cells of the choroid plexus rather than its uptake from the blood is the limiting step for copper delivery to brain parenchyma.
Key copper-metabolism proteins present in peripheral tissues are also detectable in the brain, and can be divided in three major groups: copper uptake transporters, which transfer copper into the cytosol, copper chaperones that facilitate copper distribution to intracellular protein targets and copper transporting ATPases, which translocate copper from the cytosol to the lumen of the secretory pathway and small vesicles, for the synthesis of copper-containing enzymes and their export into extracellular fluids (Figure 2.1.4A).
Copper transporter 1 (Ctr1) belongs to the first group: CTR1 mRNA is uniformly expressed in the CNS, but is higher in the choroid plexus epithelial cells [104] and in endothelial cells of the BBB. Interestingly, the Ctr1 level on the membrane in peripheral organs (like duodenum) is regulated in response to changes in the extracellular copper levels [105]. Similarly, the expression of Ctr1 in the choroid plexus can be up-regulated after dietary copper deficiency while increased copper facilitates endocytosis of Ctr1 by intracellular vesicles [106], suggesting that Ctr1 is the first pathway for copper entry into cells. The mechanism of copper transport by CTR1 is not yet fully understood: its structure suggests that it may act as a channel in which copper binding to the extracellular surface triggers the opening of the cytosolic gate, which allows copper to be released inside the cell and to be bound to cytosolic chaperones, that delivers copper to different

intracellular compartments. These chaperones include Ccs (Copper Chaperone for Superoxide dismutase 1), Cox17 (Cyclooxygenase 17) and Atox1 (antioxidant protein 1 homolog). Ccs, in the cytosol, delivers copper to the catalytic site of protein superoxide dismutase 1 (Sod1) [107]; in addition, a small fraction of Ccs is found in mitochondria, where Sod1 can enter after hypoxia or oxidative stress. Ccs is thought to incorporate copper into Sod1 that enters mitochondria, thus increasing its concentration in the inter-membrane space and protecting from oxygen reactive species also these organelles, mostly under stressful conditions. Cox17 instead, together with Sco1/2, deliver specifically copper to mitochondrial cytochrome c oxidase (Cco) [108], a terminal enzyme of the mitochondria respiratory chain, that catalyzes electron transfer to molecular oxygen and contributes to the electrochemical potential formation used for the synthesis of ATP. Lastly the small cytosolic protein Atox1, in addition to play an antioxidant role [109], mediates copper movement from the Ctr1 intra-cellular domain to the late trans-Golgi network, where it can bind copper-transporting ATPases (Atp7a and Atp7b) [110]. ATPases use the energy of ATP hydrolysis to transport copper from the cytosol into the lumen of the secretory pathway and to incorporate the metal into various copper-proteins, including blood clotting factors V and VIII, tyrosinase and, as mentioned before, ceruloplasmin. The evidence that genetic mutations in ATP7A or ATP7B are associated with severe neurological, developmental and psychiatric problems lead to the hypothesis that these membrane ATPases play a particularly important role in CNS physiology: although Atp7a and Atp7b are often co-expressed in same cells, Atp7a and Atp7b exhibit distinct expression patterns in the CNS, and they do not fully compensate for each other's function when one is lost [111]. In adult brain, Atp7a levels are greatest in the choroid plexus cells of the lateral and third ventricles [111] where it facilitates copper movement across the basolateral membrane into the intra-ventricular space of the brain. This indicates again the central role of this region in the homeostasis of copper. Atp7b instead is mainly expressed in hepatocytes and is required for copper excretion from these cells into the bile and the copper incorporation on Cp. Intracellular trafficking of copper finally requires other metallo-chaperones proteins like metallothionein, a cysteine-rich protein that chelates copper protecting against the toxicity caused by cytoplasmic excess of this ion [112].

Many diseases result from an altered copper metabolism due to genetic defects resulting in unpaired copper absorption and abnormal copper distribution, or abnormal absorption due to a wrong diet. Severe copper deprivation is associated with marked neurological defects, since inactivation of copper-dependent enzymes can result in altered cell morphology [113], increased inflammation [114], motor neuron disease [115] and embryonic death; either genetic or acquired copper deficiency moreover leads to demyelination of the neurons in the white matter of the spinal cord and brainstem [116], but the specific role of copper in myelination is not well understood.

Being essential for several metabolic processes like oxygen transport, electron transport and citric acid cycle [117], also iron is vital for all organisms. The most important biologic function of iron is the coordination of oxygen in erythrocytes, in fact in hepatocytes or mainly in erythroblasts, the 65% of the total systemic iron can be delivered to mitochondria for the synthesis, as Fe^{2+}, of the heme group. Like copper, iron is acquired from the diet and transported across the intestinal mucosa, as either inorganic iron or heme iron. The major mechanism of iron absorption in the intestine involves mucin, that chelates Fe^{3+} in the luminal space of the duodenum [118], the membrane-bound reductase Dcytb, that reduces Fe^{3+} to Fe^{2+} [119], and the divalent metal transporter known as Dmt1 [120] which imports Fe^{2+} into enterocytes. In enterocytes, iron can be incorporated in ferritin for its intracellular storage or can cross the polarized enterocytes up to the iron exporter ferroportin (FPN), the only identified mammalian iron exporter, which allow Fe^{2+} export from the enterocytes into the circulation [121]. On the extracellular side of the enterocytes a membrane bound ferroxidase, hephaestin, oxidizes the iron transported by Fpn to Fe^{3+}, which is accepted by transferrin (Tf) in the circulation [122]. This ferroxidase role in the other body compartments is covered also by hephaestin together Ceruloplasmin. The ferroxidase activity contributes to the rate of plasma iron oxidation and to the regulation of the release of this metal from the storage sites [123] through the Fpn exporter. The functioning of the Fpn channel is also regulated by hepcidin, a protein secreted by the liver that binds to fpn and induce the endocytosis and the turnover of this plasma iron

exporter [124] in response to inflammation, erythropoietic needs and iron availability [125]. Acting at the level of the Fpn expressed by enterocytes, hepcidin can also block the iron uptake from the lumen of the intestine in response to systemic iron overload.

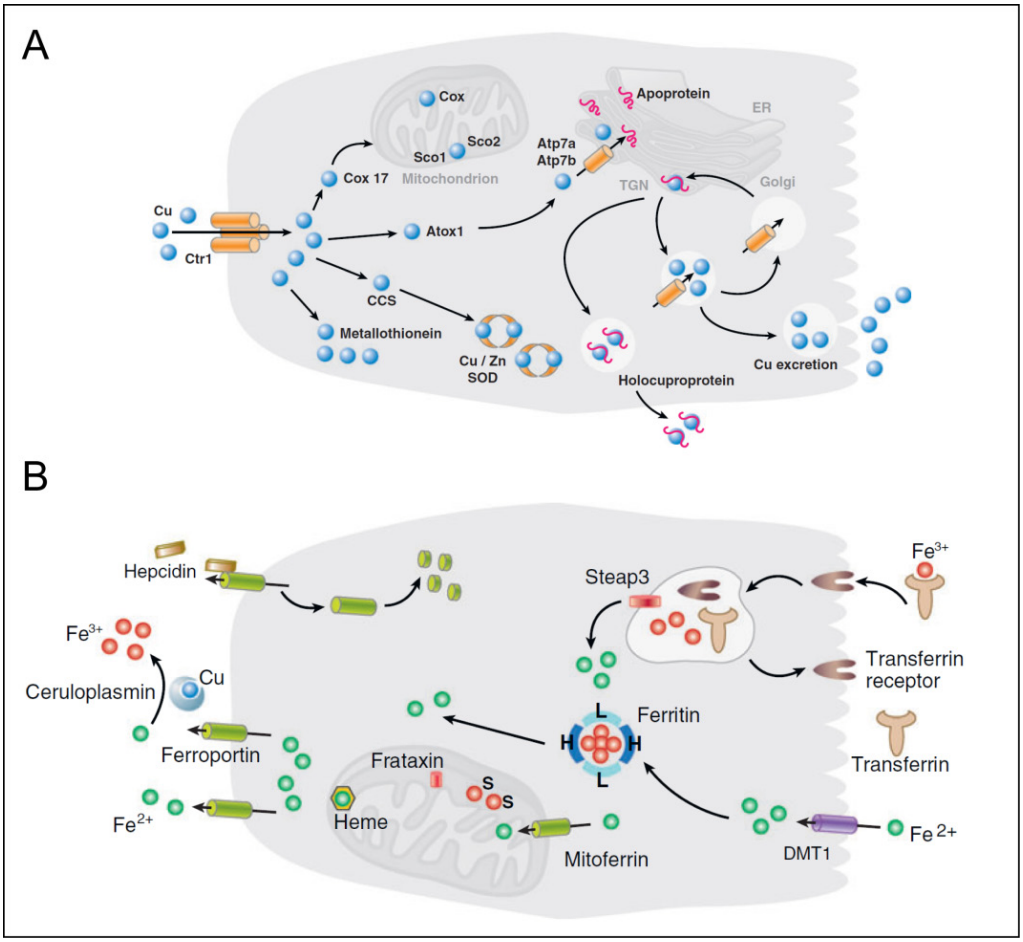

Figure 2.1.4: representation of cellular Copper (panel A) and iron (panel B) homeostasis. Adapted from [7].

Under normal physiological conditions there is almost no free iron in circulation, because a majority of it is bound to Tf, an abundant circulating protein that delivers iron to cells throughout the systemic circulation: Tf can bind to Tf receptors (TfRs) on the surface of cells that express this receptor, causing the Tf-TfR complex to be internalized in a vesicle; then, due to the slightly acid pH of the endosome, iron is released from Tf, reduced to the transportable ferrous form Fe^{2+} by the vesicular reductase Steap3 [126] and transported across the endosomal membrane into cytosol by Dmt1 present on the vesicular membrane, ready for the storage or for the incorporation in various proteins. The Tf-TfRs uptake of iron is the predominant mechanism of iron uptake of non-intestinal cells[127], but all nucleated cells also possess the capability to transport free inorganic iron [128] using the Dmt1 pathway for Fe^{2+}, or the integrin-mobilferrin pathway (IMP) for the Fe^{3+} [129]. Being iron requirements higher than the gastrointestinal absorption capacity, all of the iron utilized each day is continuously recycled from internal stores [130]: the majority of iron turnover in the body is thus accounted by the continual synthesis and destruction of erythrocytes. This recycled iron can be either reused for new erythrocyte production or delivered to the liver long-term storage system. About the Iron excretion out of the organism, several studies showed that this process is limited to the passive loss of cells lining the gastro-intestinal/urinary tracts, and skin. Anyhow, to maintain normal homeostatic iron balance dietary absorption must match endogenous losses and disequilibrium in these processes can lead to several metabolic disorders; in fact, nutritional iron deficiency has a significant impact on infant and child health in many developing countries, where it is one of the major public health problems [131]. All tissues in the body share a common system of iron delivery, except two regions that are separated from the systemic circulation by epithelial or endothelial barriers: the central nervous system, and testicles [132].

In the CNS iron is essential as a cofactor of several enzymes involved in phosphorylation, neurotransmitters production, nitric oxide metabolism, myelination and oxygen transport [133]; the concentration of iron in the brain is therefore very high compared to other organs, and is higher in the basal ganglia, where it's comparable to the one found in liver [134]. Iron is also widely distributed in all cell types within the CNS but is abundant especially in astrocytes, suggesting the idea that

these cells function as iron storage site for the whole brain.

CNS iron uptake is high in infants, when the brain is growing and developing, but measurable iron uptake is present also in adult [48]: iron is taken up through two different ways: through the brain capillary endothelial cells (BCECs) of the BBB or through the epithelial cells of the choroid plexus, which both express high levels of Dmt1 transporter and TfRs. Since the hydrophilic nature of iron bound to transferrin prevents its passage into the brain as it is, the TfRs mediated uptake is the major pathway for iron uptake by the brain: failure of the transferrin receptor expression in mice results indeed in lethal outcomes during development with severe defects in the CNS. As said above, the transferrin receptor is continuously expressed by BCECs and CPECs [135], but the expression pattern can change with age and in pathological conditions. The up-regulation of the TfRs synthesis in iron deficiency conditions increases the transport of iron into the brain, compared to standard conditions with normal available levels of iron [136]. This regulation is mediated by the five iron responsive elements (IRE) present in the un-translated region of the TfRs mRNA [137] that interact with iron regulatory proteins to protect mRNA from cleavage and degradation, thereby increasing protein synthesis if the cellular iron levels are low.

Like in other cells, binding of iron-transferrin complex to the TfRs is followed by docking and formation of an endosome that enters in the cytoplasm (Figure 2.1.4B): the slightly acid endosomal pH causes the iron to be detached from transferrin and the presence of Dmt1 transporter (in the CPECs) allows the passage of divalent cations out of the endosome and into the cytosol [137]. Dmt1 interestingly could not be detected in BCECs endosomes, suggesting that iron is transported from the luminal to the abluminal surface of these cells inside vesicles without any intermediate step, fusing with the CSF-faced membrane and leading to the exposure of the iron from the endosome into the interstitial fluid, where it can be loaded on different molecules and ready transported into the brain. The transferrin would mainly remain bound to its receptor which has a high affinity for apo-Transferrin at acidic pH [138] and would be recycled to the plasma-side of the BCECs. The BCECs are so likely to release ferric iron, whereas ferrous iron release occurs by secretion of iron from CPECs, neurons and oligodendrocytes through Fpn transporter [139]. In the last case, extracellular ceruloplasmin (the major ferroxidase present in the CNS) secreted by CPECs or GPI-bound on the membrane of astrocytes, mediates Fpn-mediated iron release from cells and its loading on Tf [140].

Being the concentration of transferrin low in the CSF and in the brain interstitial fluid, astrocytic end-feet that form intimate contacts with the abluminal side of BCECs [141], play an important role in the regulation of solutes transported through these cells, producing several alternative iron carriers (hydrogen ions, ATP, and primarily citrate [142]) that can circulate throughout the brain interstitium, supplying iron to cells within the CNS [4]. The rate of release of iron is in fact directly proportional to these molecules concentration [143]. Another interesting protein who can act as an extracellular iron carrier in the brain is lactoferrin, which is secreted in the brain by CPECs and is structurally related to transferrin but with an higher affinity for ferric iron. Lactoferrin, present in CSF, shows increased concentrations after inflammatory reaction [144], suggesting its role in the scavenging of iron released from damaged cells. Scavenging is necessary to reduce the toxic effects of free iron, that can be non-enzymatically oxidized from Fe^{2+} to Fe^{3+}, triggering the Fenton and Haber Weiss reaction ($Fe^{2+} + H_2O_2 + H^+ \rightarrow Fe^{3+} + HO\bullet + H_2O$) which in turn produce toxic hydroxyl radical, a very reactive molecule that have deleterious effects reacting with and altering the structure of several molecules including proteins, nucleic acids and lipids.

All the different cell types present in the CNS differ apart from each other by mechanism of uptake/export of iron, depending on the transport molecules they express. Neurons, containing both TfRs and Dmt1, take up both transferrin-bounded iron [135] as well as free iron: interestingly, these cells up-regulate the expression of transferrin receptors in response to iron deficiency [135], while the expression of DMT1 are unaffected by the iron interstitial concentration [145]. Moreover neurons constantly express FPN and in some regions of CNS ferritin, showing that they are able to store iron [146]. Astrocytes instead do not express TfRs, suggesting that they take up iron by different mechanisms [147], and their iron export involve Fpn and the membrane-bound form of ceruloplasmin [148]. Oligodendrocytes, not expressing TfRs too, seem to acquire iron by a mechanism that could involve uptake of iron-citrate. Also these cells use Fpn as iron export mechanism [149].

Iron leaves CNS through its uptake by the arachnoid villi in the subarachnoid space; alternatively, if the CNS iron requirements are high, iron can be stored by the ependymal cells of the choroid plexus. The dis-regulation of the brain iron equilibrium can be a primary cause of neurodegeneration, suggested by disorders like aceruloplasminemia and neuroferritinopathy [95]: in fact concentration of iron in the brain, increased also with aging, is higher in subjects with neurodegenerative diseases such as Parkinson's disease and Alzheimer's disease [150, 151], indicating a pivotal role of this metal in the development of several diseases. Moreover, being the BBB and the BCSFB the major sites of iron uptake and secretion of regulatory proteins, diseases (or also aging) that cause their secretion/barrier-functions dis-regulation could have adverse effects on brain iron homeostasis.

2.1.5 The cupro-ferroxidase Ceruloplasmin

Among all the proteins implicated in iron and copper homeostasis, Cp seems to cover a key role, being at the intersection point of the metabolisms of these two metals. Cp (EC 1.16.3.1) is a blue colored glycoprotein composed of a single chain polypeptide of 1046 amino acids, with a molecular weight of about 130 KDa, which may vary depending on the carbohydrate attachments diversity [152]: this glycosylation heterogeneity may have implications in protein half-life and enzymatic activity. The Cp gene is found on chromosome 3q25–q24 and encodes 20 exons encompassing 65 Kb of DNA: Serum Cp (300 mg/l) is expressed by the liver, but extra hepatic gene expression has been documented in the brain, lung, spleen and testis. Furthermore, Cp's gene transcription in the liver is mediated by inflammatory cytokines, and increased plasma concentrations were found in inflammation and trauma, making the protein an acute phase reactant [153]. In the CNS, Cp is expressed in retina as well in the epithelial cells of the choroid plexus and astrocytes [154]. The isoform expressed by astrocytes, due to an alternative splicing of exons 19 and 20 in Cp gene, which replace the final five amino acids of the secreted protein with an alternative 30 amino acids that constitute an hydrophobic stretch, is anchored to the cell membrane trough a glycosylphosphatidylinositol (GPI) anchor [148, 155]. Choroid plexus epithelial cells instead express the Cp soluble form, secreting it in the cerebrospinal fluid (2 mg/l).

Figure 2.1.5: 3D representation of the Cp structure (EC 1.16.3.1): each different color represents a different domain of the protein. In green, the copper trinuclear cluster, in blue, the two mononuclear copper centers.

From the structural point of view the molecule is composed of three consecutive homology units further subdivided into six compact cupredoxin-type sub-domains [156], with large loop insertions (Figure 2.1.5); this high degree of internal homology has led to the proposal that Cp arose by tandem triplication of a primordial gene that coded for a primitive two-domain oxidase. Inserted in its structure, six tightly bound copper atoms are fundamental for the structure organization and the enzymatic activity of the protein. Due to the presence of these copper atoms, characterized by different spectroscopic properties and reactivity, Cp falls in the multi-copper oxidases family; these enzymes, also called blue oxidases, commonly present at least one blue or type 1 (T1) site, able to bind a copper atom in a unique tetrahedron structure. Interestingly, these sites are the responsible of the typical blue color of this proteins family. In addition to the blue copper centers, these proteins share three other copper atoms with a common site of binding, which is thus called the tri-nuclear cluster. On the basis of their spectroscopic properties, the three copper ions can be formally distinguished in one mononuclear type 2 (T2) copper site, with a normal electron paramagnetic resonance (EPR) signal and nearly undetectable absorptions in the optical spectrum, and a pair of anti-ferromagnetically coupled copper ions, or type 3 (T3) copper site, with strong absorption at 330 nm in the oxidized state and no EPR signal, but they in fact functionally behave as a single multi-metallic unit.

The role of the Cp's T1 site in the domain 6 is the sequential uptake and transfer of single electrons from substrate to the trinuclear cluster that uses the acquired electrons to reduce oxygen to water [157, 158]. This unique structure for a copper site is exclusive to blue oxidases and enables these enzymes to catalyze the four-electron reduction of di-oxygen to two water molecules by one electron oxidations of substrates [159]. Additionally to the four atoms of the catalytic center, the remaining two copper atoms (that do not participate to the oxidation reaction) are mononuclear centers held by intra-domain sites: one located on domain 4 that has a typical T1 copper environment with a set of four ligands (two histidine, one methionine and one cysteine), and one located in domain 2 that has a different structure since it lacks the methionine which is replaced by a leucine residue [160].

Ceruloplasmin is synthesized in hepatocytes (and by the other specialized cells in brain, retina and lung) and secreted into the plasma as holo-protein, with the six integral copper atoms already incorporated during biosynthesis immediately before secretion (or before membrane anchoring in the case of the glycosylphosphatidylinositol (GPI)-linked form [161]). This process is performed by the P-type ATPase Atp7b [162], and a failure to incorporate copper during synthesis results in secretion of an unstable apo-ceruloplasmin, which has no enzymatic activity and has an half-life of approximately 5 hours [163] compared to the 5.5 days for the holo-ceruloplasmin. This rapid degradation of the apo- form is due to its different conformation respect to the active ceruloplasmin, that makes it even more susceptible to proteolytic cleavage by plasma proteases [164].

Free copper concentration is physiologically maintained low by binding proteins that delivers it to specific cells, molecules or subcellular compartments [165, 166]; as we will see later in detail, this free pool of Cu can be toxic in particular pathological conditions, catalyzing the formation of hydroxyl radicals from H_2O_2 and, in the CNS, the oxidation of dopamine to aminochrome, which is suggested to be involved in the degeneration of dopaminergic neurons of Parkinson's disease patients [167]. Still in the CNS, copper plays a role in the assembly of theβ - amyloid and prion protein aggregates [168]; ceruloplasmin, binding up to 95% of circulating copper, should have a major role in copper homeostasis and in the delivery of this metal to recipient systems. In contrast, the discovery that copper metabolism is normal in patients with aceruloplasminaemia [169] seems to refute this hypothesis, maybe because Cp's activity is compensated by the redundancy of the copper transport systems which can also easily cope with its absence.

On the contrary to the majority of multi-copper oxidases, which act only on organic substrates, Cp oxidizes both inorganic ferrous iron and different organic substrates (described below), sharing this property with only a few other enzymes of unicellular organisms. In particular, the oxidation of iron is considered as the most important antioxidant activity of Cp, because iron is particularly prone to engage redox reactions with oxygen, resulting in a flux of ROS against many molecules and cell structures [170]. However, as outlined in the review of Floris et al [171], because Fe^{2+} is readily oxidized to Fe^{3+} through a non enzymatical reaction, it would seems that there is no need for a specific catalyst. As said in the 2.1.4 chapter, non-enzymatic oxidation of Fe^{2+} to Fe^{3+} is believed to trigger Fenton/Haber-Weiss reaction with the production of deleterious oxygen radicals: the hydrogen peroxide, in the presence of ferrous iron, serves as a source of the strongly toxic hydroxyl radicals, and oxidation of Fe^{2+} by Cp with production of molecular oxygen and water prevents further dangerous reactions (Figure 2.1.6).

So, the role of Cp might be an efficient control of the level of ferrous iron oxidation, without the production of toxic hydroxyl radicals [172]. Subsequently to this enzymatic reaction, the ferric iron is loaded on transferrin [2, 148, 173], the protein responsible of the transport of the ferric iron in the plasma and in the cerebrospinal fluid. This

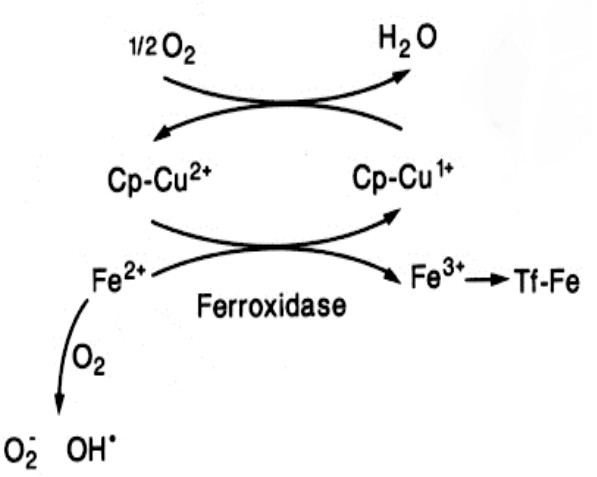

Figure 2.1.6: schematic representation of ceruloplasmin ferroxidase activity (from [2]).

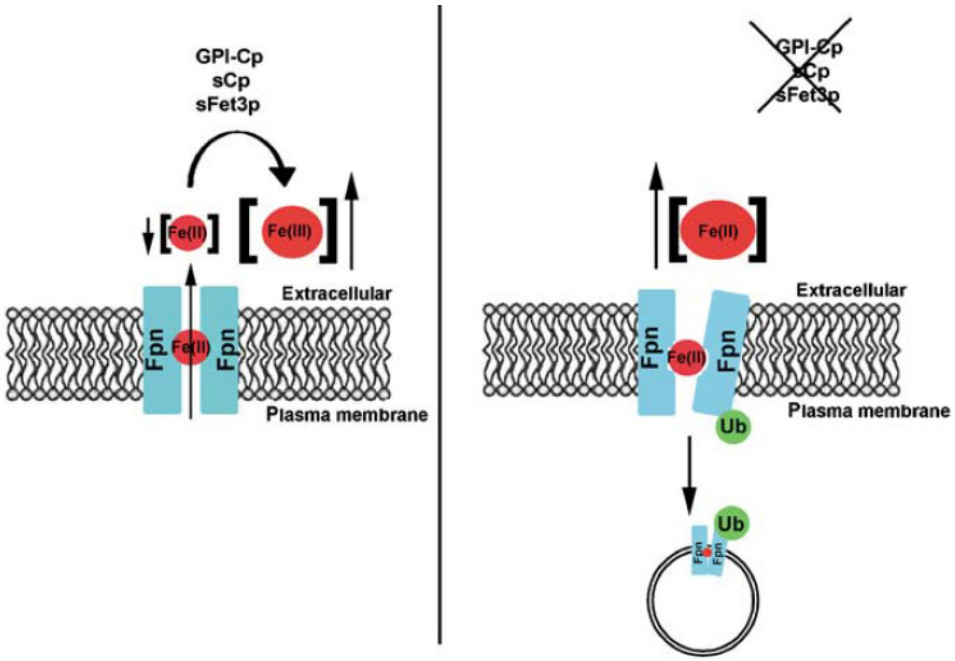

Figure 2.1.7: Cp extracellular ferrosidase activity is essential for the maintenance of the FPN exporter on the cell membrane (From [8]).

mechanism is required in order to maintain the iron efflux outside the cells through the iron exporter Ferroportin, that exports iron from cells as Fe^{2+}; a failure in the extracellular conversion of Fe^{2+} to Fe^{3+} leads the ferrous iron to be accumulated inside the cells. Moreover, the un-converted ferrous iron, blocking the Fpn channel, induces Fpn internalization, ubiquination and degradation (Figure 2.1.7). Thus, removal of Fpn-bound iron is an essential function of Cp [8], jointly with the direct oxidation of Fe^{2+} outside the cells. An important indication of this fundamental function of Cp is that humans with mutations of the Cp gene show iron accumulation in various organs including the retina, liver and brain [174].

Beside ferrous iron, Cp is able to oxidize an extensive group of other organic compounds: these include p-phenylenediamines, amino-phenols, catechols and 5-hydroxyindoles [175]. Interest in Ceruloplasmin catalyzed oxidation of arylamines and phenols has been the object of a long and detailed investigation, stimulated by the presence of catecholamines and 5-hydroxytryptamine neurotransmitters among those substrates that could relate Ceruloplasmin to neurologic diseases. The possibility that ceruloplasmin is a regulator of biogenic amine levels in the plasma and eventually in the brain, is currently controversial [171]. The main problems that hinder the resolution of the question are related to the *in vitro* conditions of the assays that cannot mimic *in vivo* conditions for the action of Ceruloplasmin, the extreme reactivity of the intermediates and the involvement of oxygen radicals in these reactions. This is particularly true for the metabolism of 6-hydroxydopamine, a neurotoxin involved in Parkinson's disease, which is oxidized *in vitro* by Ceruloplasmin [176, 177].

As said before, a role for Ceruloplasmin in this and other metabolic processes is justified by the ability to oxidize substrates at the expense of oxygen without ROS release that would otherwise be formed if substrates are engaged in direct redox reactions with oxygen. Finally, another significant activity of Cp is the one mediated by its catalytic site which involves Cys699, that performs a copper-independent glutathione peroxidase activity, with both hydrogen peroxide and/or organic peroxides [178]. This site enables ceruloplasmin to remove reactive intermediates that, in the case of hydrogen peroxide, could lead to an altered intracellular redox state. Also nitric oxide (NO) has been recently described as a substrate of ceruloplasmin: Cp has been shown to favor formation of S-nitrosoglutathione (GS-NO) when added to cultured monocytes expressing inducible NO synthase (iNOS) [179]: the role of Cp would be the oxidation of NO released by cells to nitrosonium, (NO+), a species more reactive than NO in the reaction with thiols. The mechanism exploits the property of NO to act as a ligand for copper and to engage a redox reaction with the metal once bound to it. NO appears unique among substrates of ceruloplasmin since it can reach and directly bind to blue copper sites, although with low affinity [180].

A very interesting observation is that Ceruloplasmin seems to be, in turn, a target of oxidative damage; in fact oxidative modifications by peroxylradicals and by hydrogen peroxide, during ageing, can result in the release of bound copper [181-183], with

consequent dramatic change of its EPR spectrum [184].

An elevation of plasma Cp concentration commonly accompanies a lot of pathological states and malignancies, in particular metastatic cancers [185, 186]; Cp seems to be involved in angiogenesis, an event common to a variety of physiological and pathological processes and, since it's known that this is copper-dependent process, it possibly be supported by a high level of Ceruloplasmin at a proper angiogenic site. The capability to take part in the angiogenic process and in antioxidant defense, which are two activities of Ceruloplasmin that could benefit the organism under some pathophysiological conditions, such as neovascularization of injured tissues, in the case of tumorigenesis would facilitate, rather than counter, cancer progression [187].

In conclusion, with all its functions, Cp can be included in the family of multifunctional proteins recently defined "moonlighting proteins" which are able to change their function switching between different capacity in response to changes in concentration of their ligand/substrate, their differential localization and/or differential expression [188]. A new function can be the result of a different use of a pre-existing site or of a modification of unused regions of protein surfaces, especially in the case of large molecules; in the Cp structure indeed, the presence of particularly reactive groups on the lateral chains of amino acid residues can lead to a gain of function that further expands ceruloplasmin modes of action.

2.2 Neurodegenerative diseases: metals matter

2.2.1 Alzheimer's disease

Described for the first time in 1907 by Alois Alzheimer, Alzheimer disease (AD), a progressive neurodegenerative pathology, is the most common form of dementia all over the world covering from 50 to 80% of the cases and affecting 2/1.000 individuals between 65 and 69 years, 9/1.000 between 75 and 79 years and 40/1.000 between 85 and 89 years. The pathology initially manifests itself with symptoms like memory loss, disorientation, personality and humoral and intellective changes, leading the individual incapable of make various simple daily activities. Afterwards, all these symptoms get worse, causing in the patient amnesia, aphasia, agnosia and apraxia and making, in the terminal phase of the disease, the patient to be completely not self-sufficient and helpless; death (that can take place from 3 to 20 years after first diagnosis) will occur by collateral pathologies, like opportunistic infections. Like most of other dementias, AD is mostly a sporadic disorder and the major risk factor is the aging; however, genetic autosomal dominant variants of the pathology are also known, and can be divided in early onset familiar forms (rare, age of onset under 60 years) and late onset familiar forms (much more frequent, with an age of onset above 65 years). Most of the times anyhow AD, described as a complex multifactorial pathology, is the result of the interaction of different predisposing factors, either genetic or environmental.

The etio-pathogenesis of AD is still controversial, but the most diffused hypothesis is the amyloid cascade theory: according to it, the formation of β-amyloid (Aβ) oligomers or mature fibrils is the first step of the pathology. β-amyloid (which accumulation impairs synapsis activity, proteasome function and cause neuronal death, correlating with the clinical stage), is derived from the proteolytic cleavage of the amyloid precursor (App), a membrane protein which, being a ferroxidase, is involved in the metabolism of iron in the central nervous system [189]; moreover, App seems to play a role in the formation and function of synapses [190]. Cleavage of App can follow two different ways: the first one involves both α-secretase and theγ -secretase, that cleave the App at the N-terminal and at the C-terminal respectively producing a non-amyloidogenic peptide; the second, amyloidogenic, produces the $A\beta_{1-42}$ and the $A\beta_{1-40}$ peptides, is mediated by β-secretase and γ-secretase [191]. At the level of amyloid plaques, both $A\beta_{1-40}$/$A\beta_{1-42}$ are found, but $A\beta_{1-42}$ is known to be more prone to aggregate. Moreover, under physiological conditions 90% of Aβ produced is of the $A\beta_{1-40}$ form, which is soluble and promptly degraded; on the contrary during aging, the ratio of $A\beta_{1-40}$/$A\beta_{1-42}$ production is overturned, which in turn results in $A\beta_{1-42}$ accumulation, oligomerization and formation of fibrils. Why Aβ aggregates into fibrils is not yet explained, but Aβ aggregation seems to cover an antioxidant role in the early phase of the pathology: as Aβ increases in the AD cortex, there is in fact a decrease in neuronal levels of oxidized nucleic acids, decreased oxidative damage [192] and decreased toxic free metals, being iron ions [193] sequestered within the plaques. Aβ sequence and Aβ concentration [194] are thought to be key factors in the set off of the amyloido-genic process: due to dominant mutations of three genes coding for App (APP) or Presenilin 1 and 2 (PSEN-1/PSEN-2), two proteins that are part of the γ-secretase complex, the senile augmented production of $A\beta_{1-42}$ is anticipated and enhanced, causing most common cause of early onset familiar AD (5% of the cases) [195]. Another hallmark of Alzheimer pathology, aside from extracellular amyloid plaques, is the presence of intracellular neurofibrillary tangles (NFT) composed prevalently by a hyper-phosphorylated form of Tau protein. Tau, associated to microtubules of neurons, is essential for cytoskeleton organization and for the transport of nutritive molecules inside the cell; hyper-phosphorylation (probably caused by toxic concentrations of Aβ) causes Tau to be less affine to microtubules [196], letting it to form oligomers which can aggregate into an extremely insoluble β-sheet structure that compose then the neurofibrillary tangles. The mechanism of this hyper-phosphorylation is not explained yet: many phosphokinases, including GSK3β, CDK5, and ERK2, have been investigated as potential player in this process, making them also possible treatments targets to reduce tau phosphorylation [197].

Oxidative stress plays a pivotal role in AD, because age-related accumulation of reactive oxygen species (ROS), which results in damage to major components of cells, is enhanced in AD patients: oxidized nucleic acid, lipids and proteins are indeed found in AD patients CNS [198, 199]. Free radicals are potent damaging agents responsible of cell death or other

irreversible modifications [200], and neurons appear to be particularly vulnerable to attack by these free radicals due to their low glutathione content [201], the polyunsaturated fatty acids of their membranes [202] and the high quantities of oxygen required by the their metabolism. Much is the attention spent in the last years on the study of the correlation between metals and AD, as it's known that several metals play a major catalytic role in the production of free toxic radicals, and high concentrations of metals like iron, aluminum, copper and zinc are found in AD patient's brain. The concentration of iron (which, as said in the paragraph 2.1.4, can induce oxidative environment through the Fenton Haber Weiss reaction [203]) in the brains of AD patients is elevated and transferrin, ferritin and iron have also been found localized in senile plaques [204] and NFT. Furthermore, the ability of α-secretase to cleave App can be modulated by iron [205]. Copper instead have the potential to produce oxidative damage by altering ceruloplasmin function [206] and interacting with App [207]. The involvement of copper in neurodegeneration is also suggested by the fact that this metal is essential for many enzymatic activities, including cytochrome-*c* oxidase and Cu/Zn superoxide dismutase [208]; furthermore, copper concentrations are also highly concentrated within Aβ plaques. Zinc localizes into Aβ plaques too, and binds modulating its functional properties [189].

Oxidative stress can be generated in numerous ways, and can impair various mechanisms like mitochondrial metabolism and protein degradation. Free radicals, for example, are involved in glycation processes and can foster the formation of advanced glycation end products (AGEs) [209]: AGEs, a class of posttranslational modifications, are generated by the non-enzymatic reaction of a sugar ketone or aldehyde group with the free amino groups of a protein or amino acid [210], and in the presence of transition metals these AGEs can also undergo redox cycling with consequent ROS production. Accumulation of AGEs in the brain is a feature of aging [211], and since their production is accelerated by, and result in formation of, oxygen-derived free radicals, they represent an important source of the oxidative stress in AD; in addition, AGEs were detected in association with β-amyloid [212] and NFT [213].

The secretion of ROS/reactive nitrogen species (RNS) by immune cells is the major mechanism for attacking target cells, and activated microglia have the potential to produce large amounts of ROS/RNS by various mechanisms: both activated microglia and astrocytes localize at sites of Aβ deposition [214], producing hydrogen peroxide [215] and various cytokines, chemokines and complement components [216]. Activated microglia and astrocytes can produce also large amounts of nitric oxide (NO), which in turn can react with superoxide to form the peroxynitrite radical, increasing the amounts of nitrotyrosine-modified proteins [217] and enhancing the oxidative environment.

The degradation of non-functional, oxidized proteins is an essential part of the antioxidant defenses of cells: proteasomal activity declines with age, and further studies demonstrate disease-specific alterations in the level and distribution of proteasomal subunits and decreased proteasome activity in the AD brain [218]; chronic proteasome inhibition, in addition to increased protein insolubility, induces elevated levels of protein oxidation and significantly inhibits the activity of mitochondrial complex. Moreover, disruption of membrane lysosomes [219] cause the release of lysosomal contents including redox-active iron that directly participate to oxidative stress also inducing mitochondrial damage with enhanced production of ROS [220]. Reduced energy production and increased oxidative stress, as well as damaged mitochondria, are also characteristics of AD [221]. The defect in the electron transport chain within the mitochondria is a factor that can contribute to the production of free radicals, being damaged mitochondria less efficient to produce of ATP and more efficient to produce (ROS): a reduced rate of brain metabolism is one of the best-documented abnormalities in AD [222], having the AD patients CNS an higher percentage of completely damaged mitochondria compared to aged-matched controls. The most consistent defects in mitochondria in AD are deficiencies in several key enzymes of oxidative metabolism: Mutisaya et al [223] showed, for example, that albeit normal amounts of cytochrome-*c* oxidase are found in the brains of AD patients, its oxidase activity was about 25–30% lower than normal in the cerebral cortex, suggesting that it's only the enzyme activity that is affected [224]: cytochrome-*c* oxidase defect can produce increasing amounts of free radicals, and interesting, mutations in cytochrome-*c* oxidase genes segregate with late-onset AD [225].

Summarizing, we can describe Alzheimer neuro-pathological disorder as a combination of two

different factors: a genetic defect related to a particular molecule and the age-related abnormal production of free radicals, but the exact contribution of each source of oxidative stress above described is complicated, as these sources of oxidative stress interact with each other, establishing a positive feedback. Furthermore, what may be the initiating factor and how this whole process is set off is still unclear.

The amount of risk of Alzheimer's disease that is attributable to genetics is estimated to be around 70%, but Identification of specific risk genes is problematic because, being AD a multifactorial pathology, the overall increase in risk conferred by a single gene is small and because the pathological changes in AD are highly heterogeneous. In addition to the genes related to App metabolism listed above, several other potential risk genes for AD have also been identified: the most important gene linked to an high risk to develop AD, both in familiar and sporadic forms, is the APOE gene, that encodes for apolipoprotein E (ApoE). ApoE is a protein localized in the plasma, involved in the transport of cholesterol through both the vascular system and the neurons, and known to bind Aβ protein. Three forms of apoE are known: ε2, ε3 and ε4. E4 allele is more frequent in AD subjects, and its presence determines a 4-fold increased chance to develop the pathology [226]. Apo ε2 instead seems to have a protective role. ApoE is a protein sensitive to attacks by free radicals, but the E4 isoform is more sensitive, suggesting that this feature of the E4 allele contribute to the pathology. Moreover, the level of peroxidation in the brains of AD patients is inversely proportional to the concentration of ApoE, which suggests the hypothesis that apoE has a beneficial effect against lipids peroxidation, and that the effect is more pronounced when the patient has the ε2 allele.

Alzheimer's disease can only be definitively diagnosed post mortem (observing the atrophy of parietal cortex, temporal cortex and hippocampus and a reduced brain volume of about 1/3 compared to healthy subjects), although earlier "probable" diagnosis may be possible with improved diagnostic techniques and criteria, that include a detailed history of the type and course of symptoms, computational tomography CT or (magnetic resonance imaging) MRI detection of intracranial lesions or diseases that might cause or contribute to dementia syndromes (tumors, cerebrovascular disease) [227] or detection of atrophy in hippocampus, cortex and amygdala. PET (positron emission tomography)-glucose brain metabolism analysis and Aβ neuroimaging in vivo are innovative diagnostic procedures, whose can put forward the diagnosis of the disease. AD can be also differentiated from other dementias by the combined detection of lower concentrations of CSF's $A\beta_{1-42}$ and increased concentrations of total Tau or hyper-phosphorylated Tau at threonine 231 and 181 than age-matched control individuals [228]. From the therapeutic point of view, AD is still incurable, and the therapy tries only to lighten its symptoms: cholinesterase inhibitors are used to improve patients' behavior, but the effect on cognition is moderate. Memantine improve cognitive performance [229] and might also be beneficial in the prevention and treatment of agitation and aggression [230], while antipsychotic drugs are commonly used to treat agitation, aggression, and psychosis in patients with dementia [231]. Simple non-pharmacological treatments, such as social interaction and care training, can be effective alternatives to drug. Innovative therapies include active immunotherapy with fragments of the Aβ protein, that was effective at clearing Aβ and improving conditions in transgenic mice [232], but raised skepticism about how this approach works, because only a small proportion of antibody crosses the brain barriers. Several potential therapies either inhibit β-secretase or modulate γ-secretase, with the goal of reduce $A\beta_{1-42}$ concentration. Nowadays, reduction of the risk of developing Alzheimer's disease depends mostly upon lifestyle changes and improved treatment or prevention of medical conditions that confer additional risk.

2.2.2 Parkinson's disease

Described for the first time by James Parkinson, Parkinson disease (PD) is a chronic progressive pathology, and, after AD, is the second predominant form of dementia. Although genetic familiar forms are also described, Parkinson's disease, like AD is prevalently a sporadic disorder (90-95% of the cases) and aging is the major risk factor [233], rising the incidence from 20/100000 persons between 50 and 59 years of age to 120/100000 persons after 70 years of age [234]; only 10% of people with the disease are younger than 45 years, and men are about 1.5 times more likely than women at risk to develop PD.

The diagnosis of the pathology is very difficult, being its onset gradual and the earliest symptoms that

include depression, anxiety, smell impairment and sleep disorders are non-specific, unnoticeable and linked to the normal aging process. When the disease progress and the neuronal loss is significant however, more specific and evident symptoms appear, like impairment of dexterity, resting tremor, muscular rigidity, bradykinesia, monotonous speech and postural imbalance. All these PD characteristics are the result of the degeneration of specific regions of the patients' brain, in particular of the dopaminergic neurons in the midbrain area called substantia nigra pars compacta (SN), but as well as with more widespread neuronal changes.

From the pathological point of view, the hallmark of PD is the presence of intra-cytoplasmic inclusions called Lewy bodies (LBs), a dense granular structures localized principally in the dopaminergic neurons of the caudal and ventro-lateral regions of the SN but also in the hypothalamus, basal ganglia, cortex and olfactory bulb. LBs are composed mainly by α-synuclein (α-syn) and other proteins like Ubiquitin and Parkin. LBs, that are continuously forming and disappearing in the SN, are often accompanied by the presence large eosinophilic structures thought to be the predecessor of LBs called pale bodies [235], and by Alzheimer characteristic β-amyloid aggregates in patients with severe memory loss [236, 237]. Interestingly, LBs are also present in 10% of the people older than 60 years who died without neurological evidences: this condition, called incidental LBs pathology, might be the early pre-symptomatic phase of PD [238]. Braak et al. [239] proposed a PD progression theory divided in 6 stages, based on LBs diffusion through the different CNS regions: first, the α-syn immune-reactive inclusions are found within the olfactory system, causing olfactory deficits; in stage 2, the LBs are more widespread within the medulla oblongata and also during these first stages, the individuals do not present any perceptible motor symptoms. Stage 3 is characterized by the progression of LBs in the midbrain, basal forebrain, and later into SN. In stage 4 cell loss in the SN is evident, as well as α-syn immune-reactivity in the cerebral cortex: at this time, patients may display the first PD symptoms. Finally, in stages 5 and 6, α-syn pathology begins to invade the neo cortex: at this phase, motor symptoms are clearly diagnosable, and cognitive dysfunction becomes evident.

The physiological function of α-syn protein in the healthy brain is not well understood: expressed prevalently in the neo-cortex, hippocampus, SN, thalamus, and cerebellum [240], this 140 KDa protein is present in the cytoplasm as a monomer, and high concentrations are present in the pre-synaptic space of neurons where it coordinates the neurotransmitter vesicular recycling (fundamental for the correct functioning of the synapse [241]). Characterized by a highly amyloido-genic domain (which presents a high propensity to aggregate and to form oligomeric structures and insoluble fibers under particular conditions such as elevated concentrations) α-syn can aggregate in β-sheet proto-fibrils which trigger the LBs formation. The mechanism of α-syn oligomers formation is not clear: mutations of the SNCA gene (which encodes for the α-syn) increase the tendency of the protein to oligomerize [242, 243], and many studies suggested that this aggregates, sequestering toxic α-syn, are made to prevent its cellular toxicity.

Oxidative stress, characterized by an imbalance between the generation of free radicals and antioxidant defenses, may be related to the impaired mis-folded protein clearance as well as to mitochondrial function [244]: DAergic neurons of the SN are the most oxidative-sensible cells because the dopamine (DA) metabolism, which generates highly toxic molecules, can contribute to mitochondrial dis-function increasing the oxidative damage. DA, synthesized from tyrosine by tyrosine hydroxylase, is stored in millimolar concentrations in synaptic vesicles: impairment in the storage of DA, which may be due to α-syn fibrils (which are shown to be responsible of the leakage of the neurotransmitter from the presynaptic vesicles [245]), can increase DA levels in the cytoplasm. In this condition DA can auto-oxidize its catechol ring with the production of DA-quinone, superoxide radical ($\bullet O_2$) and hydrogen peroxide (Figure 2.2.1) [246]. Alternatively, DA can be degraded by monoamino-oxidases A and B (Mao-A/B) with the production of hydrogen peroxide. DA-quinone is a very reactive molecule, and it has been shown to interact with α-syn inducing its aggregation [247], impair brain mitochondrial function [248] causing ROS production, induce proteasomal inhibition leading the cells to undergo apoptosis [249] and cyclize to become the highly reactive aminochrome, who leads the generation of superoxide and depletion of cellular NADPH. Moreover, hydrogen peroxide generated during DA metabolism, as described in the chapter 2.1.5, can be subsequently converted into the highly reactive

hydroxyl radical in the presence of high transition metal ions [250] contributing to oxidative stress (Figure 2.2.1). Interestingly, DAergic neurons physiologically show high concentration of iron and ferritin that are increased in PD [251], and iron deposits were found in microglia, oligodendrocytes, astrocytes located close to neurons and in the rim of Lewy bodies in the SN of PD patients [252]. It is so conceivable that oxidative stress is a common mechanism that leads to cellular dysfunction and death, causing the cellular and molecular modifications present in PD, like α-syn olygomerization; this hypothesis is supported by various evidences, like decreased intracellular reduced glutathione (GSH) [253, 254] found in the damaged cells of the SN, their increased levels of oxidized lipids [255], proteins and DNA [255]. Neuromelanin, the final product of DA oxidation, is furthermore accumulated in the nigral region of the human brain [256] and it can sequester free iron, acting as a neuroprotective factor [257].

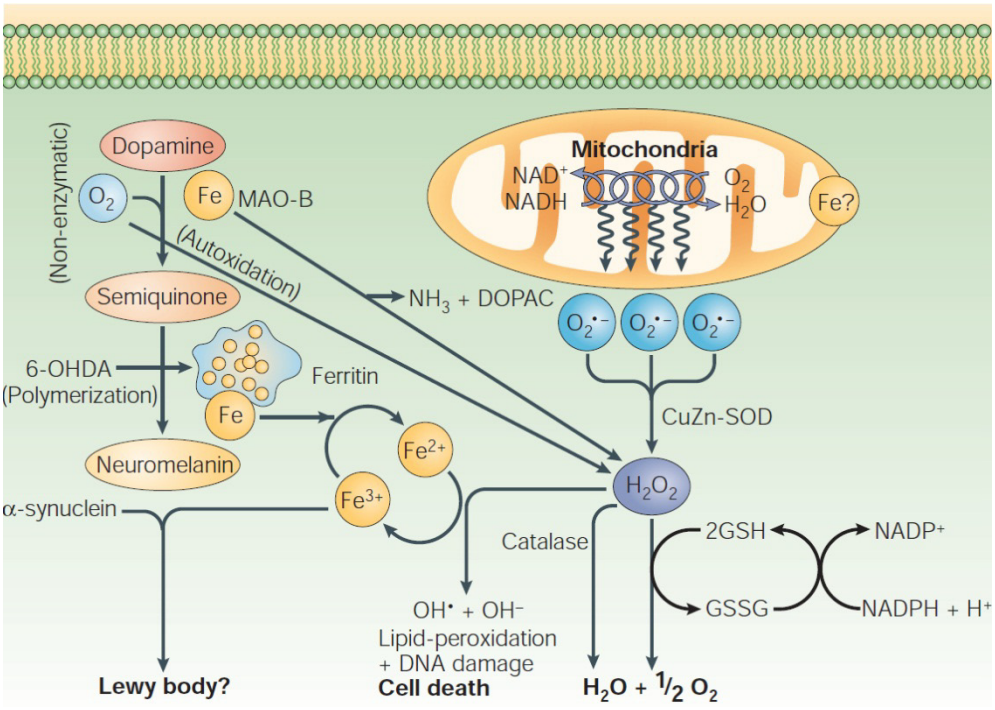

Figure 2.2.1: Iron and oxidative stress hypothesis in PD. This figure summarizes the pathological mechanism in PD, explaining the possible cell-death mechanisms. From [4].

Mitochondrial dis-function can also be provoked by α-syn: indeed α-syn aggregates induce mitochondrial release of cytochrome c (triggering apoptosis), increase mitochondrial calcium, nitric oxide, and oxidative modification of mitochondrial components. In addition, α-syn, although mostly cytosolic, seems to interact with mitochondrial membranes to inhibit Complex I [258]: higher number of respiratory chain deficient DAergic neurons have been found, in fact, in PD patients compared to age-matched controls [259]. At this point it's clear that all the pathways above mentioned are thus interconnected in a positive-feedback mechanism, because mitochondrial dysfunction itself leads to increased free radical generation, which further provokes α-syn aggregation; the net result of this "pathologic loop" is an increased cell dysfunction and a lowered threshold to apoptosis.

The theory of the mitochondrial dysfunction and oxidative stress [260] role in PD is supported today by the study of its genetics forms, either recessive or dominant and which involve several genes that often code for mitochondrial proteins. "Loss of function" mutations in four genes (PINK1, PARK7, PARK2 and PARK5) cause recessive early parkinsonism with an age of onset under 40 years: all these mutations lead to a disease that has a more benign course than Parkinson's disease and responds well to dopaminergic drugs. Pink1, localized to the mitochondrial inter-membrane space and bound to mitochondrial membranes, is thought to phosphorylate mitochondrial proteins in response to cellular stress and to protect against mitochondrial dysfunction. Interestingly, LBs localization of Pink1 was observed in patients with sporadic PD [261]. PARK7 gene encodes for a cytoplasmic protein (Dj-1) that appears to exert an antioxidant function [262] in physiological conditions, but under stress environment can also translocate into the mitochondria and nucleus [263]; deletions and point mutations in the PARK7 gene cause a loss of its protective role. Mutations in the gene PARK2 (that encodes for Parkin) and PARK5 (which encodes for Uchl1) underline the importance of the protein degradation system in the disease, being Parkin [264] and Uchl1 included in the ubiquitin-proteasome pathway, responsible of the removal of oxidative mis-

folded proteins from the cytosol. Mutations of this two genes cause an impairment of the mis-folded α-syn degradation, causing its accumulation in LBs.
Looking at the autosomal dominant genes, SNCA (coding foα -syn and described previously) and LRRK2 instead have been shown to cause with a mutation frequency of 5% [265], the majority of the cases of autosomal dominant PD; LRRK2 gene represent the most common known cause of familial PD, encoding a large multi-domain protein able to undergo phosphorylation and to phosphorylate generic substrates. Although Lrrk2 protein is mainly localized to the cytoplasm, consistent levels of the protein are associated with the outer mitochondrial membrane [266], raising an important question of whether mutant Lrrk2 kinase increased activity might directly affect mitochondrial function.
The final evidence of the key role of oxidation in PD is provided by the treatments of animal models in which PD is provoked: MPTP (1-metil-4-fenil1,2,3,6-tetraidropiridine) treatment, which block the mitochondrial respiratory chain complex I and induce DA dependent oxidative stress, induces in the animal a PD-similar phenotype. Rotenone (which acts as an inhibitor of the mitochondrial respiratory chain complex too) and Paraquat, two pesticides, cause a loss of dopaminergic neurons in rodents and increase the incidence of Parkinson disease in human professions in direct contact with them.
Neuronal loss in PD is finally associated with also chronic neuro-inflammation, which is mediated primarily by microglia, the main resident immune responsive cells in the central nervous system. Microglial reaction has been found in the SN of sporadic PD patients [267] as well as familial PD patients [268]: microglia, activated in response to injury or toxic insult as a self-defensive mechanism to remove cell debris and pathogens, release free radicals such as NO and superoxide, which can in turn contribute to oxidative stress in the microenvironment. Over-activated or chronically activated microglia causes an excessive and uncontrolled neuro-inflammatory response, leading to an increased cell apoptosis with consequent neurodegeneration [269]. The oxidized or ROS-damaged molecules released from suffering nigral DAergic neurons that trigger microglial activation include neuromelanin and α-synuclein, as demonstrated by strong microglia activation caused by intra-cerebral injection of neuromelanin, and by that a fraction of α-syn fibril released from neurons [270] is found in the cerebrospinal fluid of PD patients [270] and causes activation of microglial cells; moreover, α-syn stimulates astrocytes to produce inflammatory modulators that augment microglial chemotaxis, activation and proliferation [271]. Concluding, the understanding of the patho-physiology of the disease at cellular and molecular levels and finding the molecular targets for an efficacious neuro-protective therapy is a crucial issue in the field of Parkinson disease research.

2.2.3 Cp in in neurodegenerative diseases

Being ceruloplasmin a crucial protein in the metabolism of both iron and copper, seems quite clear that an alteration of its function at the level of CNS can result in an impairment of the homeostasis of these two metals, possibly leading to the iron and copper disequilibrium described in the previous chapters for AD and PD patients. An important evidence of this fundamental role of Cp is provided by three human genetic disorders: Aceruloplasminemia, Menkes disease and Wilson disease, which are characterized by the absence of the protein or at least by its presence in an inactive form in the whole body.
Aceruloplasminemia is an autosomal recessive disorder [272, 273] caused by 40 distinct loss-of-function mutations in the Cp's gene [274], which lead to the formation of a premature stop codon causing the formation of an inactive apo-form of the protein, that lacks the copper cluster sites critical for its enzymatic function. The rapid degradation of the apo-Cp in this way produced leads the patients to have absent serum ceruloplasmin, albeit particular mutations where patients present the clinical features of aceruloplasminemia [275] while having detectable levels of serum ceruloplasmin have also been reported; despite symptomatic heterozygous patients exist, usually these heterozygous individuals have normal iron metabolism and no clinical symptoms.
The absence of Cp in the body leads patients to have also decreased serum iron, elevated serum ferritin and iron accumulation within hepatocytes, pancreatic endocrine cells, basal ganglia and astrocytes [276]. This accumulation causes hepatic iron overload, anemia, retinal degeneration, diabetes mellitus and adult-onset neurological symptoms, which reflect the CNS sites of iron accumulation [2, 277, 278]. Despite the fact that the truncated Cp molecule loses all its coordinated copper ions, no

serious disorders of copper metabolism have been reported in aceruloplasminemic patients (and also in Cp knockout mice) [2], and none of the clinical symptoms associated with the disease is consequence of copper deficiency or toxicity. Neurological symptoms, which often occur when patients are older than 40 years [279], are usually progressive and are caused by cerebellum and basal ganglia neuronal cell loss, abnormal astrocytes morphology and deposition of ferrous iron in glia [280, 281], neurons and reticulo-endothelial cells, where in physiological conditions this metal is stored and then mobilized for recycling [282]. This increased brain iron, hallmark of aceruloplasminemia, has been detected by MRI or autopsy [283], and seems to be the responsible of the neuronal cell death through two different mechanisms: *via* iron-mediated radical stress (high levels of lipid peroxidation in aceruloplasminemia have been evidenced in various organs, including the brain) and *via* iron deficiency in regions where iron accumulated in astrocytes is not able to be exported for uptake, like neurons: The latter mechanism is due to the absence on the astrocytes of their GPI-anchored form of Cp, required for the cellular iron efflux; it's known that astrocytes GPI-Cp is essential for the stability on the cell surface of the iron exporter Fpn [8], and *in vitro* biological analyses demonstrated in fact that the ceruloplasmin-mutants astrocytes have impaired ferroportin stability on the cell surface, resulting in exacerbated iron accumulation within the cell [284].

Menkes (MD) and Wilson disease (WD) instead are not characterized by mutations of the Cp gene, but by mutations in the genes encoding copper-transporting ATPases ATP7A and ATP7B, responsible the first of the copper transport through the intestinal and brain barriers, and the second of the incorporation of copper into fully developed holo-ceruloplasmin.

MD is an X-linked fatal loss-of function disease [285], characterized by an impaired copper metabolism and delivery in the whole body including the brain, with marked metabolic and developmental changes (growth failure, hypo-pigmentation, arterial tortuosity), progressive neuro-degeneration and death of the majority of patients in early childhood. The various features of this disease are the result of abolished activity of several cupro-enzymes (including Cp) due to the lack of systemic Cu caused by the Atp7a dis-function at the level of the intestinal barrier. Neurologic features develop in early infancy, due to loss of neurons and extensive atrophy in cerebellum and cortex [286], with focal degeneration of the gray matter and de-myelination [287]; systemic copper treatment clearly is not effective in MD, as copper transport into the brain is dependent on Atp7a.

Wilson Disease is also characterized by copper deposition in the liver, brain, kidneys and cornea, with an increased copper concentration in the CSF too; symptoms of the disorder reflect the copper accumulation sites, and are the onset of hepatic cirrhosis, neurological symptoms and Kayser-Fleischer corneal rings. WD is characterized by more than 200 different loss-of function mutations (deletion, insertions and missense/nonsense mutations) of ATP7B [288, 289], whose gene is located on chromosome 13 [290]; some mutations are associated with a severe impairment of copper transport, resulting in severe liver disease, while other mutations appear to be less severe, depending on the site of mutation in the ATP7B sequence. Loss of function of Atp7b results in synthesis of an apo-ceruloplasmin that is rapidly degraded in the plasma [291], as Atp7b function is to load copper on the apo-form of ceruloplasmin; moreover, another Atp7b function is to mediate the excretion of excess copper into bile [292]. These two distinct functions require the protein to localize at different subcellular compartments: at the trans-Golgi network, where Atp7b incorporate copper into apo-ceruloplasmin, and to post-Golgi vesicles in proximity to the canalicular membrane, where Atp7b translocate when intracellular copper levels are increased to facilitate biliary copper excretion.

Due to the copper imbalance in the CNS, a large proportion of WD patients display neurological and psychiatric symptoms; in the brain of patients copper is accumulated in selected structures, such as nucleus lenticularis, substantia nigra, globus pallidum and corpus striatum, affecting in particular mitochondrial respiration and triggering activation of cell-death pathways [293]. This accumulation leads to early symptoms like hyperkinesia with typical flapping tremor, dysarthria and dementia, which consequently progress to severe Parkinsonian symptoms [294] and neuro-psychiatric illness [295] when other CNS regions are affected, including the thalamus, subthalamic nuclei, brainstem, and frontal cortex. On the contrary of MD, improvement in these symptoms can be observed upon treatment, in this case with

oral chelating agents able to restore copper homeostasis.

Aside from being involved primarily in these focused diseases, Ceruloplasmin seems to play an important role also in AD and PD patients, characterized by iron and copper anomalous homeostasis and oxidative stress [296]. In fact, Cp concentrations are often increased in AD and PD patients in particular regions characterized by extensive pathology (for example in AD hippocampus and frontal cortex and in PD substantia nigra) but not in others. However, the relationship between this regional brain Cp content and neuronal loss is unclear: probably, elevated regional Cp levels are induced by the suffering brain in order to enhance the anti-oxidant capacity of the system increasing the regional iron-oxidative activity of Cp [297].

Furthermore, although being an oxidation-protective enzyme, Cp seems to be subjected to oxidative modifications itself: in fact, besides Cp concentration in serum is the same for example in control and AD subjects, its ferroxidase activity is significantly lower [298] and free copper in serum is increased in patients, correlating with the MMSE (Mini Mental State Examination) score [299]. These observations suggest an alteration in the structure of the protein which, although being present, loses its enzymatic activity and its ability to transport copper. Also in the cerebrospinal fluid of patients Cp oxidative activity was significantly lower while its concentration is not generally affected; on the contrary, in the brain of AD patients copper has been found to be not increased [297, 298] or even significantly lowered, due to its sequestration within Aβ plaques [300].

This decreased Cp activity (and of others cupro-enzymes) in AD can be thus the result of a defect in the incorporation of copper in the protein (due to the specific copper accumulation and sequestering in Aβ plaques) or of a release of copper from the oxidation-damaged protein. Cp ferroxidase activity impairment can finally influence also iron homeostasis: in fact iron, despite is, in general, not increased in AD [300], accumulates specifically in NFT, neuritic plaques and intra-cellularly in neurons and astrocytes, indicating again a dysfunctional status in its metabolism in the brain, inducing tissue damage, axonal dysfunction and cell death.

In the case of Parkinson disease, the issue is more complicated, being described several variants of PD: one, the most common, with increased iron in the substantia nigra and low Cp concentration in serum [301], the second with normal iron in the substantia nigra and normal Cp concentration in serum, and the last with additional increased serum copper matching an increased Cp [302]. Anyhow, the common feature of these different variants of PD is again the lack of Cp ferroxidase activity, suggesting that also in PD this enzymatic activity is necessary for the correct metabolism of iron in the brain. In the second variant of PD described above in fact, albeit Cp serum concentration is not modified, its oxidative activity in serum negatively correlates with the iron content of the substantia nigra, and in the last variant (that shows biological markers similar to the Down syndrome) Cp concentration increasing might indicate that the impaired copper incorporation into the Cp molecule and the deficiency of its ferroxidase activity triggers a compensatory mechanism of the brain that synthetize high amounts of Cp [303]. Looking at these different variants of PD phenotypes, seems clear that accumulation of iron in the substantia nigra, although common in PD (and, interesting, associated with Cp gene mutations [304]), is not enough to produce the clinical symptoms of the pathology: the oxidative activity of Ceruloplasmin is indeed not only addressed to Fe oxidation, but it's also involved in the oxidation of catecholamines (like DA) in neurons where these amines function as neurotransmitter molecules, it is so reasonable that Cp oxidative activity participate also in this process to avoid the occurrence of PD. As said before, Cp is in effect able to enhance the oxidation of 6-hydroxydopamine [177], an intermediate product on the way to the formation of dopamine-melanin, and oxidation of 6-hydroxydopamine by Cp avoid H_2O_2 production [177], unlike the case of its oxidation in the absence of Cp when toxic oxygen species are generated.

In PD, a negative correlation has indeed been found between the Cp concentration and its oxidative activity in serum and iron deposits in the substantia nigra in the brain [302]; furthermore, Kyung-hee Lee at al discovered that pathological amounts of Cp in the brain induce gene expression and activate signaling molecules implicated in microglial activation [305], causing an aberrant inflammatory response inducing nitric oxide production and exacerbating the oxidative environment and cell death. The difference in sensitivity to rotenone of rats and mice, which seems to correlate with the levels of Cp in animals is, again, another evidence that suggest an involvement of Cp in the pathology [306].

2.3 Asparagine spontaneous deamidation and NGR-motif-dependent gain of function

2.3.1 Molecular timing of asparagine deamidation

Proteins and peptides are susceptible to a variety of post translational modifications (acetylation, phosphorylation, methylation and glycosylation) that can affect their structure and their biological functions. These aminoacidic modifications can occour spontaneously during the normal aging of proteins, but the normal turnover/neosyntesys keep the rate of modified proteins under control. During the ageing of an individual, due to the unbalance between deleterious *vs.* repairing systems, these modifications take over causing an accumulation of these modificated proteins. This process can be accelerated also under pathological coditions: it's very well reported in literature for example that the oxidative environment present in several neurodegenerative diseases (like AD and PD, as described before) cause an increase in this deleterious modifications of a variety of proteins, which become often unactive or even capable to trigger pathological effects. Among these modifications, the formation of isoaspartic acid (*iso*Asp), result both of the isomerization of aspartic acid (Asp) and the deamidation of asparagine (Asn) [307], occurs spontaneously in proteins and peptides either *in vitro* (for example in the storage and purification of calmodulin [308]) and *in vivo* during development and aging of cells [309]. Deamidation of Asn is a hydrolytic reaction that brings to an anomalous β-linkage formation and to the introduction of a negative charge that may cause a change in the protein primary structure, which may in turn affect the secondary, tertiary structure and its biological activity. The deamidation of the asparagine residue is a ubiquitous non-enzymatic process that is initiated by a nucleophilic attack of the peptide bond amino group on the asparagine side-chain carbonyl group, with release of NH_3 (Figure 2.3.1). The cyclic succinimide-ring-intermediate thus resulting rapidly hydrolyzes to a mixture of aspartate or *iso*aspartate, with a preference of 1:3 [310] for the formation of the latter because of the asymmetry of the succinimide structure [311]. Asparagine is not the only amino acid able to deamidate: also glutamine, the other amino acid with an amide side chain, can undergo spontaneous deamidation, but with a slower rate [312]. *Iso*aspartate can result also from the spontaneous isomerization of Aspartate, but this reaction occurs at a slower rate compared to Asp deamidation. *Iso*Asp formation is influenced by several factors like pH, temperature, oxidation [313], tertiary, secondary and primary structure of the protein: Robinson et al. [307] demonstrated indeed that the rate of asparagine deamidation can be determined by the surrounding amino acid sequence, being the Asn deamidation affected by Ser, Thr and Lys located at the N-terminal side [314] and favored when the side chain of the carboxyl-flanking amino acid is relatively small and hydrophilic (in particular Glycine and Serine). By contrast, branched hydrophobic amino acids, such as Valine, protect Asn and Gly from possible deamidation. Also the degree of local polypeptide flexibility influences the kinetic of this reaction: *iso*Asp formation generally occurs within flexible protein sequences and is less likely to be found within secondary structures such as α-helics or β-sheets [315].

Asn deamidation was considered nothing more than a purification artifact until the 1960s, when Flatmark and colleagues demonstrated that Cytochrome C becomes deamidated *in vivo* [316] spontaneously and under physiologic conditions. They thus proposed Asn deamidation as a form of protein damage and a consequence of aging, and for the majority of the proteins it is still thought to be the case: organism can use this reaction has a timer of biological events and protein survival that can be genetically programmed to regulate biological events of various durations, simply by varying the amino acids that surround asparagine residues within proteins [307]. Interestingly, a comparison of the total number of amide-containing amino acids in long-lived and short-lived proteins demonstrated an inverse correlation between this number and the half-life of a protein [317], confirming again the "molecular clock function" of asparagine deamidation [318]. But how does this "aging signal" works? It is assumed that deamidation destabilizes the proteins by making them more susceptible to proteolytic degradation [319], and this susceptibility could be determined by a change in the protein structure, cellular location, or state of aggregation. Anyhow, although this function is well-founded, the observation that such an unstable amino acid as asparagine would not be so widely distributed in nature unless its deamidation had a beneficial role

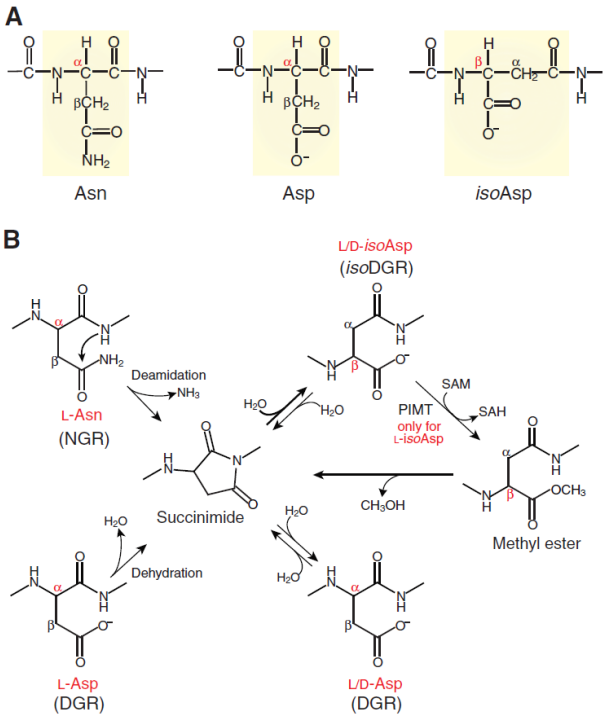

Figure 2.3.1: mechanism of spontaneous *iso*DGR formation by Asn deamidation or Asp isomerization. See the text for the detailed description of the reactions (From [6]).

[307] induced to think that certain proteins evolution may have chosen susceptible sequences in order to produce a remodeling of protein structure that serves a useful function: this is the case of Fibronectin, an extracellular matrix protein that has important roles in cell adhesion, migration, growth, and differentiation, which contains two highly conserved Asn-Gly-Arg (NGR) loops. Asn deamidation at the level of these NGR loops is capable to promote an integrin-mediated cell adhesion [320, 321], suggesting the NGR role as a molecular switch for the activation of latent integrin-binding sites.

Protein-l-isoaspartyl/d-aspartyl methyltransferase (PIMT), an ubiquitous cytosolic enzyme, partially repair deamidated and isomerized proteins catalyzing the conversion of *iso*Aspartate to Aspartate [312] in this way: enzymatic methylation of *iso*Asp sites by PIMT facilitates reformation of the cyclic succinimide intermediate, which immediately hydrolyzes spontaneously to a mixture of *iso*Asp and Asp again in a ratio of 3:1 (Figure 2.3.1). Although each cycle across this repair pathway is only 30% efficient, recycling of the generated *iso*Asp sites through the PIMT reaction results in an overall high repair efficiency; albeit repairing the isomerized Asp sites, in the case of Asn deamidation the repair is incomplete, since PIMT restores the normal peptide backbone but not the normal Asn side chain. Repair of *iso*Asp, which can restore the loss of biological function and require less energy compared to degradation and resynthesis of a new protein, has been demonstrated *in vitro* with synthetic *iso*Asp-containing peptides [322, 323] as well as with aged proteins [323]. PIMT is expressed in every organism from bacteria to humans, and in mammals PIMT levels are higher in brain and testes [324]: the findings suggest a key role of PIMT in these two organs, being both neurons and mature spermatozoa highly differentiated cells that may have special needs for damaged proteins repair. The same *iso*Asp-sensitivity of brain may play a pathological role also in human neurological diseases, ranging from childhood neurological disorders to age-related dementias: recent studies have indeed reported the formation of *iso*aspartate in age-associated neurodegenerative diseases, for example in brains of mice affected by prion disease [325]. Moreover, *iso*Asp have been found in Aβ peptide of senile plaques and Tau in NFT of AD [326], and expression of PIMT is up-regulated in AD brains compared to healthy brains. PIMT co-localize with NFT but not with senile plaques: an explanation of this different co-localization is that NFT localize intracellularly (where PIMT is present) while amyloid deposits accumulate in the extra cellular space where PIMT does not exist. Interestingly, it is observed that the site-specific deamidation/isomerization observed in the microtubule-binding domain of Tau (Asn381 and Asp387) induces a conformational change, by which the Tau protein can aggregate into NFT with an exceptional stability *in vivo* [326].

2.3.2 The NGR motif

Asparagine-Glycine-Arginine motif (NGR) confer to proteins and peptides a tumor targeting property, specifically binding aminopeptidase N (CD13) [327], a membrane-bound metallopeptidase that plays multiple functions in the regulation of various hormones and cytokines, protein degradation, antigen presentation, cell proliferation, cell migration, and angiogenesis [328]. Many cell types express CD13, including the endothelium of angiogenic blood vessels, tumor cells, pericytes, myeloid cells, antigen-presenting cells, keratinocytes and, in some cases, fibroblasts [329-331]. Noteworthy, CD13 is up-regulated in angiogenic blood vessels [327] but expressed at a very low level by the endothelium of normal blood vessels: NGR-containing peptides can hence target activated

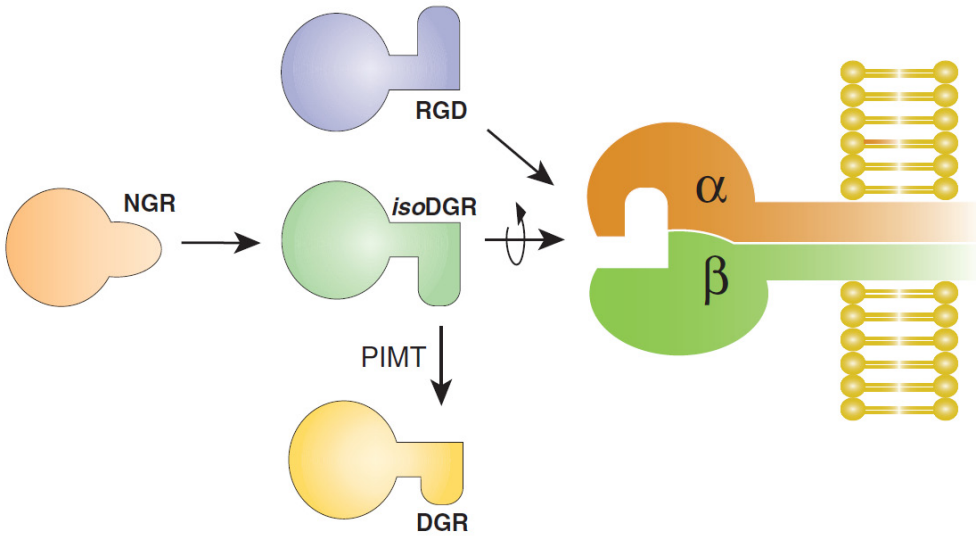

Figure 2.3.2: schematic representation of an isoDGR dependent molecular switch for integrin recognition. IsoDGR, derived from NGR's Asn deamidation, is able to interact with integrin RGD-binding pocket. IsoDGR can also be converted into DGR by PIMT enzyme, abolishing the acquired adhesive function (From [6]).

endothelial cells in tumors and in other physiologic or pathologic conditions as for example inflammation. Differentially immunoreactive forms of CD13 are expressed in tumor-associated blood vessels, myeloid cells and epithelia [330], and it's possible that the selectivity of NGR peptides for endothelial CD13 is related to differential glycosylation or conformational changes caused by complex formation with unknown compounds. The tumor-targeting property of NGR suggest its use as a carrier for the targeting of molecules to the neovasculature of tumors: various compounds and particles have been coupled or added synthetically to NGR peptides [332, 333] in order to increase their neovasculature-homing attributes, including cytotoxic drugs, cytokines and antiangiogenic compounds. Coupling CNGRC to the N-terminus of tumor necrosis factor (TNF), a cytokine endowed with potent vascular damaging properties and antitumor activity, for example led to the generation of a new compound, named NGR-TNF, with improved antitumoral activity [332, 334].

In addition to this tumor-targeting function, NGR motif has another very important property, being able to rapidly convert to *iso*DGR by asparagine deamidation: this motif (that mimic the specular structure of the integrin-binding motif RGD) can recognize members of the RGD-dependent integrin family, such as αvβ3, αvβ5, αvβ6, αvβ8 and α5β1 integrins [335] (Figure 2.3.2). Considering the known effects of structural protein elements on the deamidation rate of Asn residues discussed in the previous chapter (that range Asn deamidation kinetics ranging from hours to years), only certain NGR sites with suitable accessibility, flexibility and side chain orientation are likely to undergo deamidation under physiological conditions and subsequently bind integrins, while others need a protein reorganization in order to undergo this reaction.

Interestingly, it has been shown that also DGR has a role in integrin recognition and cell adhesion [336]: fibroblast growth factor 2 (FGF2), a pro-angiogenic heparin-binding cytokine that contains two DGR sites, can bind to αvβ3 integrin promoting endothelial cell adhesion [337] after DGR's Asp isomerization.

The search for exact matches of vertebrate proteins with NGR in the SWISS-PROT database showed that 5.02% of proteins contain this motif, and although it is likely that most of these sites are not properly folded and sufficiently exposed for receptor interaction, it is tempting to speculate that at least some of them might play a role in cell adhesion: in effects, approximately 17% of proteins that are classified by the keyword 'adhesion' in vertebrate protein databanks contain NGR sites [338]. Frequency of the DGR motif in proteins classified as having a role in cell adhesion is also high [338] suggesting that DGR too can function as a latent integrin-binding site that is differentially activated dependent on its molecular context and the conditions.

Like for NGR, also DGR flanking residues and its microenvironment can affect the kinetics of Asp isomerization into *iso*DGR. Anyhow, the rate of Asp isomerization is generally slower than that of Asn deamidation in similar peptides [310].

Competitive binding experiments showed that *iso*DGR can inhibit the binding of RGD-containing ligands to bothαvβ3 and α5β1, suggesting that the binding site is located within the same RGD binding

pocket: NMR studies and docking experiments showed subsequently that cyclic *iso*DGR peptides favorably interacts with the RGD-binding site of αvβ3 in an inverted orientation. Asn/Asp flanking residues not only influence *iso*Asp formation, but, like RGD scaffold, determine the affinity and specificity of the interaction between the resulting *iso*DGR and different integrins [335]. *Iso*DGR, being a natural fit for the RGD-binding pocket of αvβ3 integrin, supports the hypothesis that both NGR and DGR can work as "molecular timers" for generating integrin-binding sites in proteins. The rapid transition of NGR to *iso*DGR could have important implications in the biological properties of NGR-displaying phages and NGR-conjugates, but also for the physiologic or pathologic effect of NGR containing proteins, like fibronectin (Fn) and fibronectin fragments.

Four Fn modules, the first type II (Fn-II1), the fifth type I (Fn-I5), the seventh type I (Fn-I7) and the ninth type III (Fn-III9) repeats, contain NGR sequences. Full-length plasma fibronectin was shown to be considerably more resistant to Asn deamidation than short Fn fragments or peptides [339], suggesting that rapid deamidation of NGR in fibronectin requires proteolytic processing and/or conformational changes. On the contrary, NGR deamidation in the Fn-I5 fragment is very rapid (probably because Asn is followed by a Gly residue), with a half-life of the NGR site in cell culture medium of only ~4 hours [321].

The *iso*DGR-integrin interaction could exert different functions also in physiopathological mechansims: *iso*DGR peptides recognize αvβ3-integrin-positive endothelial cells in tumor vessels, inhibiting tumor growth when systemically administered to tumor-bearing mice [321, 335]. Given evidence that implicates αvβ3 integrin in angiogenesis [340], it is possible that the interaction of the *iso*DGR site in fibronectin fragments with αvβ3 integrin could have an important role in cancer and in other diseases that involve angiogenesis.

Clearly, all the possible functions described for Fn may be translated to other NGR-containing proteins which can activate latent integrin-recognition-sites in physiological or pathological condition, contributing to beneficial or unwanted/deleterious processes in various biological phenomena. Interestingly, ceruloplasmin sequence contains two NGR motifs: the first one (^{568}NGR) is exposed on the surface of the protein while the second (^{962}NGR motif), being buried inside the 3D structure of the protein, is less exposed and therefore less accessible to the solvent. Considered the rate of NGR frequency in vertebrate proteins seems plausible that, in Cp, a regulation of the deamidation of these two sites can be a mechanism able to give to the protein new properties that might participate to patho-physiological phenomena.

3 Results

3.1 Ceruloplasmin Oxidation, a Feature of Parkinson's Disease CSF, Inhibits Ferroxidase Activity and Promotes Cellular Iron Retention

Stefano Olivieri, Antonio Conti, Sandro Iannaccone, Carlo V. Cannistraci, Alessandro Campanella, Marco Barbariga, Franca Codazzi Ilaria Pelizzoni Giuseppe Magnani, Mariasabina Pesca, Diego Franciotta, Stefano F. Cappa, and Massimo Alessio

The Journal of Neuroscience, December 14, 2011 • 31(50):18568 –18577

3.1.1 Ceruloplasmin shows differing isoform patterns in PD

Cp expression was analyzed by SDS-PAGE and WB on CSF proteins. Immunoblots indicated that, once normalized for total proteins, the PD Cp expression level did not vary from that of control subjects (CN) (Figure 3.1.1) and thus confirmed data already reported [341]. As examined under 2DE, CSF Cp showed several isoforms with distinct isoelectric points (pI) and a relative molecular mass of 150 kDa; the distribution of said points differed between PD and CN (Figure 3.1.2A).

To analyze Cp patterns, we used a constant pI threshold (pH 5.6) to divide the profile into two distinct areas: region A and region B (Figure 3.1.2A). Analysis of the respective distribution of the signal to the two regions, each distribution being evaluated as a percentage of the total Cp signal, showed significantly higher values (t test, p< 0.0001) in the acidic region A for PD than for CN patients (Figure 3.1.2B). This represents the fraction of total Cp that is modified in the CSF of PD patients. The distribution of Cp signal in the two regions was investigated by means of ROC curve analysis, which showed a PD versus CN area under the curve of 0.919 (p= 0.00012) (Figure 3.1.2A). Application of a signal cutoff value in region A>46.02% enabled discrimination of PD from CN patients with a sensitivity of 71.4% and a specificity of 93.3% (likelihood ratio, 10.7). Interestingly, PD patients' clinical status (as UPDRS score, Table 5.1) and Cp acidification (signal in region A as percentage of total WB Cp signal) were found to

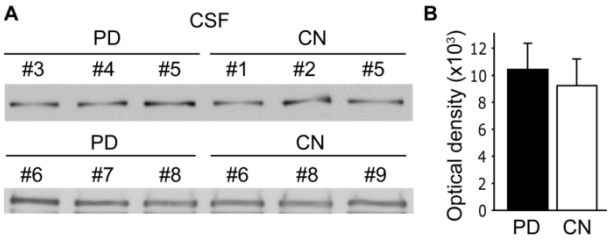

Figure 3.1.1: **A**) Cp expression levels in the CSF of control (CN) or Parkinson disease patients (PD) analyzed in western blot; **B**) quantification of Cp signal in panel **A**.

correlate (Pearson's correlation coefficient r=0.745; p= 0.0022) (Figure 3.1.3B). To understand whether Cp isoform acidification is a feature shared by other neurological pathologies, we analyzed the Cp pattern in CSF from patients affected by AD, ALS, and PN. Cp signal distribution enabled us to discriminate PD from the other neurological pathologies (t test: PD vs AD, p=0.0310; PD vs ALS, p=0.0119; PD vs PN, p=0.0022) (Figure 3.1.2A,B). The analysis also showed a difference between CN and, respectively, AD (p=0.0060) and ALS (p=0.0253), while no differences between CN and PN were observed (p>0.05) (Figure 3.1.2A,B). A statistically significant result was obtained even when the five independent groups were evaluated together by ANOVA test (p=0.0001). Postanalysis test was significant for PD versus CN (p<0.001) and PD versus PN (p<0.01) comparisons (Figure 3.1.2B). Collectively, these results suggest that the Cp present in PD CSF is affected by modifications that induce protein acidification, which in turn is

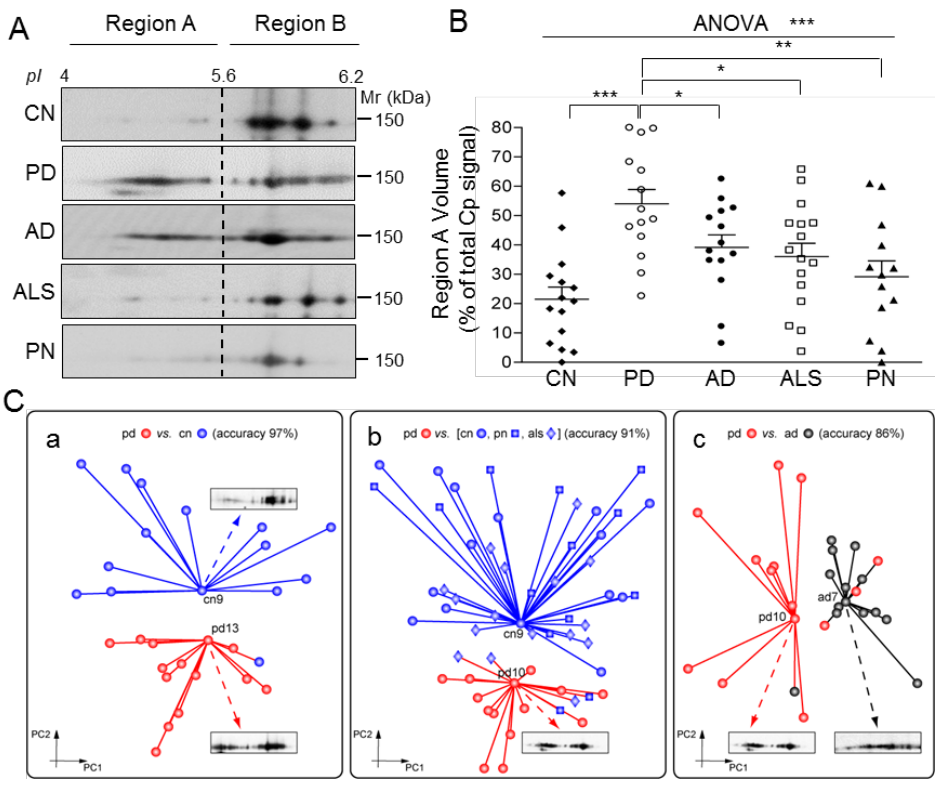

Figure 3.1.2: CSF Cp 2DE profile discriminates PD from AD, ALS, PN, and CN. ***A***, Representative results for WB analysis performed with anti-Cp on 2DE-resolved proteins. On the basis of pI threshold value, Cp signal distribution was divided into two distinct areas, regions A and B. ***B***, Analysis of WB signal optical density value distribution in region A, evaluated as a percentage of the total Cp signal. Data were analyzed both by Student's t test and by ANOVA. Single patient distributions as well as means and SE are shown (PD, n=14; CN, n=15; AD, n=14; ALS, n=16; PN, n=13) (*p<0.05; **p<0.005; ***p<0.001). **C**, Unsupervised cluster identification discriminates Cp pattern of PD patients from other groups. Dimensionality reduction of the anti-Cp WB images data set executed by principal component analysis (the first two principal components, PC1 and PC2, are shown), and clusters of homogeneous subjects were identified by unsupervised minimum curvilinear affinity propagation clustering analysis. Red clusters are for PD attribution, and blue and black clusters for non-PD attribution. Markers associated with sample names indicate the exemplars for the respective cluster. An original 2DE-WB image is displayed for each exemplar. **a**, Clustering of PD and CN. Sample cn13 proved to be misclassified. **b**, Clustering of PD, CN, PN, and ALS subjects. Five of 58 samples were misclassified, from left to right, als7, als5, pn4, als10, pn6. **c**, Clustering of PD and AD patients. Four of 28 samples proved to be misclassified (from left to right, ad8, pd13, pd14, pd11).

underlined by signal accumulation in the acidic region A.

3.1.2 Unsupervised analysis uncovers a discriminative pattern for Cp in PD patients

We applied a fully unsupervised automatic computational classification method; by means of unsupervised machine learning applied to the image pixels, this classification offers dimensionality reduction, feature selection, and clustering of the 2DE anti-Cp WB map data set. Dimensionality reduction allowed the display of images in a new two-dimensional projection space, within which cluster analysis identified two groups, one corresponding to CN and the other to PD (Figure 3.1.2Ca, dark gray and light gray clusters, respectively). This identification confirms that Cp pattern is able to distinguish PD from CN (accuracy, 96%), with the single exception of CN13. Moreover, MCAP clustering revealed two respectively representative exemplars (CN9 and PD13) for the given clusters (Figure 3.1.2Ca). The WB map for the cluster exemplars provides an explanatory comparison between prototypes of the two states (Figure 3.1.2Ca). Similarly, Cp pattern is able to distinguish the PD cluster from the cluster comprised of those CN, PN, and ALS subjects who proved to be homogeneous (Figure 3.1.2Cb); accuracy was 91%, with 5 of 58 subjects misclassified (ALS 5, 7, 10, and PN4, 6). When analyzed together with other groups, AD patients failed to be homogeneously distributed in a single cluster and thus obstructed unsupervised analysis. Interestingly, when directly compared, AD and PD groups were 86% accurately recognized by unsupervised Cp pattern analysis (Figure 3.1.2Cc) (4 of 28 subjects misclassified; AD 8 and PD 11, 13, 14). Comparison of the WB maps corresponding to the

cluster exemplars (Figure 3.1.2Cc, PD 10 and AD 17) shows that, of the two prototypal states, AD Cp undergoes lesser modification.

3.1.3 *In vitro* oxidative stress induces Cp interconversion to acidic isoforms and an increase in CSF total protein carbonylation

It has been shown that, because of its interaction with metal cofactors, Cp is sensitive to oxidative stress [182]. We accordingly hypothesized that the oxidative stress affecting CNS in PD patients might induce sufficient protein modifications to change pI. Given the hypothesis that Cp is a protein with a 5.5 days half-life [342], chronic exposure even to mild oxidative conditions may result in extensive oxidative modifications. To confirm this hypothesis, we induced *in vitro* oxidative stress on CN CSF, and we analyzed the resulting Cp pattern. It is known that, in *in vivo* experiments, an increase in H_2O_2 concentration correlates with an increase in ROS concentration [343]; we accordingly used a high H_2O_2 concentration treatment to mimic the prolonged exposure of the Cp to an oxidative environment. We observed that increased H_2O_2 concentration led to proportional shifts in Cp isoforms to the acid region (Figure 3.1.4A). Oxidation also induced the progressive generation of two Cp products, amounting to ~120 and 80–100 kDa, respectively (Figure 3.1.4A, indicated by arrows). These products were probably degradation fragments, as previously reported [181]. Interestingly, the 120 kDa product was detectable in most (10 out 14) PD patients (Figure 3.1.2A). The CSF Cp pattern obtained by oxidative treatment was similar to that observed in PD patients, a finding that suggests that changes might be due to oxidative modifications. Among several modifications induced by oxidative stress, one of the most common is protein carbonylation [344], and we accordingly analyzed this modification in CSF. Metal-catalyzed oxidation induced by treatments with high concentration of ascorbate, both with and without $FeCl_3$, produced mild and strong carbonylation, respectively [see OxyBlot assay manufacturer indications and the study by Musci et al. [184]], and resulted in a proportional increase in OxyBlot reactivity (Figure 3.1.4B). Subsequently to these treatments, the Cp 2DE pattern showed a shift to

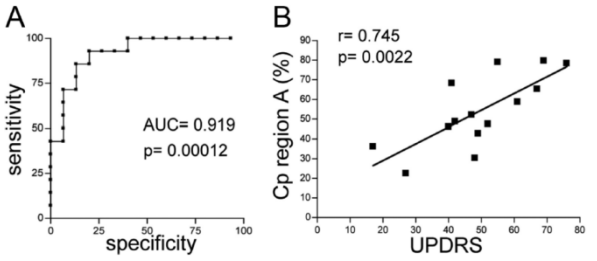

Figure 3.1.3: Cp pattern acidification discriminates healthy subjects and correlates with Parkinson's disease grading. **A**, The ROC curve was used to define the ability of the assay to discriminate between PD and CN groups, and to define the threshold value at which OD gave the best ratio between sensitivity and specificity. PD versus CN showed an area under the curve (AUC) of 0.919 with p=0.00012. A signal cutoff value in region A>46.02% enabled discrimination of PD from CN patients with a sensitivity of 71.4% and a specificity of 93.3%. **B**, Correlation analysis was evaluated as Pearson's coefficient (r) between Cp signal in region A (as a percentage of total WB Cp signal) and PD clinical status (as UPDRS score) for each patient. UPDRS and Cp signal in region A values passed the normality test for Gaussian distribution as assessed by Kolmogorov–Smirnov test. Correlation showed a coefficient *r*=0.745 with p=0.0022.

Figure 3.1.4: *In vitro* oxidative stress induces Cp to convert to acidic isoforms and total CSF protein carbonylation to increase. *A*,WB analysis of Cp profile in the CSF from a representative CN subject resolved by 2DE under resting conditions or after treatment with increasing amounts of H_2O_2 (1, 5, 10 mM); percentages indicate the amount of total Cp signal present in regions A and B (Figure 3.1.1); the arrows indicate low-molecular-weight products generated by protein oxidation. *B*, Detection of protein carbonylation by OxyBlot assay on total CSF proteins resolved by SDS-PAGE and stained for carbonyl groups, under resting conditions or after oxidation obtained by treatment with Asc with or without ferrous chloride ($FeCl_3$). *C*,WB analysis of 2DE Cp profile in the CSF under resting conditions or after oxidation treatments as in *B*; percentages indicate total Cp signal present in regions A and B (Figure 3.1.2).

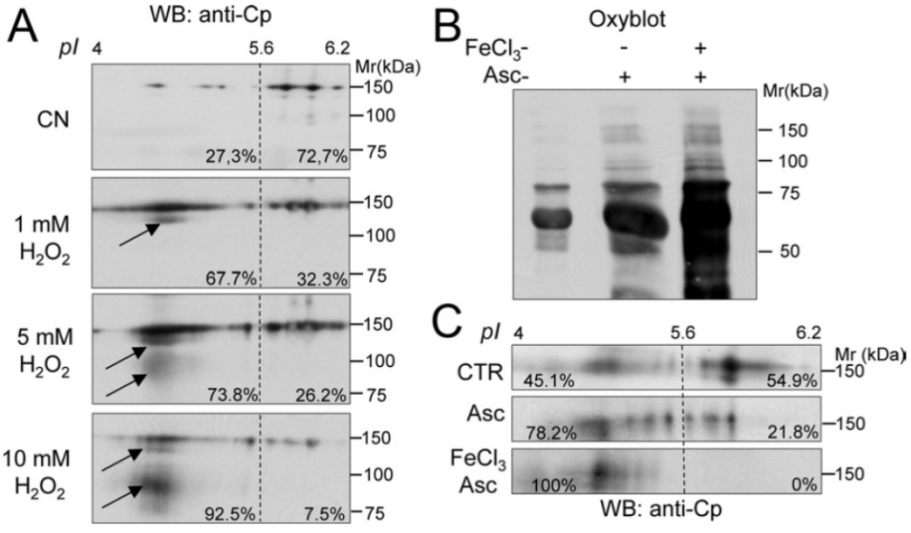

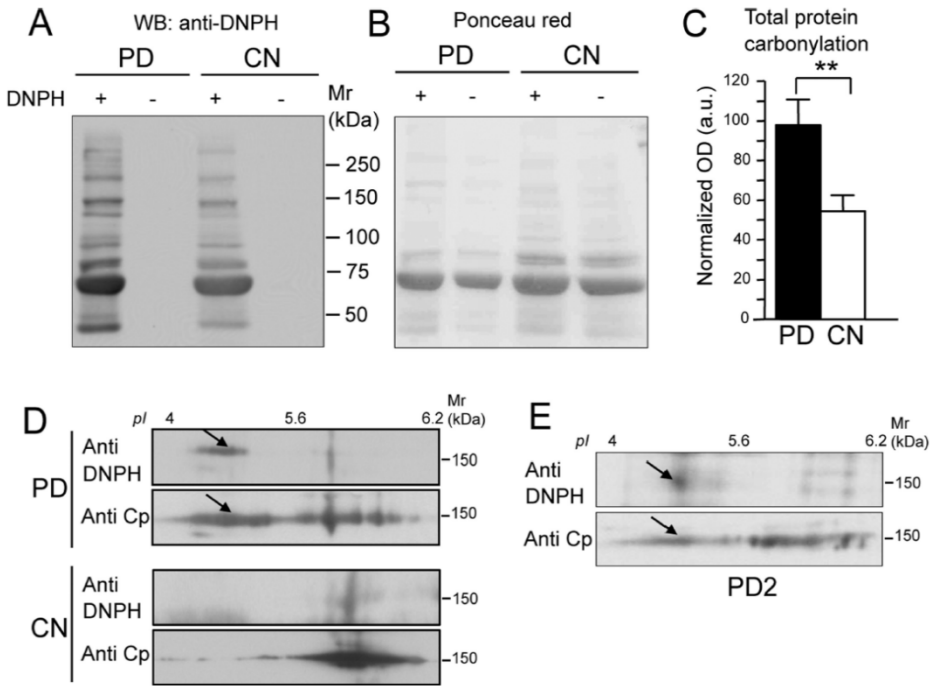

Figure 3.1.5: CSF total protein carbonylation is increased in PD patients and Cp is a carbonylation target. **A**, Representative gel of OxyBlot assay for carbonyl group detection. CSF total proteins from PD patients and healthy subjects (CN) were resolved by SDS-PAGE either after derivatization with DNPH (+) or without derivatization (-), and analyzed by WB with anti-DNPH for carbonylation detection. **B**, Ponceau red staining of the nitrocellulose used for OxyBlot assay shows that proteins were loaded in equal amounts. **C**, Evaluation of total protein carbonylation detected in the CSF of PD patients (n=14) and CN subjects (n=15): the y-axis indicates OxyBlot signal OD values (in arbitrary units) normalized by total protein loading. Data were analyzed by Student's t test; means with SE are indicated (**p<0.005). **D**, CSF proteins from both the PD patient pool and the CN subject pool were resolved by 2DE after derivatization with DNPH. Carbonylation was revealed with anti-DNPH antibody, and the same nitrocellulose membrane was further stained with anti-Cp to detect signal colocalization. **E**, The same analysis as in **D**, performed on a single PD patient (PD2), from whom greater amounts of CSF had by chance been collected showed identical results. The arrows indicate the colocalization of carbonylated spots with Cp acidic spots.

region A that was proportional to the degree of carbonylation (Figure 3.1.4B, C). Albeit at different levels, these changes were similar to those obtained with H_2O_2 treatment (Figure 3.1.4A, C) and hence suggest that protein oxidation contributes to Cp isoform changes.

3.1.4 CSF total protein carbonylation increase in PD patients

Analysis of total protein carbonylation in the CSF obtained from PD patients showed a significantly greater level than that of control subjects (p=0.0015) (Figure 3.1.5A, C). This suggests that CSF proteins undergo oxidative modifications during the course of PD pathological events. However, in contrast with Cp 2DE shift, no correlations were observed between severity of disease and CSF total protein carbonylation levels. This finding is plausible, given the diversity of the parameters that we tracked: on the one hand, electrophoretic mobility changes in single/individual Cp proteins, as possibly induced by several, differing forms of modification; on the other hand, specific changes in carbonylation levels as evaluated in total CSF proteins as a collective whole.

3.1.5 Cp carbonylation occurs in PD patients, and modified Cp corresponds to acidic isoforms

OxyBlot analysis, performed on 2DE-resolved CSF proteins from both the pool of PD patients and the pool of CN subjects, followed by staining on the same nitrocellulose for Cp expression, showed that the Cp present in PD CSF was carbonylated (Figure 3.1.5D). Moreover, the carbonylation signal was found to correspond mainly with more acidic Cp isoform, a feature that did not appear in the CN subjects (Figure 3.1.5D, see arrows). This analysis was restricted to the pooled samples due to the limited amount of samples available. However, the same analysis performed on a single PD patient (PD2), from whom we had by chance collected a larger amount of CSF, showed the same results (Figure 3.1.5E). Carbonylation converts side chains of many amino acids to reactive aldehyde and ketone groups, and thus may causes loss of positive charges, which in turn results in protein acidification. For this reason, it is conceivable that oxidative stress-induced Cp carbonylation might contribute to the isoform switch observed both *in vitro* and in PD patients. However, the complexity of the Cp 2DE pattern observed indicates that the oxidation-induced changes involved multiple target sites and varying events (e.g., methionine and cysteine oxidation, asparagine deamidation, glucidic moiety modifications, etc.). In particular, the shift to acidic pI values may have resulted from the formation

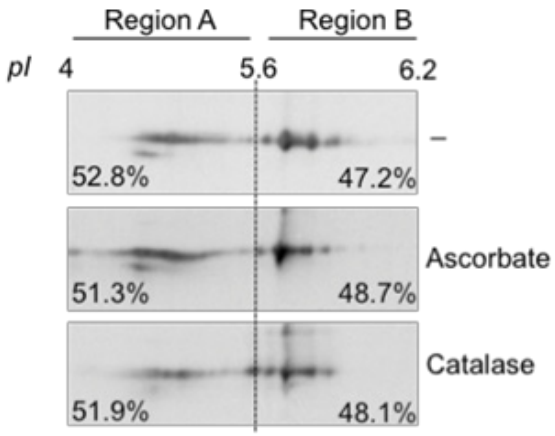

Figure 3.1.6: The oxidative modifications that triggered Cp acidification in PD patients were irreversible. CSF from PD (15 µg of total proteins) was separately incubated with the antioxidant 200 µM ascorbate (2 hrs at 25°C under shaking conditions, 600 rpm) or the catalase enzyme (Sigma C30, 65 units; 16 min at 25°C under shaking conditions, 600 rpm). (-): untreated condition.

of sulfinic acid on some of the 15 cysteine residues present in Cp. These alterations are now under investigation. Moreover, the oxidative modifications that triggered Cp acidification in PD patients were irreversible, since neither antioxidant (200 µM ascorbate) nor catalase treatment reverted the isoform switch (Figure 3.1.6).

3.1.6 Oxidation decreases Cp ferroxidase activity

The literature reports a reduced level of ferroxidase activity in PD CSF [345, 346], and it is noteworthy that CSF ferroxidase activity mainly corresponds to Cp activity [7, 347]. To investigate the connection between oxidative modifications and Cp function, we analyzed the ferroxidase activity of purified Cp. We observed that a reduction in ferroxidase activity correlated with increases in H_2O_2 concentrations (Figure 3.1.7A). Apparently, ferroxidase activity inhibition was not complete (Figure 3.1.7A), as a result of the interference of the copper (Cu) atoms released by Cp during denaturation by oxidative treatment with the Btp assay [348]. As already reported, Cp heat denaturation leads to Cu release [182], and under this condition we obtained ferroxidase activity profiles that closely resemble those obtained with strong protein oxidation (Figure 3.1.7B). A similar decrease in iron detection was observed in an assay that used a mere 20 nM Cu, a concentration that equates to the Cu concentration releasable after denaturation of the total amount of Cp used in our assay (Figure 3.1.7B). These results indicate that Cp oxidation impairs ferroxidase activity; as reported [184], this impairment induces structural changes that lead in turn to the release of Cp coordinated Cu atoms, which are necessary for enzymatic activity.

3.1.7 Extracellular oxidized Cp favors intracellular iron accumulation

Impairment of the extracellular ferroxidase activity of GPI-bound membrane Cp has been reported to block iron efflux from cells by downmodulation of Fpn, a membrane ferrous iron transporter [8, 174], with the ensuing increase of intracellular iron accumulation. We investigated whether similar iron retention might be induced by nonfunctional soluble Cp in dopamine hydroxylase-positive cells that do not express membrane GPI-Cp.

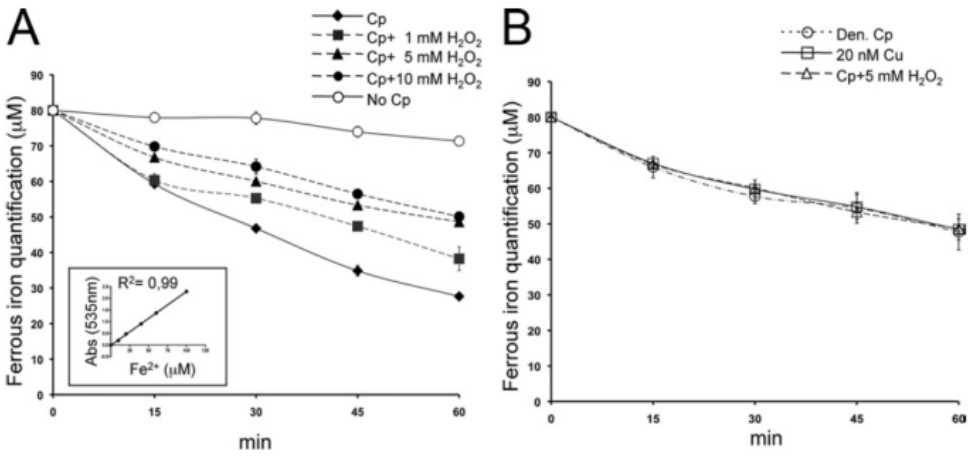

Figure 3.1.7: Oxidation decreases Cp ferroxidase activity. **A**, Ferroxidase activity was analyzed by Btp assay. Purified Cp (1.25 µg) was incubated with 60µM $FeCl_3$ (ferrous form) and analyzed at five different times (0, 15, 30, 45, 60 min) with a solution of 1 mM Btp. The decrease in absorbance at 535 nm of Btp-Fe^{2+} complex is due to ferrous iron oxidation into ferric form (Fe^{3+}). Ferroxidase activity was also analyzed after oxidation by H_2O_2 treatments (1, 5, 10 mM). By way of control, the assay was performed in the presence of buffer alone (No Cp). Means with SE are indicated (n=5). The inset shows linear regression of the Btp- Fe^{2+} complex optical density at 535 nm with different Fe^{2+} micromolar concentrations.**B**, Btp assay performed with Cp after 50 mM H_2O_2 treatments, with heat-denatured Cp (Den Cp), and with buffer alone containing 20 nM Cu^{2+}, the concentration reached by the Cu released from 1.25 µg of denatured Cp.

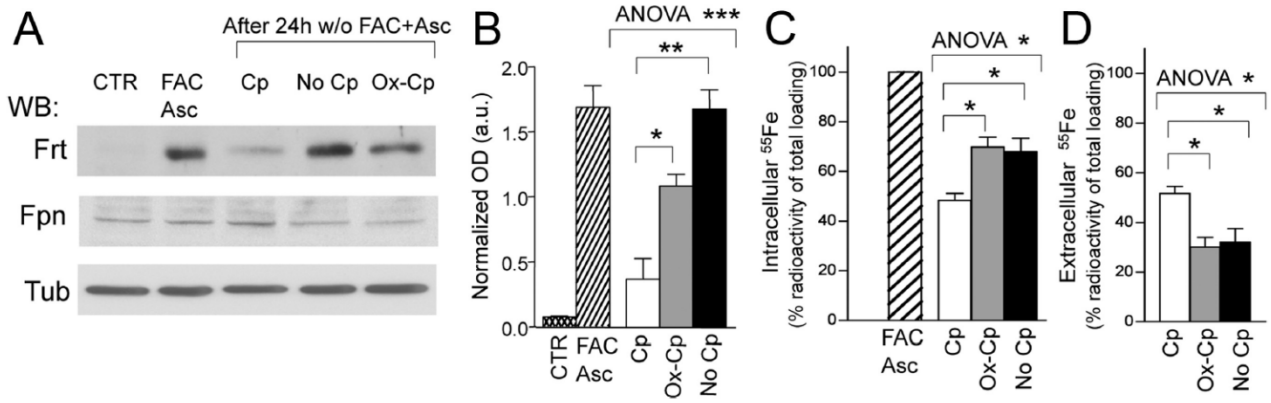

Figure 3.1.8: Extracellular oxidized Cp favors intracellular iron accumulation. **A**, SH-SY5Y neuroblastoma cells maintained in medium supplemented with 10% FBS (CTR) were iron loaded by treatment (20 h) with FAC (100μM) and Asc (200 μM). Extracellular iron and ascorbate were subseque ntly removed (w/o FAC+Asc) and cells further incubated (24 h) in the medium alone without serum (No Cp) or in the presence either of functional Cp (5 μg/ml) or of inactive oxidized Cp (Ox-Cp). Cell lysates resolved by SDS-PAGE were used for WB performed with anti-Ferritin (Frt) and anti-Ferroportin (Fpn); reactivity of anti-β-tubulin (Tub) was used for signal normalization. **B**, Analysis of Ferritin OD normalized signals (in arbitrary units) in treated SH-SY5Y. **C**, Evaluation of Fe retained in the cells. SH-SY5Y cells were iron loaded as previously described but with 95μM FAC supplemented with ^{55}Fe citrate (5 μM) as a tracer. After 20 h incubation, the cells were washed, and one aliquot (2x10 5 cells/well, in triplicate) was kept for 100% iron-loading evaluation (FAC), while other aliquots were further incubated (24 h) in serum-free medium alone (No Cp), or in the presence either of functional Cp or of inactive oxidized Cp (Ox-Cp). Cells were then washed, lysed, and counted. Radioactive counts per minute in each well (in triplicate for each condition) were normalized on the basis of total protein contents and used to evaluate the differences in percentages of total intracellular iron contents. **D**, Evaluation of Fe released by the cells. Spent media after 24 h incubation in serum-free medium alone (No Cp), or in the presence either of functional Cp or of inactive oxidized Cp (Ox-Cp), were collected and counted. Radioactive counts per minute of medium from each well (in triplicate for each condition) were used for the calculation of percentages of iron released from total intracellular iron loading. Data in **B–D** were analyzed by both unpaired ANOVA and Student's t test; respective means with SE of five (**B**) and three (**C, D**) independent experiments are indicated (p values: *p<0.05; **p<0.005; ***p<0.0001).

The SH-SY5Y neuroblastoma cell line was iron loaded by treatment with ferrous ammonium citrate (FAC) and with Asc in the presence of serum, and duly demonstrated the upregulation of the Fe storage protein ferritin (Figure 3.1.8A, B); extracellular iron was subsequently removed, and cells were further incubated in the medium alone (without serum), or in the presence either of functional Cp, or of oxidized Cp. In the presence of functional Cp, we observed a decrease of ferritin expression (Figure 3.1.8A, B), which, in turn, indicates functional Fe^{2+} exportation from cells. In contrast, the absence of extracellular ferroxidase activity (absence of Cp or presence of Ox-Cp) witnessed high ferritin levels (p=0.0040 and p=0.0173, respectively), which suggests a impairment in iron efflux from cells (Figure 3.1.8A, B). A similar conclusion was inferred from the direct evaluation of the radioactive Fe released into the medium or retained in the cells. Both in the absence of Cp and in the presence of Ox-Cp, cells showed, in comparison with functional Cp, a 13–23% increase in iron retention (Figure 3.1.8C), and a corresponding reduction in Fe^{2+} export that ranged from 26.5 to 46.9% (Figure 3.1.8D) (Cp vs No Cp, p=0.0325; Cp vs Ox-Cp, p=0.0112; Student's t test). The reduced iron efflux was not paralleled by a statistically significant down modulation in Fpn expression level as assessed by WB, even though a trend of expression decrease was observed in the absence of extracellular ferroxidase activity (Figure 3.1.8A, No Cp and Ox-Cp). To evaluate whether Cp contribution to pathological mechanism is effective in primary cells, which proved to be more sensitive to intracellular iron accumulation than did the cell line model [349], we also tested Cp functionality on iron homeostasis in rat primary neuronal culture. This culture produced ferritin expression results that resemble those acquired with the dopaminergic cell line, a finding that in turn implies intracellular iron retention. The iron load, induced by treatment with FAC and Asc, promoted an upregulation of ferritin (Figure 3.1.7A, B). After iron removal, the neurons were maintained for 24 h in medium with low serum (1.25% derived from the presence of neuron culture conditioned medium) in the absence (No Cp) or in the presence of functional (Cp) or oxidized (Ox-Cp) ceruloplasmin. A significant reduction of ferritin expression was observed only in the presence of extracellular functional Cp (p=0.0303, Mann–Whitney test), while neither Ox-Cp nor No-Cp conditions were able to promote iron export (Figure 3.1.9A, B). The decrease in ferritin expression in the presence of extracellular functional Cp was significant compared with neuron invariability observed in the presence of Ox-Cp

(p=0.0041, Mann–Whitney test) (Figure 3.1.9A, B). The high variability observed with primary culture in multiple experiments (n=5) might be due to the residual ferroxidase activity in the serum. Similar results, albeit with lower differences, were obtained when primary cultures after FAC loading were kept only 6 h under treatment conditions in the presence of low serum to exclude a putative role of neuronal suffering during the treatment.

We ruled out the hypothesis that astrocyte expressed GPI-Cp plays a role in the cocultures because astrocyte levels in the cultures were very low, as evaluated by anti-GFPA/ anti-βIII-tubulin reactivity ratio (range, 0.013-0.011). This estimation excludes also a contribution of astrocytes in the ferritin signal obtained in hippocampal cultures. Moreover, in pure hippocampal astrocyte cultures, subjected to the same treatments, the ferritin levels and variations were almost undetectable. Since GPI-anchored Cp as expressed by astrocytes plays a major role in brain iron homeostasis, we investigated whether this Cp isoform might also be the target of pathological oxidative conditions. Pure primary rat astrocytes exposed to oxidative conditions compatible with cell survival (0.6mM H_2O_2) showed that the GPI-Cp 2DE pattern profile (which differs from its soluble Cp equivalent [350] had shifted to a more acidic pH (Figure 3.1.9C). This finding indicates that astrocyte-expressed membrane GPI-Cp undergoes oxidative modifications too.

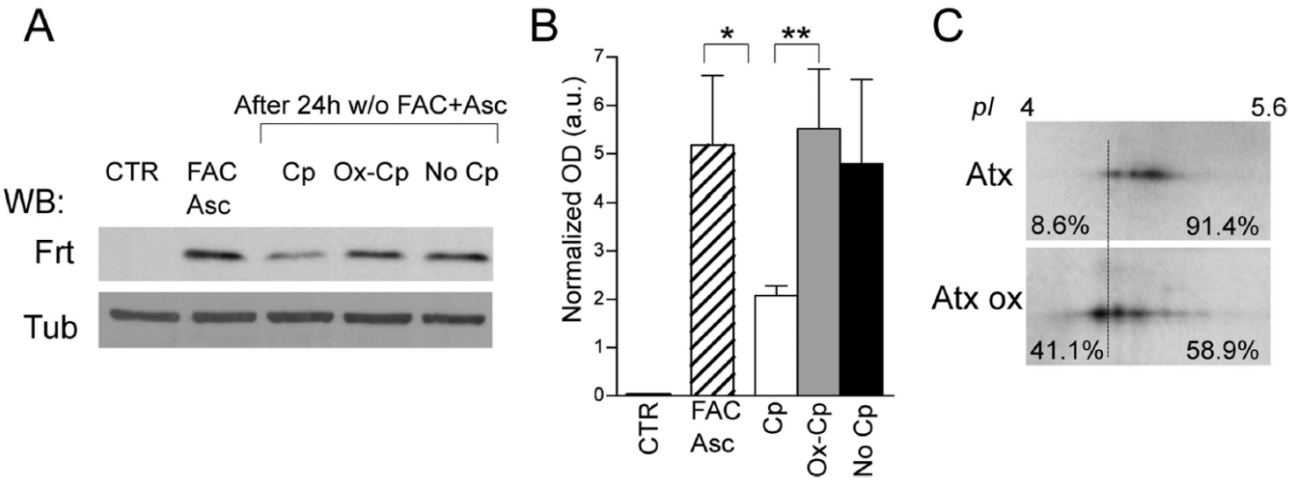

Figure 3.1.9: Extracellular oxidized Cp favors intracellular iron accumulation in primary neuron. **A**, Rat primary hippocampal neurons maintained in medium supplemented with 5% FBS (CTR) were iron loaded by treatment (20 h) with FAC (100 µM) and Asc (200 µM). Extracellular iron and ascorbate were subsequently removed (w/o FAC+Asc) and cells further incubated (24 h) in the medium with low serum (1.25% derived from the presence of neuronal culture conditioned medium) in the absence (No Cp) or in the presence either of functional Cp (5µg/ml) or of inactive oxidized Cp (Ox-Cp). Cell lysates resolved by SDS-PAGE were used for WB performed with anti-Ferritin (Frt); reactivity of anti-βIII-tubulin (Tub) was used for signal normalization. **B**, Analysis of Ferritin OD normalized signals (in arbitrary units) in rat primary hippocampal neuron culture. **C**, Membrane anchored GPI-Cp expressed by astrocytes undergo oxidative modifications. Pure primary rat astrocytes (Atx) were exposed to oxidation (1 h at 0.6 mM H_2O_2) (Atx ox), and GPI-Cp 2DE pattern profile was analyzed by 2DE and by WB performed with anti-Cp. Percentages indicate the amount of total Cp signal present in the regions defined by the threshold line. The data in B were analyzed by Mann–Whitney test; means with SE of five independent experiments are indicated (p values: *p<0.05; **p<0.005; ***p<0.0001).

3.2 Oxidation-induced structural changes of ceruloplasmin foster NGR-motifs deamidation that promote integrin binding and signalling

Marco Barbariga, Flavio Curnis, Andrea Spitaleri, Annapaola Andolfo, Chiara Zucchelli, Massimo Lazzaro, Giuseppe Magnani, Giovanna Musco, Angelo Corti, Massimo Alessio

J Biol Chem. 2013 Dec 23 (In Press).

3.2.1 Accelerated aging of Cp under oxidative conditions causes deamidation of NGR sites

Sequence analysis of purified Cp by tandem mass spectrometry (MS) showed that both ^{568}NGR and ^{962}NGR motifs were not deamidated (Figure 3.2.1A and B, Untreated) and that protein oxidation by incubation in 10 mM H_2O_2 at 37°C cannot convert NGR to DGR/isoDGR (Figure 3.2.1A and B, ox). In contrast, protein incubation in 100 mM ammonium bicarbonate (AmBic) or Ambic plus 10 mM H_2O_2, i.e., solutions that respectively mimic accelerated asparagine aging conditions (AmBic) [321] and accelerated asparagine aging under oxidative conditions (ox/AmBic), the ^{568}NGR motif was partially deamidated (Figure 3.2.1A). Interestingly, the ^{962}NGR motif was partially deamidated exclusively following Cp aging under oxidative conditions (Figure 3.2.1B, ox/AmBic). The presence of Asp (D) in place of Asn (N) in the AmBic-treated Cp indicate that a deamidation reaction occurred at the two NGR sites of Cp, although MS did not ascertain whether DGR or isoDGR isoform were present.

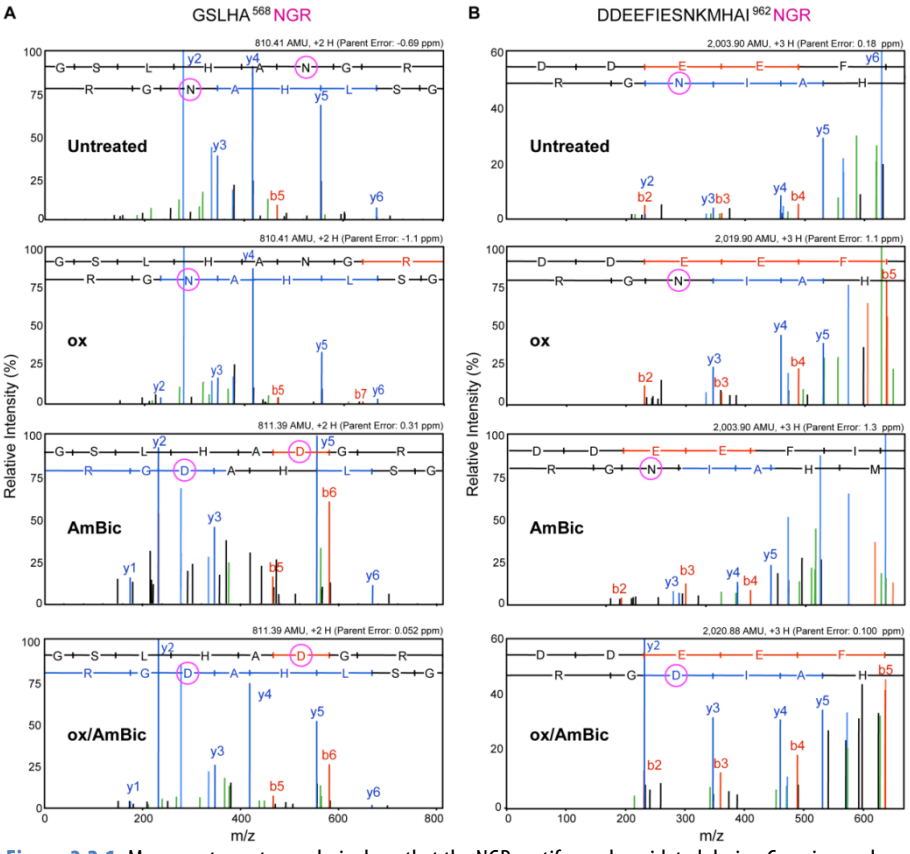

Figure 3.2.1: Mass spectrometry analysis show that the NGR motifs are deamidated during Cp aging under oxidative conditions. **A**) zoomed annotated ESI-MS/MS spectra of the peptide 563-570 derived from trypsin digestion of Cp upon different treatments: Untreated, resting conditions; ox, oxidation by Cp incubation in the presence of H2O2; AmBic, accelerated Asn aging by Cp incubation in the presence of Ammonium Bicarbonate buffer; ox/AmBic, mimicking accelerated Asn aging under oxidative conditions by Cp incubation in the presence of AmBic and H2O2. **B**) zoomed annotated ESI-MS/MS spectra of the peptide 948-964 derived from trypsin digestion of Cp upon different treatments as in A. Only principal fragmentation series (b and y) are indicated. The MW, the charge state and the error of the peptides are reported. Deamidation was inferred by sequencing the D amino acid corresponding to N+1Da increased molecular mass.

A possible explanation for the different behaviour of the ^{568}NGR and ^{962}NGR motifs may arise from analysis of the crystallographic Cp structure (PDB 2j5W) [351], which reveals that the ^{568}NGR motif is exposed

on the surface of the protein, while the ^{962}NGR motif is less exposed and therefore less accessible to the solvent (Figure 3.2.2A and B). The two sequences display differing tertiary contexts (Figure 3.2.2C and D) that might in turn influence deamidation rates differentially. We then attempted to clarify the structural differences between the two sequences by a computational approach. Molecular dynamics simulations on wild type Cp (PDB 2j5w) showed a relatively stable structure with large fluctuations of loop regions (Figure 3.2.2E). Notably, the root means square fluctuations, as calculated throughout the simulation, suggest that the two NGR sequences are more rigid than the other residues (Figure 3.2.2F). Importantly, the ^{568}NGR sequence is steadily accessible to the solvent throughout the simulation, while ^{962}NGR is buried inside the protein and is blocked in a stable conformation by polar interactions with neighbouring aminoacids (Figure 3.2.2C and D). Accordingly, we hypothesized that oxidation might affect the Cp-structure and promote the exposure of the ^{962}NGR motif, which in turn adopts a favorable conformation for deamidation. Indeed, it has been previously inferred that Cp structure is affected by oxidation [182, 184, 352, 353].

3.2.2 Cp oxidation induces secondary structure changes

Circular dichroism (CD) spectra obtained for purified Cp indicated that the secondary structure of Cp, which is principally composed of β-strands (45,5%, as evaluated by Uniprot tool, www.uniprot.org/uniprot/P00450), was partially affected by Cp-Ambic treatment (Figure 3.2.2G, black *vs.* blue lines); notably, large spectra changes occurred upon Cp-ox and -ox/AmBic treatment, suggesting structural alterations (Figure 3.2.2G, black *vs.* Green *vs.* orange lines). Interestingly, the spectra profile obtained with heat-denatured Cp (Figure 3.2.2G, red line), which showed a pronounced minimum towards random coil structure (~200 nm), differed from that of Cp obtained in -ox/AmBic conditions. These data suggest that Cp oxidation or accelerated Asn deamidation under oxidative conditions induce secondary structure changes but do not unfold the protein. Comparison of the protein melting temperatures (Tm) before and after the

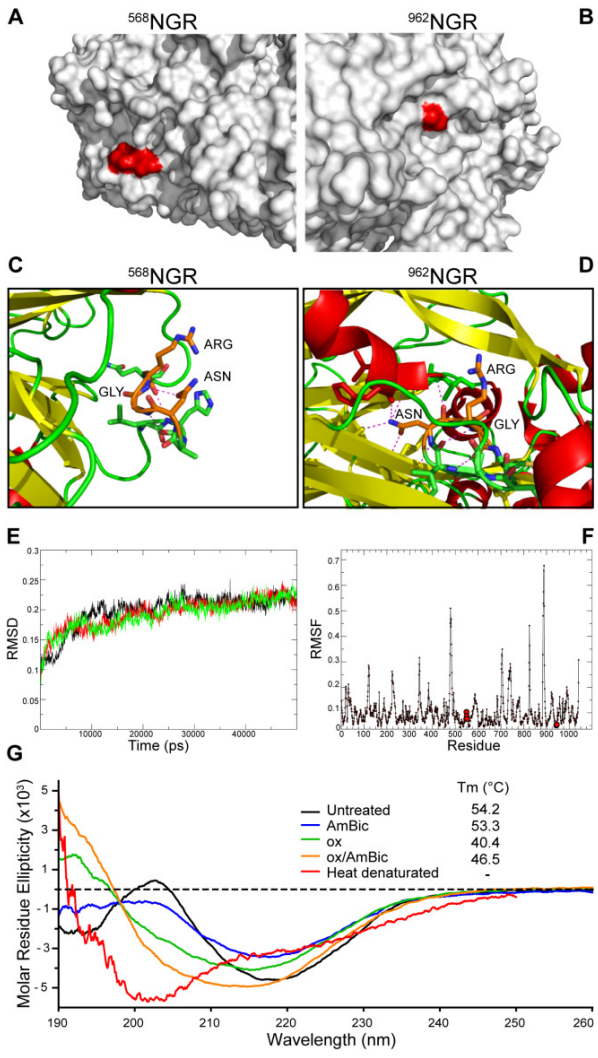

Figure 3.2.2: NGR-motifs structural analysis, Cp molecular dynamics modelling and circular dichroism analysis indicate that ^{962}NGR is buried inside Cp structure and that secondary structure changes induced by oxidative conditions might allow its surface exposure. **A** and **B**) Surface representation of Cp, in red are highlighted the ^{568}NGR and ^{962}NGR sequences, respectively, as calculated by the GROMACS g_sas tool on crystallographic Cp structure (PDB 2j5W). The higher solvent accessible surface of ^{568}NGR is represented by the larger size of the red coloured region. C and D) Cartoon representation of ^{568}NGR and ^{962}NGR sequences in Cp. The NGR aminoacids are shown in orange sticks. The hydrogen bonds are shown in red dashed lines. ^{568}NGR is engaged in short range polar interactions between GLY and ASN, whereas ^{962}NGR sequence is mostly involved in strong interactions with the rest of the protein. **E**) Cα root-mean square deviations (RMSD) from the initial Cp structure. The three different trajectories calculated by molecular dynamics modelling, shown in red, black and green, respectively, indicate a relatively stable structure. **F**) Cα root-mean square fluctuations (RMSF) of the concatenated molecular dynamics simulations (3x50 ns, 150 ns total simulation time). ^{568}NGR and ^{962}NGR are indicated with red circles. The plot shows large fluctuations localized in the loop regions, notably the two NGR sequences show a rigid behaviour, with low RMSF values along the whole simulation. **G**) Circular dichroism spectra of Cp after different treatments: resting conditions (Untreated, black line); accelerated Asn aging (AmBic, blue line); oxidation (ox, green line); accelerated Asn aging under oxidative conditions (ox/AmBic, orange line); and heat-denaturation (red line). Each spectrum was averaged using four accumulations collected in 0.1 nm wavelength intervals with an average time of 0.5 sec. The observed ellipticity (mdeg) was converted into molar residue ellipticity [θ] (deg cm2 dmol-1). For each treatment the melting temperature (Tm) is also indicated.

different treatments shows that oxidation induces the strongest destabilizing effect, as assessed by the decreased Tm after oxidation (Cp= 54.2°C; Cp-ox/AmBic= 46.5°C; Cp-ox= 40.4°C); in contrast, the AmBic treatment did not change the Cp thermostability (Cp-AmBic= 53.3°C) (Figure 3.2.2G).

3.2.3 Cp aged under oxidative conditions binds integrins

We investigated whether Cp's Asn accelerated aging under oxidative conditions, i.e. the condition that may occur in some neurodegenerative diseases, can induce integrin binding via isoDGR formation. *In vitro* binding assays to purified integrins showed negligible binding of untreated Cp, while after accelerated Asn aging in AmBic alone or in the presence of oxidative conditions (-ox/AmBic), Cp acquired clear binding properties to αvβ5, αvβ6, αvβ3 and αvβ8, albeit to differing degrees (Figure 3.2.3A). Of note, oxidation alone was ineffective. In the light of the observed additional increase in binding to αvβ6 of Cp aged under oxidative conditions, in comparison with Cp aged alone, and being the αvβ6 integrin expressed by the epithelial cells, this integrin was used for the further analysis. Interestingly, the -ox/AmBic treatment increased the binding to αvβ6 (Figure 3.2.3A), in a dose-dependent manner (Figure 3.2.3B). Competitive binding experiments, performed either with the isoDGR-peptide capable to bind the RGD binding pocket of integrins [335] or with the control ARA-peptide, showed that the isoDGR-peptide is able to abolish the binding of oxidized-aged Cp to the αvβ6 integrin (student's t-test, p<0.0001) (Figure 3.2.3C) supporting the role of Cp NGR-deamidation in the acquisition of binding activity after aging. The effect of Cp accelerated aging under oxidative conditions was also investigated by Western blot (WB) analysis. Untreated Cp showed a principal band of 150 kDa, as expected for a full-length protein (Figure 3.2.3D), whereas the treatment caused the appearance of an additional band >250 kDa. This data suggests that treatment may cause partial protein aggregation likely due to reactive succinimide intermediate reaction with amino-group present in neighboring Cp molecules [354]. Remarkably, both products, full-length Cp and aggregates, bind αvβ6 integrin (Figure 3.2.3D). Taken together, these results indicate that accelerated Asn aging under oxidative conditions promotes the Cp ability to bind integrins' RGD-binding pocket, presumably *via* NGR-to-isoDGR conversion.

3.2.4 Molecular dynamics simulations and docking calculations indicate that ^{568}isoDGR-Cp can interact with αvβ6 integrin

Our results indicated that the accelerated Asn aging under oxidative conditions leads to the deamidation of both ^{568}NGR and ^{962}NGR motifs in the Cp sequence. Computational approaches have been exploited to evaluate the possibility for deamidated Cp to bind αvβ6 integrin. However, the experimental evidences reported in Figure 3.2.2, suggest that the deamidation of ^{962}NGR in oxidative conditions causes a considerable structural re-arrangement, that cannot be predicted by computational methods. Thus, we decided to perform molecular dynamics simulation

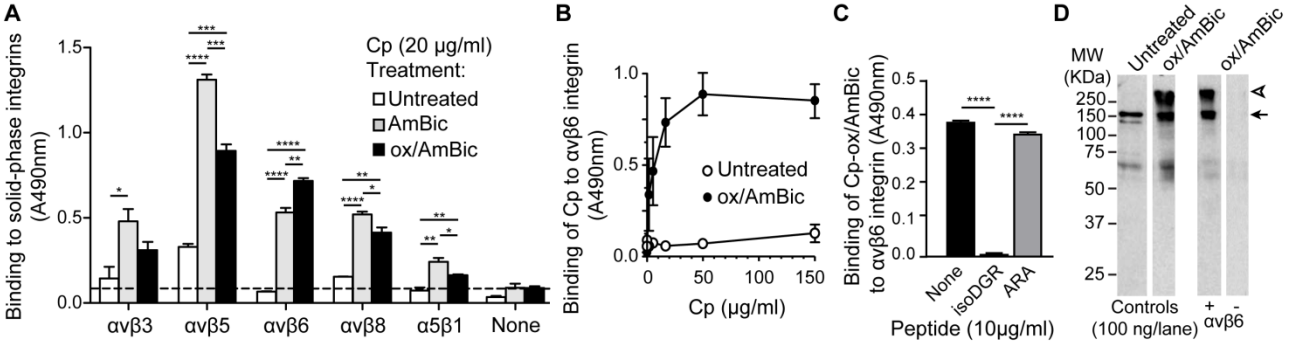

Figure 3.2.3: Cp aged under oxidative conditions is able to bind integrins via isoDGR-motifs. **A**) Screening by ELISA of the binding to several integrins of Cp under resting conditions (Untreated), after Asn accelerated aging (AmBic) or after Asn accelerated aging under oxidative conditions (ox/AmBic). **B**) Analysis of the dose-dependent binding to αvβ6 of untreated Cp or aged/oxidized-Cp (ox/AmBic). **C**) Competitive binding of aged/oxidized-Cp (Cp-ox/AmBic) to αvβ6 with the isoDGR-peptide and control ARA-peptide. **D**) Western blot analysis of the Cp-ox/AmBic compared to the untreated Cp (Controls) and of the Cp-ox/AmBic eluted from the ELISA microplate either coated (+) or non-coated (-) with αvβ6. All the assays were performed in triplicate for 3 independent experiments (n= 3). Statistical significance reported as p values was evaluated by student's t-test. ****=p<0.0001, ***=p<0.001, **=p<0.01, *=p<0.05.

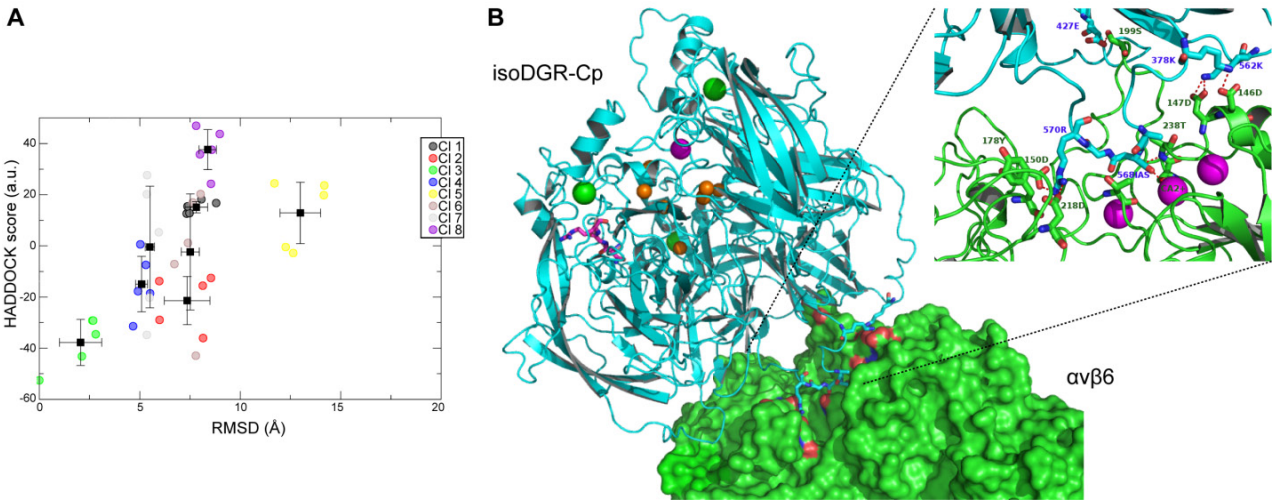

Figure 3.2.4: Molecular docking model of isoDGR-Cp/αvβ6 integrin binding site. **A**) HADDOCK scores versus RMSD from the lowest energy complex structure for docking run performed of Cp-αvβ6. Different Clusters are shown (circles) represented in different colors. They were obtained fitting the models on the backbone of the αvβ6-binding site and then calculating the RMSD values from the lowest energy solutions over the heavy atoms of the Cp protein. Structures belong to the same cluster if they differ by less than 2 Å in the pairwise RMSD matrix. The HADDOCK score corresponds to the weighted sum of different energy terms (van der Waals, electrostatic, and restraint energies). The cluster 3 is the best solution which is represented in panel B. **B**) HADDOCK model of isoDGR-Cp/αvβ6 integrin binding site. Surface representation of αvβ6 binding pocket (green) in complex with isoDGR-Cp (cyan cartoon). The side-chains of the residues forming stable interactions (as reported in text) are shown in licorice. Orange spheres correspond to Cu^{2+} ions; magenta sphere corresponds to Ca^{2+} cation; green spheres correspond to Na^{+} ions. Red dotted lines denote the hydrogen bonds of the Cp with αv and β6-subunits. In magenta licorice is shown the ^{962}NGR motif. The arginine of ^{568}isoDGR predominantly interacts with D^{150} of αv domain, whereas the same arginine can transiently interact with D^{218}. The isoaspartyl residue of isoDGR interacts with Ca^{2+} MIDAS ion located in the β6 domain (see zoomed area). Other interactions between ^{568}isoDGR-Cp and αvβ6 have been highlighted, in particular we noticed a strong and stable network of salt bridges between K^{562} and K^{369} of isoDGR-Cp and D^{146} and D^{147} of β6 domain of αvβ6 integrin (interaction reported in text).

only on ^{568}isoDGR-Cp protein in order to generate a set of reliable structures to be docked onto αvβ6.

Cluster analysis on the ^{568}isoDGR-Cp molecular dynamics allowed to extract a number of representative structures of the simulations. A bundle of 27 isoDGR structures, corresponding to the center of the clusters, were docked onto a bundle of 10 αvβ6 structures, which are the center of the clusters obtained from 10ns of molecular dynamics of the free αvβ6. To restrict the number of possible docked solutions, we defined a set of restrains (Cp-^{568}IAS: αvβ6-^{150}D, ^{218}D, ^{143}A, ^{184}P, ^{185}F, ^{238}T; Cp-^{569}G: αvβ6-^{150}D, ^{218}D, ^{143}A, ^{184}P, ^{185}F, ^{238}T; Cp-^{570}R: αvβ6-^{150}D, ^{218}D, ^{143}A, ^{184}P, ^{185}F, ^{238}T) corresponding to canonical RGD- or isoDGR-integrin binding site [355] as suggested from competition experiments. The docking calculations lead to different solutions (Figure 3.2.4A) whereby the cluster 3, representing the best solution, showed that the ^{568}isoDGR-Cp docked onto αvβ6 integrin recapitulates the classical RGD/isoDGR receptor interactions [355] and creates some additional interactions (αvβ6/Cp: ^{199}S β6/ ^{427}E, 1.7 ± 0.1Å; ^{178}Y αv/^{570}R, 2.1 ± 0.1Å; ^{146}D β6/^{378}K, 1.9 ± 0.3Å; ^{238}T β6/^{568}IAS, 1.9 ± 0.2Å; ^{150}D αv/^{570}R, 1.8 ± 0.2Å; ^{147}D β6/^{562}K, 1.9 ± 0.3Å) (Figure 3.2.4B).

3.2.5 Deamidated Cp mediates cellular adhesion and spreading

The binding to integrins observed *in vitro* might not reflect the real binding properties of deamidated Cp, given the possibility that adsorption of purified integrins on microtiter plates might alter their conformation. Furthermore, it has been previously shown that the isoDGR site of fibronectin but not its corresponding NGR site can promote cell adhesion [6, 321, 335, 355]. To assess whether Cp can generate an isoDGR motif able to recognize integrins in physiological conformations, we analyzed the effect of Cp aged under oxidative conditions on the adhesion of human epithelial (HaCaT), endothelial (E.A.hy926) and glioblastoma (T98G) cell lines. Preliminary flow cytometry analysis showed αvβ6-expression by HaCaT, αvβ3- and αvβ5- expression by EA.hy926 and αvβ8-expression by TG98.

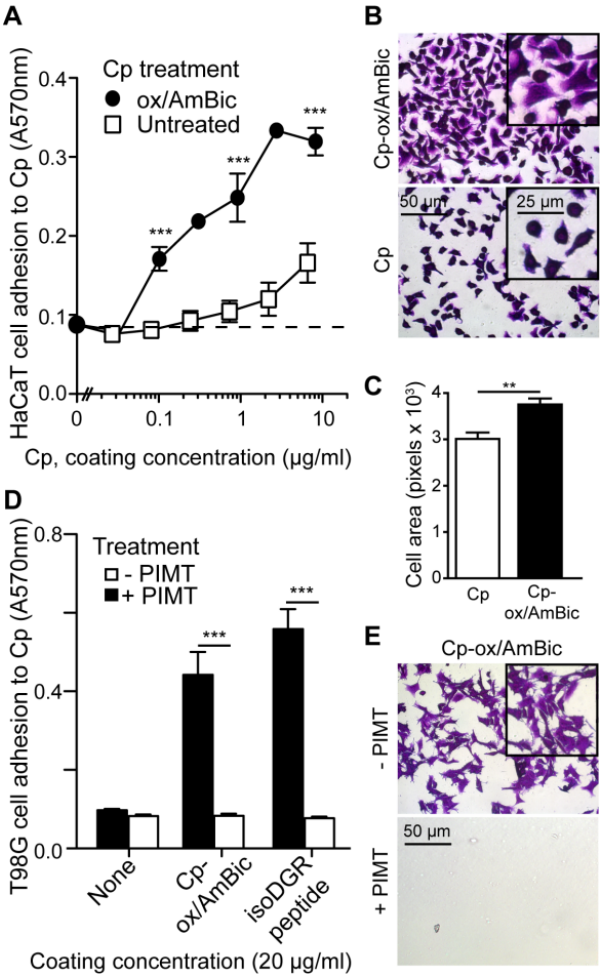

Figure 3.2.5: Cp deamidation mediate cells adhesion and spreading via isoDGR-integrins interaction. **A**) Adhesion of epithelial HaCat cells to plates coated with different concentrations of either Cp (Untreated) or aged/oxidized-Cp (ox/AmBic). Adhesion was evaluated as adsorbance at 570nm of the crystal violet stained cells. **B**) Microscopy images of stained cells adherent to Cp-ox/AmBic, untreated Cp or BSA-coated plates (None). Cell spreading is visible at higher magnification showed in the boxes. **C**) Cells spreading was evaluated as pixel area automatically detected by image software analysis. Statistical significance was evaluated on cells measurement in 3 different microscopy fields for each conditions (Cp, n= 112; Cp-ox/AmBic n=208), **p=0.0087. **D**) Adhesion of glioblastoma T98G cells to plastic coated either with BSA (None), aged/oxidized-Cp (ox/AmBic) or the isoDGR-peptide. Inhibition of cells adhesion occurred after treatment of coating proteins with PIMT (+) compared to the untreated wells (-). **E**) Microscopy images of stained cells adherent to ox/AmBic-Cp treated with (+) or without (-) PIMT enzyme. All the adhesion assays were performed in triplicate for 3 independent experiments (n= 3). Statistical significance reported as p values was evaluated by student's t-test; ***=p<0.0001.

Plates coated with ox/AmBic-Cp increased in a dose-dependent manner the adhesion and spreading of HaCaT cells, while untreated Cp induced little cell adhesion (Figure 3.2.5A and B). Cells spreading showed a cell's area significant increase (p=0.0087) of about 20% in HaCat cells adhering to ox/ambic-Cp coated plates compared to cells adhering to Cp (Figure 3.2.5C). Similar pro-adhesive effects were observed with glioblastoma (Figure 3.2.5D and E) and endothelial cell lines (Figure 3.2.6). To assess whether cell adhesion was mediated by isoDGR, we incubated ox/AmBic-treated Cp with PIMT (Protein-l-isoaspartyl/d-aspartyl methyltransferase), an enzyme that converts L-isoAsp residues to L-Asp [321, 356]. PIMT treatment almost completely inhibited the pro-adhesive activity of ox/AmBic-treated Cp and of isoDGR-peptide, the latter serving as a control (student's t-test, p<0.0001) (Figure 3.2.5D and E). These results suggest that isoAsp formation, presumably at NGR site(s) of Cp, is associated with a "gain of function" in cell adhesion assays.

3.2.6 Cp aged under oxidative conditions transduces intracellular signal through integrin engagement

Having observed that Cp after accelerated Asn aging under oxidative conditions was able to bind integrins expressed on the cell surface, we investigated whether this binding could also induce intracellular signalling. Signal transduction pathway analysis, as performed by reverse-phase protein arrays on epithelial cells, indicated that cells incubation with ox/AmBic-treated Cp can induce coordinated phosphorylation events that recapitulate many of the steps of classical integrin-mediated signal transduction. Hierarchical clustering analysis of the comparison of treatment with either ox/AmBic-Cp or untreated Cp revealed that after 30 minutes: 1) there was an increase in the phosphorylation of the

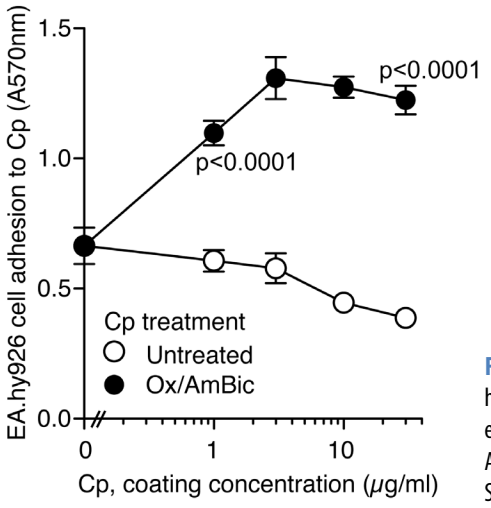

Figure 3.2.6 Deamidated Cp mediates cellular adhesion and spreading. Adhesion of human endothelial cells (EA.hy926) to plates coated with different concentrations of either Cp (Untreated) or Cp after accelerated aging under oxidative conditions (ox/AmBic). Adhesion was evaluated as wells adsorbance at 570nm of the crystal violet stained cells. Statistical significance is evaluated by student's t test.

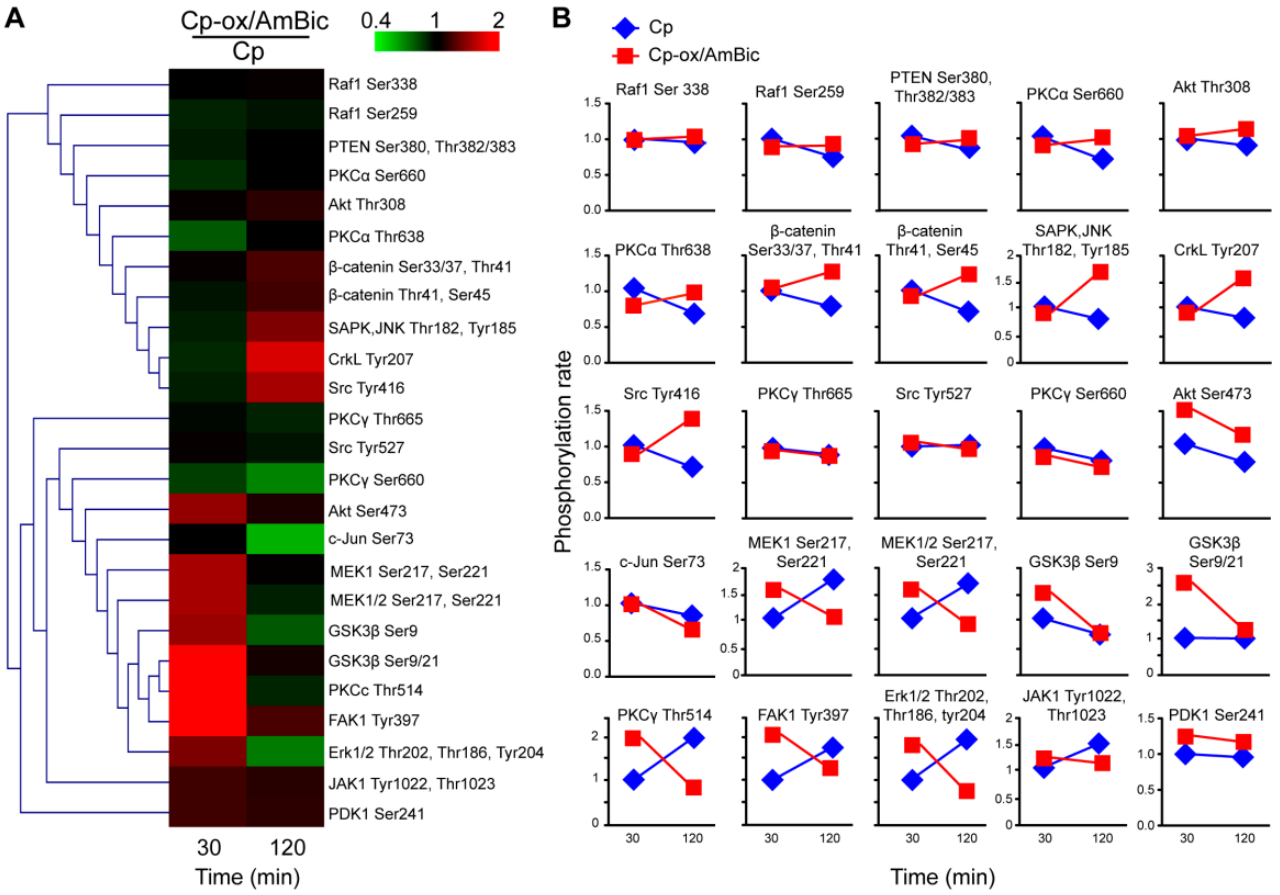

Figure 3.2.7: Phosphorylation rate analysis of proteins belonging to the integrins signalling pathway as consequence of epithelial cells treatment with aged/oxidized-Cp. **A**) Hierarchical clustering analysis of the reactivity of specific antibodies assessed by reverse phase protein arrays; the columns represent the rate of ox/AmBic-Cp *vs.* Cp at two different treatment time [(Cp-ox/AmBic)/Cp 30 and 120 minutes)], while the rows represent individual protein residue/s phosphorylation; the up- and down-regulated residue phosphorylation rate are respectively indicated in red and green. The intensity of colour increases as the rate differences increase, as shown in the bar. **B**) Expression profiles of clustered proteins. Y axes indicate the specific residue/s phosphorylation rate as normalized with the total protein expression and compared with the phosphorylation level of control conditions (Cp) at 30 minutes treatment; X axes indicate the two different time (30 and 120 minutes) of Cp (blue) and ox/AmBic-Cp (red) treatments.

activation residues of several molecules e.g. p-Tyr^{397}FAK1, p-Thr^{514}PKCγ, p-Ser$^{217/221}$MEK1, p-Thr$^{185/202}$Tyr^{204}ERK1/2, p-Ser^{241}PDK1, p-Ser^{473}Akt, and 2) the phosphorylation of inhibitory residues e.g p-Ser$^{9/21}$GSK3β which in turn maintain β-catenin activity by preventing its phosphorylation (Figure 3.2.7A and B). Several other proteins were unaffected (such as CrkI, SAPK/JNK, c-Jun and Raf1) or slightly inhibited (PTEN and PKCα) (Figure 3.2.7A and B). These results suggest that early signals mediated by deamidated-Cp mostly addressed gene activation regulation, cell cycle and MAPK signaling pathway (Figure 3.2.8). In contrast late signals (i.e. immediately after 120 minutes of treatment) seemed to sustain actin cytoskeleton rearrangement rather than cell survival, proliferation and MAPK pathway activation (Figure 3.2.8). Src and CrkL were activated, and the phosphorylation of FAK1 was inhibited, concomitantly with the slight phosphorylation of PTEN and Raf1 inhibitory molecules, which block MEK1 and ERK1/2 activation (Figure 3.2.7A and B; Figure 3.2.8). Similarly, Akt inactivation results in β-catenin inhibition by Ser$^{33/37/45}$Thr^{41}-phosphorylation, as mediated by GSK3β activation (Figure 3.2.7A and B; Figure 3.2.8).

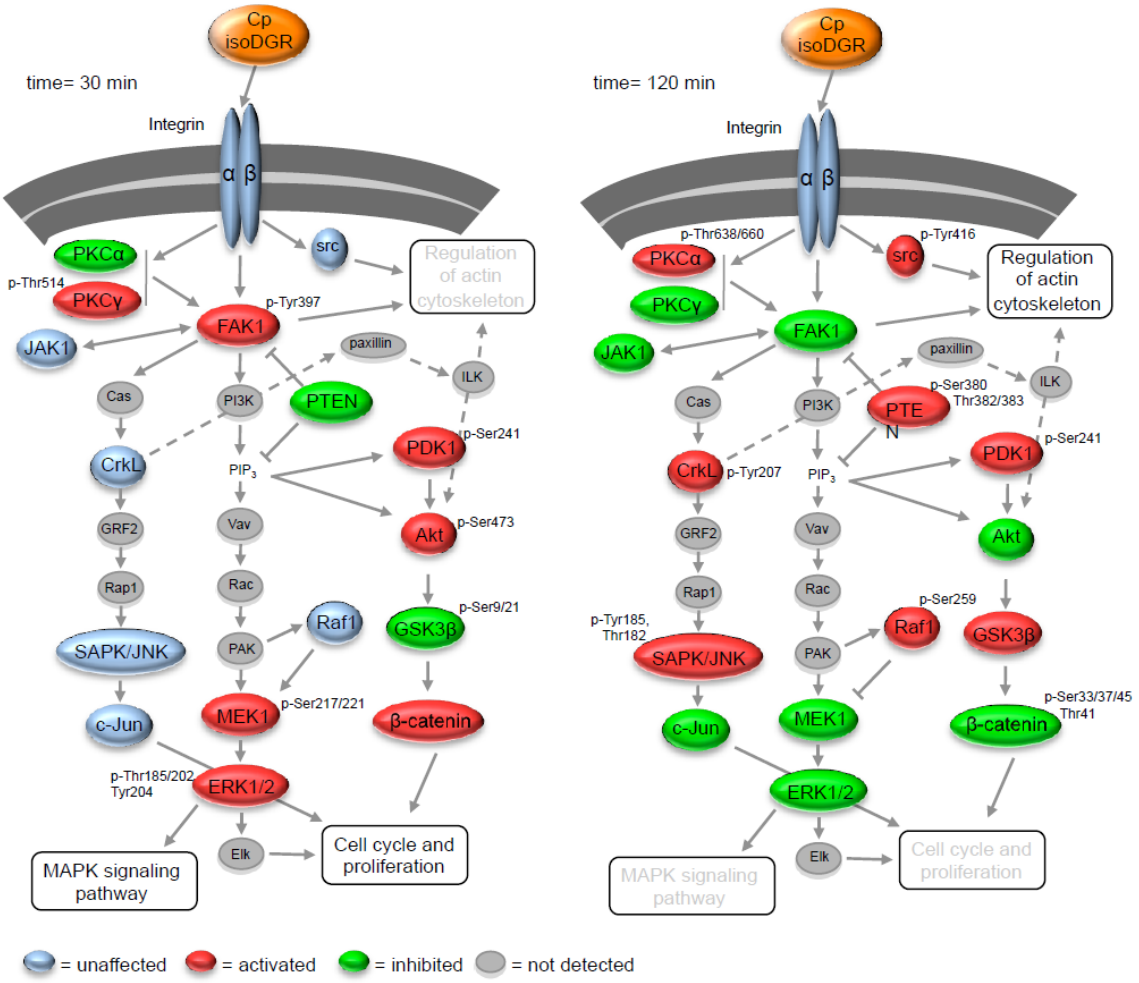

Figure 3.2.8: Schematic representation of the signalling transduction throughout integrin engagement by Cp aged under oxidative conditions. Changes in molecules' phosphorylation after 30 and 120 minutes of treatment with deamidated Cp suggest that early signal is address to gene activation, cell cycle induction and MAPK signalling pathway activation, while late signal sustains actin cytoskeleton rearrangement, and cell cycle and proliferation arrest. The schematic evaluation is based on the results obtained by activation signal analysis performed with reverse phase protein arrays Figure 3.2.7 and reports the rate of phospohrylation compared to control conditions consisting in cells treated with non-modified Cp.

3.2.7 Pathological CSF from Alzheimer disease fosters integrin binding of spiked purified Cp and inhibits its ferroxidase activity

To investigate whether Cp deamidation might occur also *in vivo*, in particular in pro-oxidant pathological CSF environment, we added purified Cp to CSF from healthy subjects or CSF from Alzheimer disease (AD) patients, and incubated the mixture for 0, 3, 6, 9 and 12 days at 37°C. Cp was added in large amounts due to the presence of other integrin-binding molecules in CSF (e.g. fibronectin, tenascin) that can compete the binding of Cp. Aging in a pathological milieu was able to induce a time-dependent Cp significant binding to αvβ6 ($p<0.0001$) (Figure 3.2.9A, CSF/AD), while binding was absent or very weak when aging occurred in normal CSF (Figure 3.2.9A, CSF). Thus, Cp deamidation showed a faster kinetic in the CSF from AD patients then from healthy subjects. By comparison with the binding ability of the same amount of *in vitro* chemically aged Cp (Cp-ox/AmBic), we ascertained that about 40% of the added Cp was converted to pro-adhesive Cp after 12 days of aging in AD patients CSF (Figure 3.2.9B). Also in the case of purified Cp aging in the CSF, the gain in integrin-binding properties was mediated by Cp deamidated NGR motifs, as demonstrated by competition with an isoDGR-peptide, which abolished binding to αvβ6 ($p= 0.0004$) (Figure 3.2.9C, grey bars). To investigate whether the Cp aged in pathological conditions was also able to recognize integrins in their physiological conformation, we performed cell adhesion experiments. HaCat cells were seeded on plates coated with Cp immunoprecipitated from either AD CSF (black bars) or control CSF (white bars) at time

zero or after 9 days of aging. The Cp aged in pathological CSF was able to promote the HaCat cells adhesion, whereas little or no adhesion was observed on Cp aged in control CSF (Figure 3.2.9D). Additionally to the gain of integrin binding function, Cp aged in AD's CSF showed a complete loss of ferroxidase activity ($p<0.0001$), while the Cp aged in healthy CSF showed a reduction of about 40% (Figure 3.2.9E, 9 days).

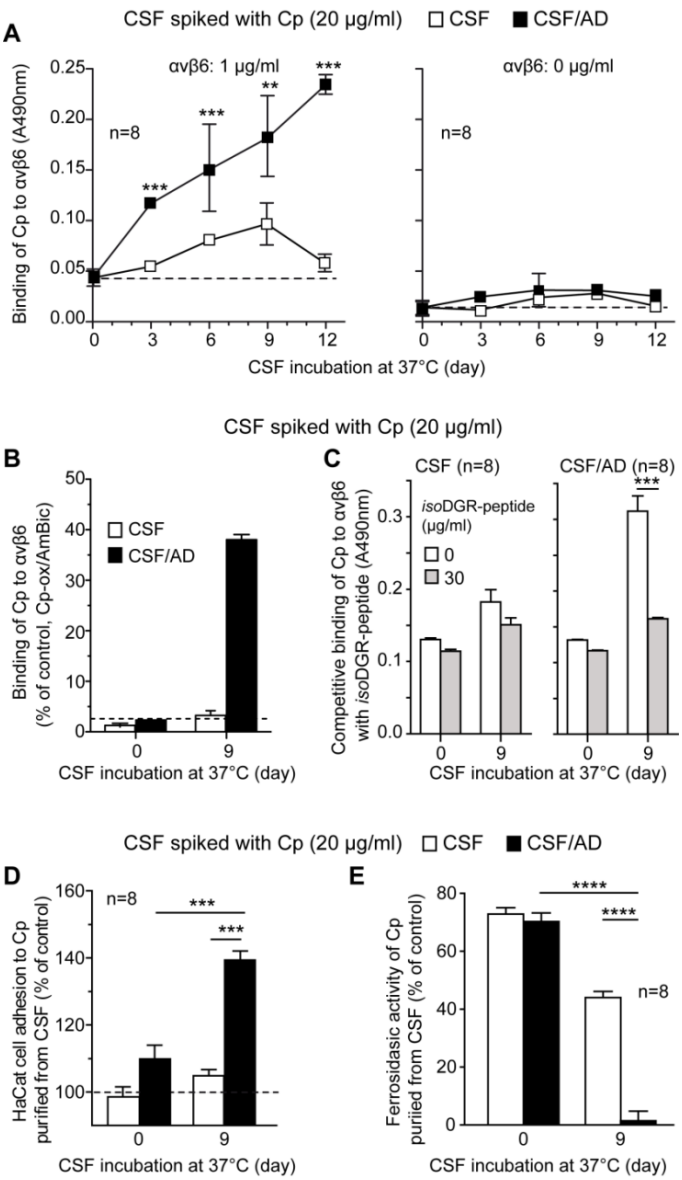

Figure 3.2.9: Cerebrospinal fluid from Alzheimer's diseases foster NGR-motif deamidation and binding toαvβ6 -integrin of spiked purified Cp. **A**) Binding toαvβ6 of purified Cp added to CSF from healthy subjects (CSF, white squares) or AD patients (CSF/AD, Black squares) aged for 0, 3, 6, 9, 12 days at 37°C. **B**) Quantitation of the Cp bound toαvβ6 integrin after *ex vivo* aging in CSF evaluated by the comparison with binding of chemically *in vitro* aged Cp (Cp-ox/AmBic, 100%). Aging from 0 to 9 days at 37°C of purified Cp in the CSF from AD patients (CSF/AD) showed about 40% of the protein binding ability toαvβ6, while the same aging conditions in th e CSF from healthy subjects showed negligible binding ability (3-4%). **C**) Competition with isoDGR-peptide (grey bars) of the binding to αvβ6 of Cp aged in CSF from healthy subjects (CSF, white bars) or AD patients (CSF/AD, black bars). **D**) HaCat cell adhesion to plates coated with immunoprecipitated purified Cp (5µg/ml) after *ex vivo* aging (0 or 9 days) in CSF from healthy subjects (CSF) or AD patients (CSF/AD). Adhesion was evaluated as adsorbance (570 nm) of the crystal violet stained cells and expressed as % of control (cells in adhesion on BSA-coated wells). **E**) Cp ferroxidase activity after incubation in CSF from healthy subjects (CSF, white bars) or AD patients (CSF/AD, black bars). Ferroxidase activity of immunoprecipitated Cp (1.25µg) was evaluated by the decrease in Btp-Fe^{2+} complex absorbance at 535 nm. Values are expressed as % of total ferroxidase activity measured for 1.25 µg of untreated Cp.
All the assays were performed in triplicate for 2 independent experiments, by using CSF from n=8 different subjects each group (see Table 5.2). Statistical p value was evaluated by student's t test. ****=$p<0.0001$, ***=$p<0.001$, **=$p<0.01$.

3.3 Cerebrospinal fluid from Parkinson's disease promote oxidation, deamidation and integrin binding of spiked ceruloplasmin

Marco Barbariga, BCs, Flavio Curnis, PhD, Annapaola Andolfo, PhD, Alan Zanardi, BCs, Massimo Lazzaro, PhD, Antonio Conti, PhD, Giuseppe Magnani, MD, Elisabetta Coppi, MD, Laura Ferrari, MD, Angelo Corti, PhD, Massimo Alessio, PhD.

In preparation

3.3.1 CSF from PD induces structural changes to spiked purified Cp's fostering 968NGR-motif deamidation, gain of integrin binding function, and ferroxidase activity inhibition.

To investigate whether pathological PD-CSF may promote Cp modifications, we added *ex-vivo* the purified Cp to the CSF either from healthy subjects, peripheral neuropathies (PN) or PD patients. Cp aging from 0 to 12 days in the CSF from PD was able to induce a time-dependent Cp binding to αvβ6-integrin (at 9 and 12 days, p=0.0091 and p=0.0083, respectively) indicating Cp-deamidation [357], while binding was negligible when aging occurred in healthy or PN CSFs (Figure 3.3.1A). The gain in integrin-binding properties of purified Cp aged in PD's CSF was mediated by deamidated NGR-motifs, as demonstrated

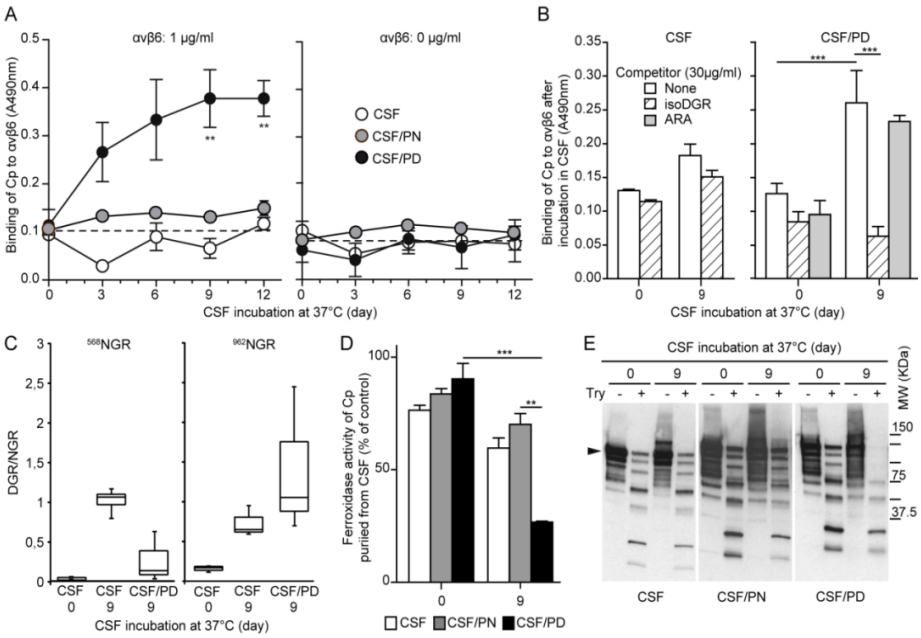

Figure 3.3.1: Aging of purified Cp in CSF from PD patients induces changes in Cp structure and biological function. **A**) Binding to αvβ6 of purified Cp added to CSF from healthy subjects (CSF, white circles), PN patients (CSF/PN, gray circles) or PD patients (CSF/PD, black circles) aged for 0, 3, 6, 9, 12 days at 37°C. **B**) Competitive binding of Cp aged in CSF either from healthy (CSF) or PD (CSF/PD) for 0 or 9 days at 37°C to αvβ6 with the isoDGR-peptide (striped bars) and control ARA-peptide (gray bars). **C**) Rate of NGR-motifs deamidation. Semi-quantitative label free protein evaluation based on the intensities of precursors performed with MaxQuant software on the peptides observed by mass spectrometry containing either ^{568}NGR- or ^{962}NGR-motif as they are or deamidated. Analysis was performed on resting purified Cp (CSF-0) and on purified Cp immunoprecipitated after 9 days of aging at 37°C either in CSF from healthy subjects (CSF-9), or PD patients (CSF/PD-9). Data are reported as ratio of DGR/NGR quantitation. **D**) Evaluation of Cp ferroxidase activity after incubation in CSF from healthy subjects (CSF, white bars), PN patients (CSF/PN gray bars), or PD patients (CSF/PD, black bars). Values are expressed as % of total ferroxidase activity measured for 1.2μg of untreated Cp. **E**) Western blot analysis after limited trypsin proteolysis (+) of the Cp aged for 9 days at 37°C in CSF from PD patients (CSF/PD) compared to Cp aged in healthy subjects CSF (CSF) or in CSF from PN patients (CSF/PN). All the assays were performed in triplicate for 2 independent experiments, by using CSF from n=8 different subjects each group (see Table 5.4); in the MS-analysis experiments n=6. Data were analyzed by student's t test; means with standard error are indicated (***=p<0.001, **=p<0.01).

by binding-competition observed using an isoDGR-peptide (p= 0.0009), but not using a control ARA-peptide (Figure 3.3.1B, striped and gray bars, respectively). Semiquantitative mass spectrometry (MS) analysis of spiked Cp immunoprecipited after 9 days of aging in normal and PD CSF environments showed that a partial deamidation occurred at the ^{568}NGR-motif in the CSF from healthy subjects (Figure 3.3.1C), likely reflecting the spontaneous deamidation rate of the surface exposed ^{568}NGR-motif; strangely, ^{568}NGR-motif of Cp aged in PD's CSF showed a very low deamidation rate.

Interestingly, even though not significant, in PD the deamidation rate of ^{962}NGR-motif, normally hidden inside the Cp structure [357], showed a trend of increase in comparison to healthy subjects (Figure 3.3.1C,CSF/PD vs. CSF respectively), a finding which suggests (although MS did not ascertain whether the pro-adhesive isoDGR isoform was present) that Cp-structural changes occurred in PD CSF and that the ^{962}NGR-motif plays a major role in the acquisition of the integrin binding properties (Figure 3.3.1 A and B). Additionally, Cp aged in PD's CSF showed a great significant reduction of ferroxidase activity (p=0.0011), while the Cp aged in healthy or PN CSFs didn't (Figure 3.3.1D, 9 days). Similarly, Cp aged in PD CSF showed higher sensitivity to limited trypsin proteolysis compared to Cp aged in healthy or PN CSF (Figure 3.3.1E) confirming the occurrence of Cp-structural changes. Together these findings indicated that purified-Cp was modified by the pathological PD CSF environment.

3.3.2 Oxidative stress contributes to ceruloplasmin structural changes

Increased carbonylation of total CSF's proteins and carbonylation of oxidized/acidic-Cp isoforms have been reported in PD (3.1.3) suggesting that oxidative modifications may occur during PD pathological events. Also the *ex-vivo* aging in PD CSF of spiked Cp showed an increase in Cp carbonylation, such increase was not observed if aging occurred in PN CSF even though a weak basal carbonylation was detectable in comparison to the incubation in healthy subjects CSF (Figure 3.3.2A, 0 *vs.* 9 days). Noteworthy, CSF of PD patients showed a significant higher concentration (48 µM) of H_2O_2 compared to healthy (p<0.0001) or PN (p=0.0001) CSFs (25 and 26 µM, respectively) (Figure 3.3.2B). Finally, the abolishment of the gain of integrin-binding ability of Cp after 9 days of aging in the pathological PD CSF

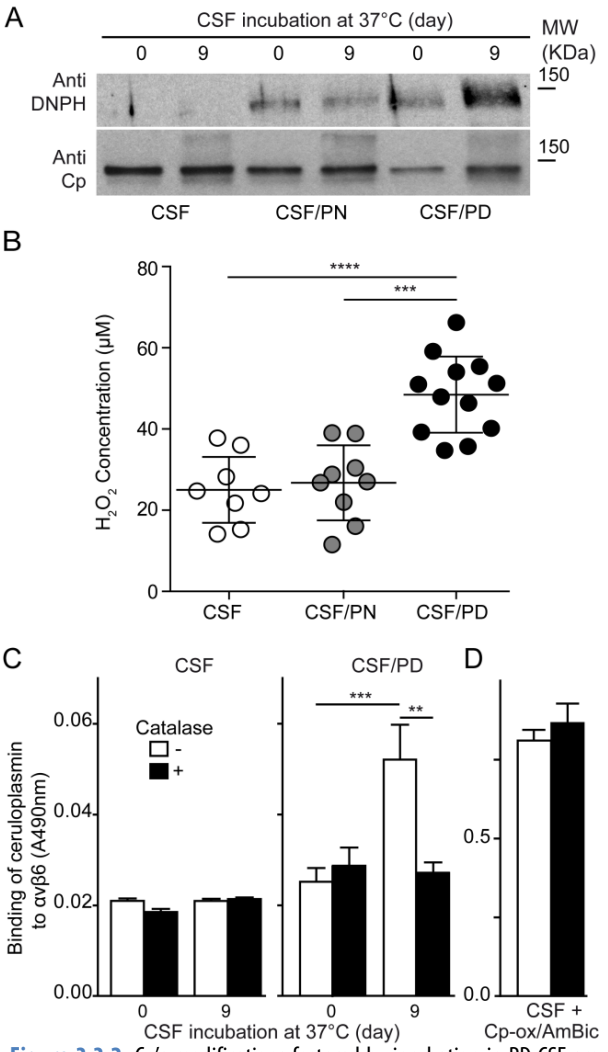

Figure 3.3.2: Cp's modifications fostered by incubation in PD CSF are generated by oxidative stress. **A**) Detection of Cp carbonylation after aging in CSF from either healthy controls (CSF), PN patients (CSF/PN) or PD patients (CSF/PD). Carbonylation was assessed by using OxyBlot assay on DNPH-derivatized proteins from Cp-spiked CSF at time 0 or after 9 days incubation at 37°C. Western blot, performed on proteins resolved by SDS-PAGE, were done using either an anti DNPH or anti-Cp antibodies. **B**) Evaluation of the hydrogen peroxide concentration in the CSF of healthy subjects (CSF, n=8), of PN patients (CSF/PN, n=9) and PD patients (CSF/PD, n=12) performed using AmplexRed®. **C**) Binding to αvβ6 of purified Cp after incubation 9 days at 37°C in the CSF from healthy subjects (CSF, n=8) or in the CSF of PD patients (CSF/PD, n=8) either in the presence (black bars) or in the absence (white bars) of catalase (60µg/ml). **D**) Binding toαvβ6 of the in vitro oxidized Cp (Cp-ox/AmBic) added in healthy subjects CSF either in the presence (black bars) or in the absence (white bars) of catalase (60 µg/ml). Statistical p value was evaluated by student's t test, means with standard error are indicated (****=p<0,0001 ***=p<0.001, **=p<0.01).

supplemented with catalase (p=0.009) indicate that the H_2O_2 present in the CSF contributed to the Cp gain of function (Figure 3.3.2C). As control, the binding ability of the already *in vitro* oxidized-Cp (Cp-ox/AmBic) added to healthy subjects CSF wasn't affected by the presence of catalase (Figure 3.3.2D).

3.4 The effects of deamidated ceruloplasmin on cellular patho/physiology

3.4.1 Integrin signaling induced by deamidated-Cp interaction produces proliferation arrest in both epithelial and neural stem cells.

Epithelial HaCat cells treated with Cp-ox/AmBic showed a proliferation reduction in the first 24 h and a proliferation arrest in the subsequent 24 h (Figure 3.4.1A). The proliferation inhibition was dose-dependent and was not observable when cells were incubated with untreated Cp or with control - ox/AmBic-treated BSA (Figure 3.4.1B). Flow cytometry analysis assessed whether the proliferation inhibition was the result of apoptosis induction or of cell cycle blockage. In contrast with untreated cells or cells treated either with non-modified Cp or with ox/AmBic-treated BSA, epithelial cells incubated with aged/oxidized-Cp started to accumulate after 48 h, i.e. in the late-S/G2-entry phase of the cell cycle (Figure 3.4.2); this result suggests that cell arrest occurred and that it took place in the G0/G1 phase. The effect was more dramatic at 72 h, when very few cells treated with Cp-ox/AmBic were in the S phase, and an accumulation was observable in the G2/M phase (Figure 3.4.2). It is noteworthy both that the rate of EdU incorporation had already reduced in Cp-ox/AmBic treated cells at 24 h, thus indicating an early effect (Figure 3.4.2), and that a similar reduction was observed for the control treatments (Cp and BSA-ox/AmBic) at 72 h (Figure 3.4.2). In contrast with cell cycle, apoptosis induction, as assessed by AnnexinV staining, proved to be negligible at 24 and 48 h for all treatments (0.5-4.5 % of the cells), and started to be substantial at 72 h and exclusively for the ox/AmBic-Cp-treated cells (14.5% positive cells). These data confirmed the hypothesis derived from signaling analysis, namely that signaling elicited by deamidated-Cp/integrin interaction modulates the effect of cell proliferation by acting on the cell cycle. Interestingly, the blockage in cell proliferation upon exposure to deamidated-Cp was cell-specific, as it was not observed in the SH-SY5Y neuronal cell line, whereas it was dose-dependently evident in mouse adult subventricular zone neural stem cells cultured as neurospheres (Figure 3.4.3C) (p=0.0068). To investigate whether cell proliferation inhibition may be mediated also by Cp aged *ex-vivo* in pro-oxidant pathological CSF environment, we incubated HaCat cells for 24, 48 and 72 h in the presence of the immunoprecipitated Cp aged in CSF from healthy subjects or CSF from Alzheimer disease (AD) patients for 0 days (w/o aging) or for 9 days. Growing HaCat cells with Cp derived from aging in AD CSF was able to reduce their proliferative activity (Figure 3.4.3, CSF/AD 9) (p=0.0091), while inhibition was absent when Cp from aging in normal CSF was added (Figure 3.4.3, CSF 9). Incubation of cells with Cp not subjected to

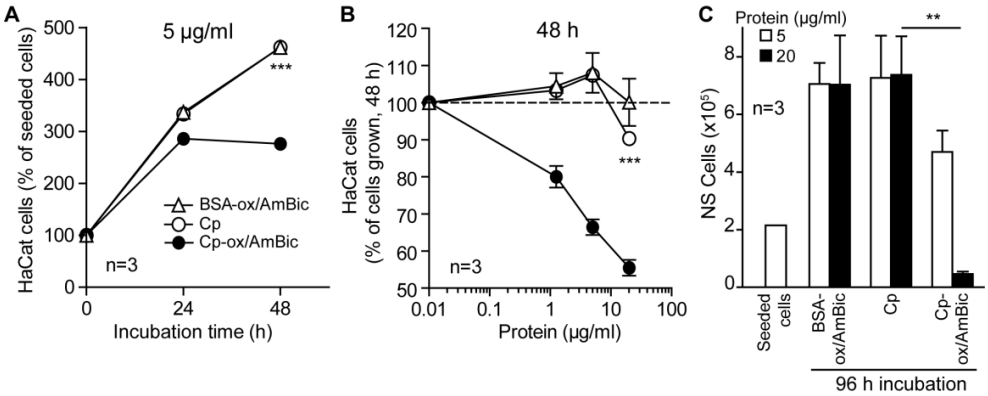

Figure 3.4.1: Integrin signaling induced by deamidated-Cp interaction results in a reduction of epithelial and neural stem cell proliferation. **A** and **B**) Proliferation was measured by MTT assay on HaCaT, after starvation in 0.1% FBS containing medium. Cells were incubated for 24 or 48 h with different concentration (1, 5, 20 µg/ml) of untreated Cp, aged/oxidized-Cp (Cpox/ AmBic) or aged/oxidized-BSA (BSA-ox/AmBic). Cells number was reported as percentages of the seeded cells. Statistical significance, reported as p value, was evaluated by student's t test (3 experiments with 6 replicates each). **C**) Short-term proliferation assay of neural stem cells (NSCs) isolated from the subventircular zone of postnatal day 40 FVB mice. NSCs, cells were plated ($8x10^3$ cells/cm^2) in mitogen containing medium in the presence of either Cp, aged/oxidized-Cp or aged/oxidized-BSA (5 and 20 µg/ml). Formed neurospheres were collected 96 h later and total number of viable cells was assessed by Trypan Blue exclusion. Statistical significance, reported as p value, was evaluated by student's t test. **= p<0.01; ***= p<0.001.

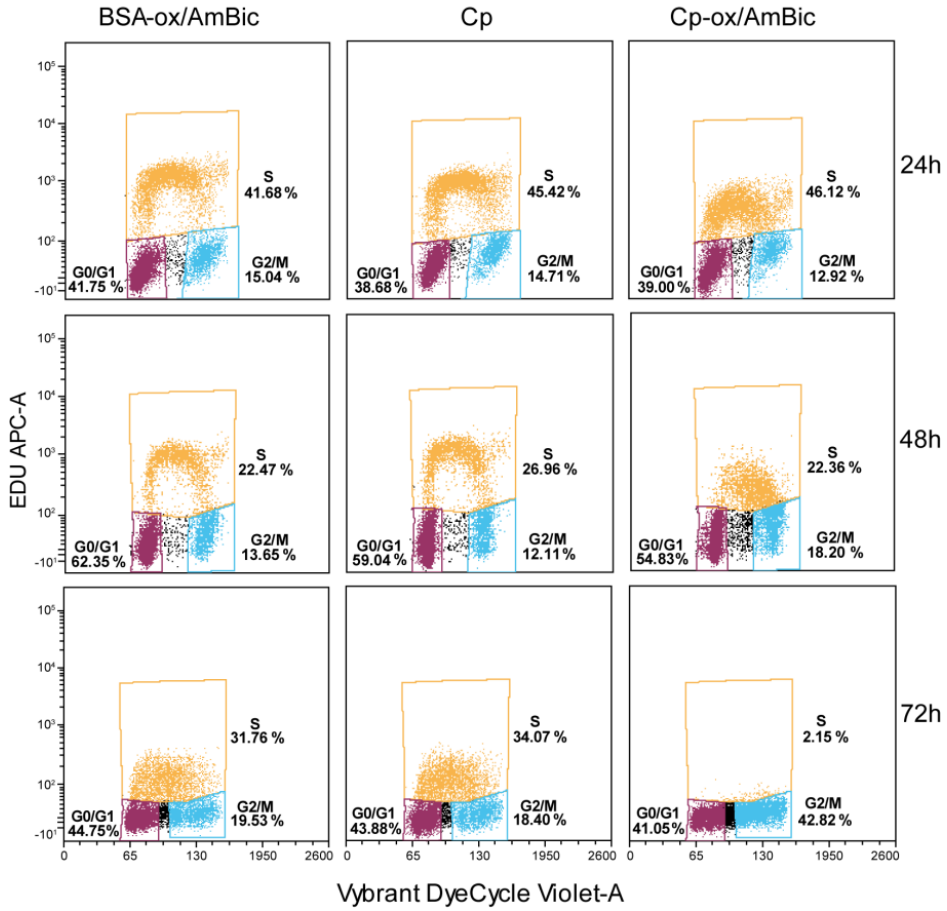

Figure 3.4.3 Cell cycle flow cytometry analysis of Cp-stimulated HaCat cells. After starvation, HaCaT cells were treated for 24, 48 and 72 h either with untreated Cp, aged/oxidized-Cp (Cp-ox/AmBic) or aged/oxidized-BSA (BSA-ox/AmBic) (5 µg/ml). Cells were stained with thymidine analog (EdU) in order to separate cells in S phase from those in G0/G1 and G2+M (y axes) and with Vybrant®DyeCycle™Violet (Invitrogen) for total DNA, discriminating between G0/G1 and G2 phase (x axes). Percentages of gated cells are reported: G0/G1 magenta, S orange, G2+M blue.

aging treatment (Figure 3.4.3, CSF 0; CSF/AD 0) was also not effective to reduce their proliferative ability.

3.4.2 Human Choroid Plexus epithelial Cells characterization

Being the epithelial cells of the choroid plexus layer the cells that regulate the synthesis and the composition of the CSF, aside from being in direct contact with it, we focused our attention on the study of the possible effects that deamidated-Cp can induce on their biology. The shape of the commercially available HCPEpiC's is quite different compared to the typical polygonal epithelial shape (Figure 3.4.4A), and so we analysed the expression of epithelial cells-specific markers in order to rule out that the cells that we used were un-differentiated precursors or contaminated by fibroblasts.

Immunofluorescence analysis showed the expression of choroid plexus-specific protein transthyretin (Figure 3.4.4B) and the Western blot analysis showed the expression of cytokeratin-19 (an epithelial marker) and the absence of Vimentin expression (epithelial-to-mesenchimal transition marker) (Figure 3.4.4C). As a control, HaCat epithelial cell line expresses the same markers of HCPEpiC, while primary fibroblasts showed an inverted protein expression (Figure 3.4.4C). These results suggest that, albeit with an altered shape, HCPEpi cells can be considered as epithelial cells and can be used in our experiments with the exception of cell-layer permeability assays, being reported that these cells were not adapt for this kind of experiments [358]. Furthermore, these cells express and secrete ceruloplasmin (Figure 3.4.4D), a feature exclusive (at least in the CNS) of the choroid plexus tissue.

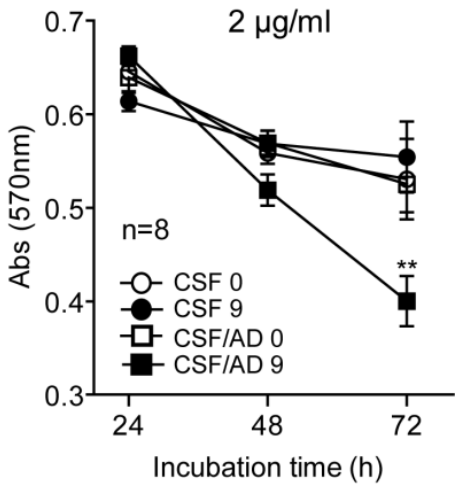

Figure 3.4.2: Proliferation of HaCat cells incubating cells in 0.1% FBS DMEM with 2µg/ml of purified Cp immunoprecipitated after aging (0 or 9 days at 37°C) in healthy or Alzheimer's disease CSF (CSF and CSF/AD respectively). Statistical significance, reported as p value, was evaluated by student's t test. **= $p<0.01$.

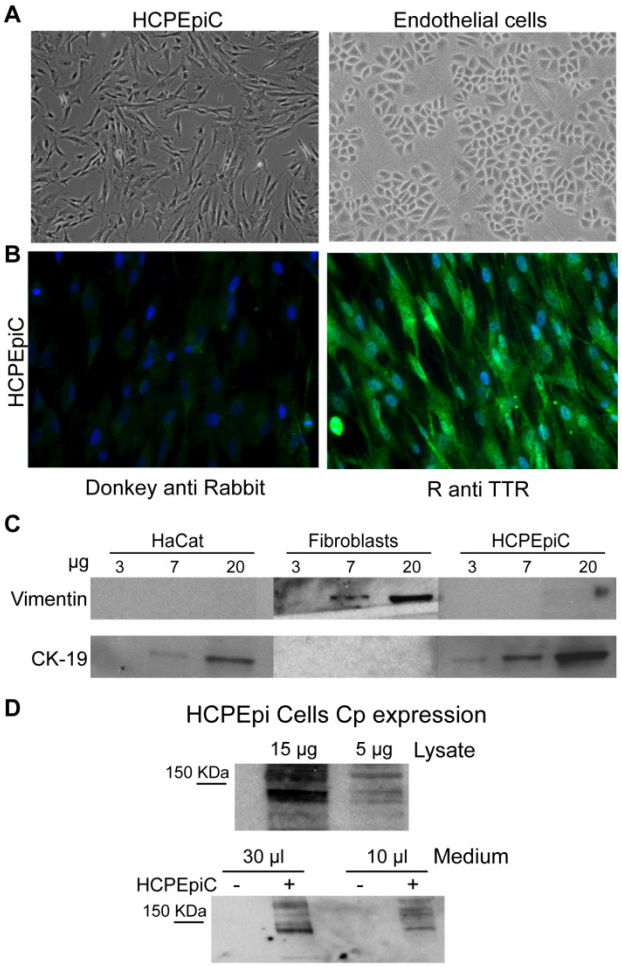

Figure 3.4.5: Epithelial cell markers expressed by HCPEpiC. (**A**) Cells showed an elongated unusual cellular shape compared to other epithelial cells; **B**) HCPEpi cells were tested by the expression of transthyretin (TTR); **C**) expression of vimentin and CK-19. Fibroblast and epithelia HaCat cell lysates were used as controls. **D**) Expression of ceruloplasmin in HCPEpiC cell lysate and as secreted form in the colture medium.

3.4.3 Deamidated Cp mediates HCPEpiC adhesion and spreading

To assess whether Cp aged under oxidative conditions can bind membrane integrins expressed by HCPEpi cells, similarly to what we observed for the HaCat cell (seen in chapter 3.2.5), we analyzed the adhesion of the choroid plexus-derived cells to plates coated with ox/AmBic-Cp. Flow cytometry analysis showed that HCPEpiC express αvβ3, αvβ5 and α5β1 integrins on surface membrane. The adhesion and spreading of HCPEpi cells on plates coated with ox/AmBic-Cp increased in a dose-dependent manner, while coating with untreated Cp did not induce cell adhesion (Figure 3.4.5A).

Subsequently, to assess whether cell adhesion was mediated by isoDGR, we incubated ox/AmBic-treated Cp with PIMT, which converts L-isoAsp residues to L-Asp which is not able to bind integrins: PIMT treatment inhibited the pro-adhesive activity of ox/AmBic-treated Cp (Figure 3.4.5B) (p=0.0061), indicating that deamidated Cp can interact also with the integrins present on the surface of HCPEpi cells, presumably through its isoDGR motifs.

3.4.4 Cp aged under oxidative conditions transduces intracellular signal through integrin engagement

In order to investigate whether the binding of Cp-ox/AmBic to integrins expressed by HCPEpi cells could induce intracellular signalling like we observed in HaCat epithelial cells, we incubated HCPEpiC with either untreated or ox/AmBic-Cp stimulus, and analysed by Western blot the activation status of some molecules representative of the triggered integrin activation pathway already seen modified (in their phosphorylation rate) after HaCat cells stimulation (see chapter 3.2.6).

After 120 min of treatment there was an increase in the phosphorylation of the activation residues of p-Tyr397 FAK1 and p-Thr202Tyr204 ERK1/2, accompanied by the phosphorylation of inhibitory residue p-Ser9GSK3β which maintain β-catenin

Figure 3.4.4: Cp deamidation mediate HCPEpi cell adhesion via isoDGR-integrins interaction. **A**) Adhesion of HCPEpiC to plates coated with different concentrations of either Cp (Untreated) or aged/oxidized-Cp (ox/AmBic). Adhesion was evaluated as absorbance at 570nm of the crystal violet stained cells. **B**) Adhesion of HCPEpi cells to plastic coated either with aged/oxidized-Cp (ox/AmBic): inhibition of cells adhesion occurred after treatment of coating proteins with PIMT (+) compared to the untreated wells (-). Images of stained cells adherent to ox/AmBic-Cp treated with (+) or without (-) PIMT enzyme are also reported. All the adhesion assays were performed in triplicate for 3 independent experiments (n= 3). Statistical significance reported as p values was evaluated by student's t-test; **= p<0.01, ****=p<0.0001.

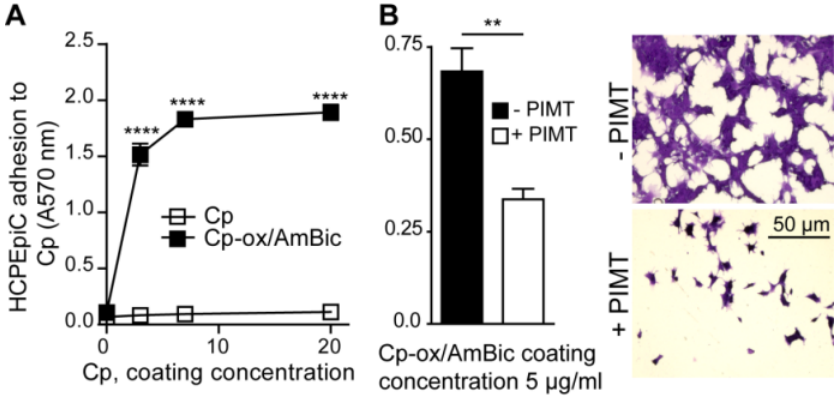

activity by preventing its phosphorylation. These results suggest that the signal mediated by deamidated-Cp mostly addressed gene activation regulation, cell cycle and MAPK signaling pathway, a pattern of activation that resembles the one seen in the HaCat cells after 30 min of stimulus (Chapter 3.2.6).

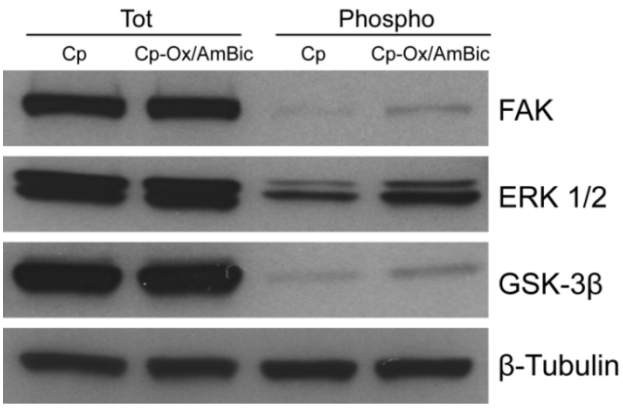

Figure 3.4.6: Phosphorylation rate analysis of representative proteins belonging to the integrins signalling pathway in choroid plexus epithelial cells treated with aged/oxidized ceruloplasmin (Cp-ox/AmBic); expression level of focal adhesion kinase (FAK), extracellular-signal-regulated kinases (ERK), Glycogen synthase kinase-3 (GSK3-β) and the phosphorylation level of specific residues were investigated by Western blot performed on HCPEpi cell lysates after treatments (30 min) with untreated Cp or aged/oxidized ceruloplasmin. Tubulin expression was evaluated for signal normalization.

4 Discussion

Based on the first set of experimental evidences which revealed modifications in the CSF' proteins of neurodegenerative diseases, we propose changes in Cp electrophoretic profile as a potential marker for the evaluation of oxidative stress levels in the CNS of PD and AD patients. This suggestion derives from the link between pI modification of Cp isoforms and CSF oxidation. The observed Cp oxidative modifications seem to be relevant in the neurological diseases in which damage is mostly confined to the brain, being AD patients Cp's modifications similar (but distinguishable) from those observed in PD patients; on the contrary, ALS patients, in whom spinal motor neurons are involved, have not shown substantial Cp modifications. Alternatively, it might be that neurodegenerative diseases differ in the lead times they need before CNS oxidative damage becomes considerable; the analysis of CSF' Cp oxidation during the progression of neurological disease could reveal a link between gradual CNS oxidative damage and specific pathological symptoms. Previous studies suggested a correlation of low serum Cp expression with the development of PD [359] and with nigral iron deposition [360], while other studies have concluded that Cp levels are not of diagnostic value [341, 361]. However, these studies evaluated Cp merely as an expression level in sera, where we have not found alterations: the novelty of our results, therefore, is that they introduce Cp isoform patterns in CSF as a way to discriminate between patients. Noticeable is, in fact, the correlation we observed between the PD clinical grading (UPDRS) and the amount of oxidized Cp, and the identification of representative pathological clusters by unsupervised pattern recognition procedures confirms the potential role of Cp analysis for clinical applications. Cp analysis in PD patients under treatment, for example, might be used to monitor therapy efficacy by modulating the iron chelator or antioxidant compound treatments.

In vitro CSF oxidation induced Cp modifications similar to those observed in patients; moreover, CSF analysis of PD patients confirmed that carbonylation of total proteins increases and that this modification might affect Cp contributing, together with others additional oxidative modifications, to its pI shift. Although CSF protein carbonylation level has already been proposed as a marker for oxidative damage [344], the evaluation of Cp electrophoretic pattern seems to be the most sensitive technique for oxidative status analysis, probably due to the presence of six copper ions in the molecule [182]. In PD, imbalances between the generation of oxidant products and ROS scavenging systems, together with improper iron metabolism, contribute to neurological damage [362]; reduced CSF ferroxidase activity [345, 346], increased oxidative stress in CNS, and iron overload in SN [363] are PD features that are potentially connected to the Cp oxidation here observed, being the functionality reduction that follows Cp oxidation correlated with a Cp electrophoretic pattern similar to that observed in CSF of PD. Given that CSF ferroxidase activity is substantially due to Cp [7], it is reasonable to associate the Cp oxidative modifications found in PD patients with the reported reduction in CSF ferroxidase activity [345, 346]. Furthermore, oxidative modification in Cp leads to copper release [182], possibly explaining why copper increases in the CSF of both PD and AD patients [346, 364]; copper ions are necessary for the Cp ferroxidase activity, thus when released from oxidized Cp impair its enzymatic function [184, 353]. Being similar pI shifts and increased carbonyl contents reported for serum Cp during aging [184], the changes observed in this work in CSF Cp from PD and AD patients might reflect accelerated protein aging induced by oxidative pathological conditions [365]. Iron metabolism impairment is the major consequence of the loss of Cp activity. Indeed, both aceruloplasminemia patients and the Cp-deficient mice are characterized by an increase in intracellular iron that correlates with motor dysfunction [123, 366]. Intracellular iron concentration is controlled both by the storage protein ferritin, which accumulates Fe^{3+}, and by Fe^{2+} efflux through Fpn accompanied by Cp extracellular ferroxidase activity [7]. In our experimental model, the absence of extracellular ferroxidase activity as a result of Cp oxidation leads to cellular iron retention both in SH-

SY5Y cell line and in primary neuronal culture, which is more susceptible to intracellular iron accumulation than the cell line counterpart [349], a feature that presumably better reflects what occurs *in vivo* under pathological conditions. The weak Fpn down modulation and the lack of a complete intracellular iron retention that we observed suggested the presence of compensatory mechanisms. One of these may consist in the described role of the β-amyloid precursor protein (APP), which like Cp is expressed in trans-membrane and secreted forms, and has been reported to exert ferroxidase activity that in turn promotes neuronal iron export through the Fpn [189]. Also the inhibition of APP-ferroxidase activity results in neuronal iron accumulation, suggesting that various molecules in varying tissues and pathologies may share the same function. The iron retention we detected in the absence of extracellular ferroxidase activity might be generated by Fpn functionality impairment rather than by membrane down modulation. This explanation is supported by data reporting that Fpn expression does not change in the absence of extracellular ferroxidase activity in cells that do not express membrane GPI-Cp [8], as is the case in the neuroblastoma cell line we used. It has been proposed that 60% of brain ferroxidase activity derives from the membrane GPI-Cp isoform, which is expressed by astrocytes, and 40% from APP, which is expressed by neurons [189]. However, account must also be taken of the ferroxidase activity exerted by the soluble forms of Cp and APP contained in CSF, which permeates the brain. We hypothesize that increases in oxidative stress in PD patients, both at neuronal and CSF levels, induce the reduction of extracellular ferroxidase activity through the oxidation both of membrane-bound and of soluble Cp; in turn, this reduction might contribute to the iron loading observed in SN [360, 367]. The possibility that Cp plays a role in PD implies in the future the analysis of GPI-Cp expression and modifications on astrocytes, because this isoform is the predominant in the brain and can be modified too by oxidative environment. Interestingly, GPI-Cp has been reported to be down modulated by oxidative stress in astroglial cells, and as such to contribute to intracellular iron deposition [368].

Considering that Cp showed oxidative modifications in the CSF of neurodegenerative diseases, we decided to investigate specific post-translational modfications fostered by oxidation. Among these, the asparagine (Asn) deamidation that leads to the formation of aspartate (Asp) and isoaspartate (*iso*Asp), resulted to be particularly intriguing because occurs in vivo during protein aging [309] and is accelerated under oxidative conditions [369]; aging under oxidative conditions is the condition that we hypothesise occurs for proteins in the CSF of AD and PD patients. The second reason that made Asn deamidation interesting was the fact that if it occurs at the level of the NGR-motif can give rise to the acquisition of integrin-binding function [6], and the Cp sequence contains two NGR-motifs in its amino acidic sequence. Thus we decided to evaluate in vitro primarily and successively ex-vivo whether this kind of modifications may occurred in Cp.

The results of this second part of investigations demonstrated how AD and PD CSF favor Cp deamidation and how this effect manifests as a functional gain in cells-integrin binding with an intracellular signal transduction. This new pro-adhesive function is derived from the deamidation at the NGR-sites within Cp, in particular the ^{962}NGR, whose deamidation is promoted by prolonged oxidative conditions. Since asparagine deamidation during protein aging depends on neighbouring residues as well as on secondary and tertiary structural elements and by environmental factors such as pH, temperature and ionic strength [307, 370], the combination of these features controls the kinetic of deamidation reactions, ranging from hours to years [307, 370]. Thus, for each protein it is important to assess whether specific Asn residues can undergo or not this post-translational modification: for example, the deamidation of an NGR-site of fibronectin and the consequent formation of isoDGR can work as a molecular switch for integrin-ligand recognition and does not occur in the intact protein, whereas it can rapidly occur in protein fragments [321]. It is of relevance that, in contrast to fibronectin, the binding to integrin occurs for the intact full length deamidated-Cp.

Our results show that deamidation of the ^{568}NGR-site, which is exposed on the protein surface, does not require structural changes. In contrast, deamidation of the ^{962}NGR-site, which is buried inside two β-strands of the protein structure and is blocked in a stable conformation by polar interactions with neighbouring aminoacids, can occur only after structural changes induced by an oxidative microenvironment. Conformational changes similar to those we reported after protein oxidation have

been described for Cp in the absence of copper ions [353].

The NGR-to-isoDGR conversion in Cp induces a gain-of-function in terms of binding to several αv-integrins and the interaction of deamidated Cp with integrins can trigger an intracellular signalling cascade. Consistently with binding data, our docking studies show that at least the ^{568}isoDGR motif of intact Cp can interact with the canonical RGD binding pocket of the αvβ6, having the stereochemical and electrostatic requirements for a correct recognition. Since it is not possible to predict *a priori* the putative structural rearrangement induced by the oxidation, we cannot describe *in silico* the possible interactions occurring between integrin and the ^{962}*iso*DGR sequence in the context of full-length Cp. These findings, together with the high conservation of these tripeptide-sequences across differing species from hamster to human (Figure 4.1), suggest that the Cp deamidation can produce a relevant biological gain-of-function. Remarkably, very few substitutions in various species were also shown in the ^{962}NGR flanking sequences, which, as said above, are likely crucial for regulating the deamidation rate.

Cp's NGR-deamidation might occur in a relevant manner in certain pathological conditions, as suggested by the observation that Cp aged *ex vivo* in the CSF from AD and PD patients acquires integrin-binding and cell adhesion properties. The faster kinetic of Cp-deamidation observed in CSF from AD and PD patients compared to the CSF from healthy subjects, supports the hypothesis of a generally accelerated protein aging in neurodegenerative diseases, as a consequence of pathological environment [4, 365]. Based on the observation that after 12 days of aging in the pathological CSF about 40% of the Cp was able to bind integrin, and given that the Cp concentration in the CSF is about 2 µg/ml and that its physiological half-life is of about 5.5 days *in vivo* [342], it is conceivable that NGR deamidation might occur in patients to an extent that yields functionally relevant concentration of deamidated-Cp (about 200 ng/ml). The observed Cp's modifications suggest the presence of pro-oxidant compounds in patients CSF: the hydrogen peroxide concentration and the evidence that catalase prevents the acquisition of Cp integrin-binding properties in CSF suggest that H_2O_2 (known to be produced in neurodegeneration [371] can be one of them. However, an in-depth investigation of the differential composition of healthy and AD/PD CSFs, along with the identification of the crucial factors underlying increases in deamidation rates, are required. The *ex vivo* gain of function, besides making Cp-modifications an effective marker for the deleterious environment in patients, arises warnings about the therapeutic use of intravenous Cp-administration proposed by Ayton and colleagues in order o reduce the iron accumulation at the brain level. In fact, in PD mice model Cp-administration ameliorated the pathological signs with a reduction of iron deposition and neurodegeneration [372].

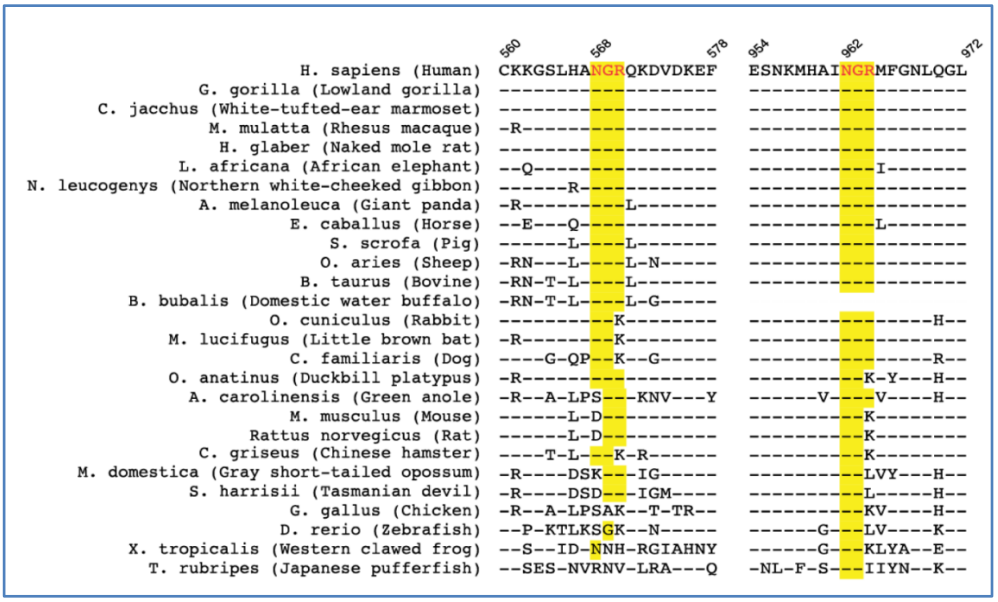

Figure 3.4.1: Analysis of the conservation of the Cp's NGR motifs in different species, performed with ClustalX software (Conway Institute UCD, Dublin; www.clustal.org). The functional relevance of the Cp's NGR motifs is underlined by their conservation along species; in particular the ^{962}NGR motif is inserted in an amino acids stretch that shows very few substitutions.

However, the proposed therapeutic usage of Cp in human must be carefully evaluated in the light of the reduced ferroxidase activity that can be fostered in the CSF and taking into account the possible side-effect due to the acquisition of integrin binding function. Referred to the latter, Cp-administration might be done, for example, in combination with helpful molecules like the *iso*DGR repairing enzyme PIMT.

As said before, since protein aging under oxidative stress is a condition that may occur in some neurodegenerative diseases [4, 373], we hypothesize that Cp aging under pathological conditions promotes modifications that favour structural changes which in turn foster both NGR-deamidation and Cu-ions release which subsequently results in loss of ferroxidase function and gain in integrin binding properties. Such Cu ions release from Cp might contribute to the reported increase of the pool of free-Cu and to the decrease of active Cp found in the CSF of AD patients [297, 299, 364]. Moreover, it is conceivable that this increase, affecting the redox environment [374], might contribute to the observed Cp modifications by a feed-back mechanism, facilitating Fenton's reaction and amplifying general protein damage [182]. The observed loss of ferroxidase activity of Cp aged in AD and PD CSF suggests again that changes in the Cp structure can be fostered also *ex vivo*. Given the role of Cp, ferroxidase activity reduction may affect the iron homeostasis [366], causing an increase in iron retention. A relationship between oxidation and protein deamidation in neurodegenerative disease is also suggested by the observation that several proteins found to be deamidated in the brain of PIMT-knock out mouse were oxidized in the brain of AD patients [356]. Thus, the Cp alterations observed in PD and AD patients might reflect accelerated protein aging, as a consequence of changes in the environmental redox status of pathological CSF [4, 365]. Therefore, it is plausible that the reported Cp oxidation-induced changes also *in vivo* include Asn deamidation of NGR-motifs. Literature reports that Cp immunostaining on neurons was observed both in neurodegenerative diseases [375] and in ischemia, all of which generate reactive oxygen species [376]. However, Cp cellular expression is known to be restricted to astrocytes [342]; the reported neuronal staining may therefore be the consequence of the acquisition by Cp of integrin-binding properties [376]. Oxidative aggregation of Cp induced by H_2O_2 has been reported [377], as the cooperative effect of Cp and H_2O_2 in inducing α-synuclein aggregation, which may have a role in PD [378]. It would be of interest to investigate in future whether the Cp aggregates we observed to be formed *in vitro* as consequence of aging under oxidative conditions, might have pro-fibrillogenic properties that can be favoured by asparagine deamidation, as is the case for β-amyloid in AD [369].

It is well known that integrin binding may activate intracellular signaling cascades, which in turn can affect cell differentiation, survival, growth and division [379]. Literature reports that an aberrant signalling mediated via integrin (e.g. αvβ1, α2β1, αvβ3 and αvβ5) engagement by fibrillar β-amyloid in the CNS resulted in an unconventional FAK activation and its down-stream signalling (i.e. MAPK, GSK3β etc.). This mechanism can lead to cell cycle arrest in the G1/S transition, neuronal dystrophy and death [380, 381]. A similar signalling mechanism is triggered by deamidated-Cp: after 2 hours of cell incubation with *in vitro* oxidized/aged-Cp, we observed an inhibition of FAK and MAPK signalling, which subsequently led to cell cycle arrest in the G0/G1 phase and to proliferation inhibition in epithelial and neural stem cells. Thus, even when β-amyloid fibrils are absent, as in PD, deamidated-Cp might induce similar, detrimental effects. In addition, we demonstrated that not only the *in vitro* deamidated-Cp, but also the protein deamidated *ex vivo* in the CSF of AD patients, is able to cause a proliferation arrest of epithelial cells. It is interesting that the cellular integrin expression pattern can itself be modulated by the oxidative pathological environment [382], and thus alters cellular signal sensitivity. Various cell types in the CNS might be activated via integrins, including microglial cells, which contribute to the inflammation mechanisms in neurodegenerative diseases [383]; interestingly, it has been reported that Cp can activate microglial cells [305], although the receptor underlying this mechanism has not yet been identified: one possibility is that deamidated Cp interacts with integrins. Experimental evidence supports the idea that niches of neural stem cells (NSC) are in deep contact with the ependymal layer [384]. Thus, disruption of, or functional alteration to, both the ependymal epithelium and neural stem/progenitor cells, may alter the balance in CNS cells between injury and self-repair, and thus force the system toward neurodegeneration [385]. In this perspective, we can speculate that, in addition to alterations in epithelial cells, the observed inhibition of NSC proliferation as induced by the pro-adhesive deamidated-Cp might exert a deleterious *in vivo* effect on reparative systems, and thus facilitate neurodegeneration. An anomalous engagement of NSC's integrins might also interfere with NSC-niche organization, as well as with functions that are

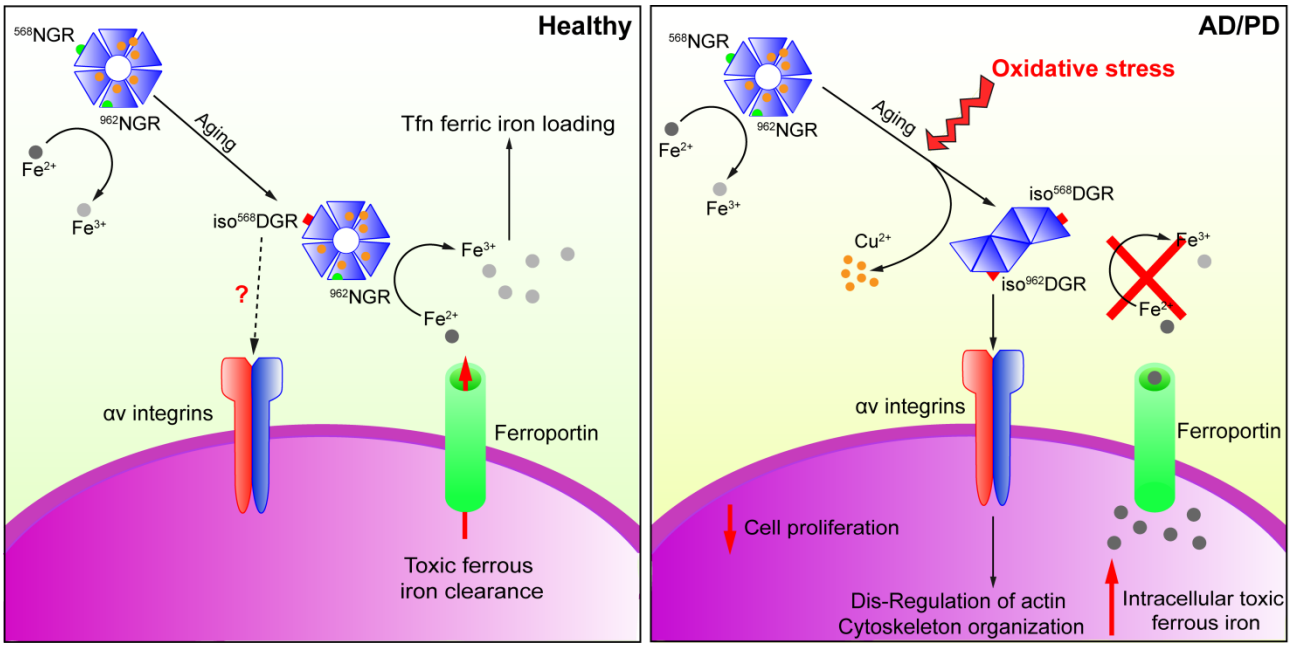

Figure 3.4.2: schematic representation of the mechanism of action of the deamidated-Cp we purpose.

mediated by interaction with the extracellular matrix [27, 386].

Further potential targets for deamidated Cp include the specialized epithelial cells of the ependymal layer and choroid plexus, which are directly in contact with the CSF. Morphometric and functional alterations to choroid plexus epithelia have been reported as age-related deficiencies that are exacerbated in AD by β-amyloid accumulation, which in turn can lead to CSF barrier dysfunction [387, 388]. Thus, the epithelial cell proliferation blockage and the cell cycle arrest we observed as consequences of deamidated-Cp treatment might approximate the detrimental effect that occurs *in vivo* on choroid plexus epithelia. Our characterization of the commercial line of human primary choroid plexus epithelial cells (HCPEpiC) allow us to perform, in the next future, proliferation, secretion and barrier-maintenance experiments after deamidated-Cp stimulation also on this highly specific cell type.

In conclusion, our findings suggest that Cp oxidation in soluble and possibly in GPI-Cp forms might play a role in the pathogenesis of PD by contributing to iron dismetabolism, and that Cp should possibly be taken into consideration as a putative target of antioxidant therapies [182], though Cp *ex vivo* modifications suggest to keep the therapeutic approach aimed to the prevention of the upstream events occurring in patients rather than the Cp replacement; the study of these events (which can be responsible also of other protein-modifications seen in PD patients, like α-syn) would be important for the understanding of the pathology and for the design of a therapy which can be beneficial not only for the Cp activity alone, but for the CNS activity *in toto*. The putative pathogenic role of Cp is mirrored by variations in patient CSF Cp electrophoretic patterns, variations that, correlating with disease stage, can be considered as potential markers for the evaluation of oxidative damage in the CNS. Our results show also that Asn deamidation, which may occur in Cp upon aging, can convert this protein into an *iso*DGR-containing ligand of αv integrins, which can transduce an integrin-mediated intracellular signalling. In particular, oxidation-induced structural changes foster the NGR-to-*iso*DGR transition at the NGR site buried in the protein structure. Even though the mechanism we described results from mainly *in vitro* observations, the *ex vivo* evidences that the CSF from AD and PD patients promotes Cp deamidation suggest that Cp modifications might occur also in patients. Further investigations are needed to assess the biological role of *in vivo* Cp-deamidation, and the consequences for neurodegenerative diseases. The Cp alterations induced by the pathological oxidative environment, might contribute to the pathological mechanisms of neurodegeneration via two distinct processes (Figure 4.1): firstly, the described loss of ferroxidase function and consequent intracellular iron retention and secondly, by a *de novo* functional gain in integrin binding that enables transduction of an anomalous/unwanted intracellular signaling, which might represent a novel pathological mechanism that affects several cell types.

5 Materials and methods

5.1 Methods related to Chapter 1 results

5.1.1 Patients

Having secured approval from the ethical review board of the hospital, and informed consent from patients, CSF samples (0.8–1 ml) were collected by means of lumbar puncture in the framework of the Institute of Experimental Neurology INSPE-BioBank (San Raffaele Scientific Institute, Milan). The analyzed groups were as follows: sporadic PD (n=14; 8 males and 6 females), sporadic amyotrophic lateral sclerosis (ALS) (n = 16; 5 males and 11 females), peripheral neuropathies (PN) (n = 13; 8 males and 5 females), Alzheimer's disease (AD) (n=14; 5 males and 9 females), and healthy controls (CN) (n=15; 7 males and 8 females). Table 5.1 summarizes the demographic and clinical features of the patients and control subjects enrolled on this discovery study. All patients were at first diagnosis and drug-free. Current criteria for the diagnosis of PD [389], of ALS [390], and of AD [391] were used for the admission of patients into the study. PN diagnosis was as described by Conti et al. [392]. The Unified Parkinson's Disease Rating Scale (UPDRS) [393, 394] was used to grade the disease. ALS and PN samples were from aliquots collected for previous studies [350, 392]. Exclusion criteria consisted of the following: HIV or HCV (hepatitis C virus) seropositivity, the appearance of other neurodegenerative diseases or previous cerebral ischemic events, and severe metabolic disorders (e.g., diabetes). Control CSF was obtained from patients who underwent lumbar puncture on account of a suspected neurological disease and who proved to be normal and free from pathological alterations after complete CSF analysis and thorough clinico-neuroimaging assessment. Sample selection ensured that age and gender distributions were homogeneous with those of the PD patients.

5.1.2 Two-dimensional electrophoresis, Western blot and image analysis

Immediately after collection, the CSF samples were centrifuged at 4°C to eliminate cells, and protein concentrations were determined. The samples were then either immediately processed, or stored at -80°C in an N_2-supplemented atmosphere to avoid oxidation. Protein samples (30 µg) were resuspended in twodimensional electrophoresis (2DE) buffer (8 M urea, 4% w/v CHAPS, 65 mM DTT, 0.2% v/v IPG buffer 3-10NL, and applied to 7 cm IPG strips pH 3-10NL (GE

	PD				CN			ALS			PN			AD		
	Sex	Age	[C] (mg/ml)	UPDRS	Sex	Age	[C] (mg/ml)	Sex	Age	[C] (mg/ml)	Sex	Age	[C] (mg/ml)	Sex	Age	[C] (mg/ml)
1	M	65	0.38	17	M	70	0.37	M	61	0.32	F	53	0.57	M	61	0.51
2	F	80	0.85	49	F	50	0.20	M	71	0.17	F	60	0.35	M	70	0.44
3	F	68	0.51	40	M	71	0.38	M	63	0.28	F	69	0.75	F	78	0.19
4	F	64	0.37	47	M	62	0.16	M	64	0.27	M	74	0.26	M	78	0.46
5	M	71	0.36	76	F	53	0.25	F	68	0.30	M	50	1.06	F	72	0.33
6	M	61	0.32	61	M	63	0.85	F	70	0.46	F	64	0.32	F	65	0.36
7	M	70	0.73	67	M	73	0.47	F	75	0.36	M	74	0.53	F	58	0.35
8	M	70	0.39	69	F	72	0.40	F	70	0.40	M	64	0.39	M	74	0.38
9	M	77	0.63	52	F	50	0.19	M	61	0.27	M	80	0.41	F	63	0.26
10	F	56	0.46	42	F	77	0.50	F	61	0.26	F	44	0.30	F	74	0.45
11	M	56	0.30	55	M	71	0.43	F	69	0.23	M	50	0.58	F	62	0.53
12	F	73	0.46	41	M	68	0.32	F	57	0.23	M	60	0.33	F	68	0.31
13	F	66	0.60	48	F	63	0.18	F	71	0.21	M	46	0.45	M	56	0.48
14	M	77	0.28	27	F	77	0.51	F	62	0.58				F	73	0.31
15					F	60	0.30	F	62	0.82						
16								F	76	0.30						
	8 M				7 M			5 M			8 M			5 M		
	6 F				8 F			11 F			5 F			9 F		
Mean		68.1	0.47			65.3	0.37		66.3	0.34		60.6	0.48		68.0	0.38
SD		1.98	0.17			9.03	0.18		5.63	0.16		11.5	0.22		7.23	0.10

Table 5.1: Demographic and clinical features of patients and controls. Gender: No statistical differences among groups (Fisher's exact test). Age: No statistical differences among groups (Student's t test). Protein concentration [C]: No statistical differences among groups except for PD versus ALS, p=0.008, and PN versus ALS, p=0.020 (Mann–Whitney test). [C], CSF total protein concentration.

Healthcare). The 2DE separations were performed as described by Conti et al. [350]; briefly, focusing was performed with an IPGphor system (GE Healthcare) at 50 µA max each IPG strip with a gradient voltage (5000 V max) for a total of 30 k•Vh. Strips were equilibrated for 15 min in 50 mM pH 8.8 Tris-HCl buffer containing 6 M urea, 30% glycerol, 2% SDS and 2% DTT, then for 15 min in the same buffer replacing DTT by 2.5% iodoacetamide. The strips were then transferred onto 10% acrylamide SDS-PAGE gels for the second dimension separation. Proteins resolved by 2DE or by SDS-PAGE were electrotransferred onto nitrocellulose membranes and Western blot (WB) was performed as described by Conti et al. [350] incubating the membranes, previously blocked with 5% dry-milk in TBS, 1h at 20°C with a sheep anti-human Cp antibody (Abcam) diluted in 5% milk-TBS. After washing with 0.5/milk-TBS, the reactivity was revealed by incubation (1h at 20°C) with secondary donkey-anti-goat Ig antibody conjugated with horse radish peroxidase (Abcam) followed by enanched chemiluminescence (ECL, GE-Healthcare) reaction and films exposure.Images were acquired by means of a laser densitometer (GE Healthcare), and evaluation of relative abundance of Cp isoforms consisted in the analysis of optical density normalized to percentage by means of Progenesis PG240 software (Nonlinear Dynamics).

5.1.3 CSF oxidation by treatment with Fe-citrate and H_2O_2

Proteins (100 µg) were oxidized by incubation (3 h at 37°C) with differing concentrations of hydrogen peroxide (1, 5, and 10 mM) and were subsequently resolved by 2DE or SDS-PAGE; Cp profile was identified by WB. For the assessment of correlation between specific oxidative modifications (carbonylation) and Cp pI shift, CSF proteins were incubated (5 h at 37°C) with 25 mM sodium ascorbate with or without 100 µM ferrous chloride to induce protein carbonylation (as indicated by the OxyBlot kit manufacturer) [184]. Carbonylation was analyzed by means of the Oxy-Blot Protein Oxidation Detection Kit (Millipore Bioscience Research Reagents) on the basis of carbonyl group derivatization with 2,4-dinitrophenilhydrazine (DNPH).

Cp carbonylation was analyzed in two pools of CSF that were harvested from all PD patients and from CN subjects, respectively. Equal amounts (5 µg) of CSF proteins were taken from each patient to generate a total 70 µg of proteins per pool. After derivatization with DNPH, proteins were resolved either by 2DE or by SDS-PAGE, and carbonyl groups were detected by Western blot with an anti-DNPH antibody, while Cp profiles were detected by means of an anti-Cp antibody on the same nitrocellulose membrane.

5.1.4 Bathophenanthroline assay

Cp ferroxidase activity was analyzed by bathophenanthroline (Btp) assay. Purified Cp (1.25 µg) (Alexis) was incubated with 80 µM $FeSO_4$ (ferrous form) and analyzed with a solution of 1 mM Btp in acetate buffer, pH 6.2, at five intervals (0, 15, 30, 45, and 60 min). Decrease in Btp-Fe^{2+} complex absorbance at 535 nm derives from ferrous iron oxidation into ferric form (F^{3+}). Cp ferroxidase activity was also analyzed after *in vitro* oxidation by hydrogen peroxide treatment, as described above (1, 5, 10 mM H_2O_2; Cp vs H_2O_2 molar ratio, 1/3000, 1/15,000, 1/30,000, respectively), and after heat treatment (99°C for 30 min). To identify the interference of copper released during protein oxidation/denaturation, we performed Btp assay without Cp, but in the presence of 20 nM Cu.

5.1.5 Cell cultures and iron challenge

The human neuroblastoma SH-SY5Y (American Type Culture Collection) was cultured (37°C in a 5% CO2 atmosphere) in a 1:1 mixture of Eagle's Minimum Essential Medium (ATCC) and F12 medium (ATCC) supplemented with 10% fetal bovine serum.

Primary rat hippocampal neurons (~80% purity) or pure astrocytes were prepared from 2- to 3-d-old Sprague Dawley rats, in respective accordance with Codazzi et al. [395] and Bettegazzi et al. [396]. The Institutional Animal Care and Use Committee of the San Raffaele Scientific Institute approved the experimental procedures. Briefly, after subdivision of hippocampus matter into small sections, the tissue was incubated into Hanks solution that contained 3.5 mg/ml trypsin type IX (Sigma-Aldrich) and 0.5 mg/ml DNase type IV (Calbiochem). After mechanical dissociation, cells were plated onto poly-ornithine-coated coverslips and maintained in MEM supplemented with 5% fetal calf serum, B27 supplements (Invitrogen), and 3 µM Ara-C (1-β-D-cytosinearabinofuranoside) (Sigma-Aldrich). Neuron cultures were maintained at 37°C in a 5% CO_2 humidified incubator and used as of 8-10 d from plating.

Pure astrocytes were grown in MEM supplemented with 10% horse serum. Two steps of overnight

shaking at 230 rpm were performed to induce selective detachment of microglia. Upon achievement of confluence, astrocytes were trypsinized and replated onto poly-lysine-coated plastic multiwells. Experiments were performed within 3 d of replating. Protein expression was tested in cell lysates by WB as realized with anti-H-Ferritin [397] (donated by Dr. S. Levi, Vita-Salute San Raffaele University, Milan, Italy) and with anti-Ferroportin (Fpn) (Abcam). To induce iron loading, cells were cultured for 20 h in a medium containing 10 and 5% serum for the SH-SY5Y cell line and the primary culture, respectively. The medium was supplemented with ferric ammonium citrate (FAC) (100 μM) and with ascorbic acid (200 μM) to cause iron reduction and its internalization by DMT1 transporter. Extracellular iron and ascorbate (Asc) were subsequently removed, and the expression of ferroportin and ferritin were analyzed after further cell incubations (24 h), either with serum-free medium for SH-SY5Y or with low serum (1.25% derived from the presence of neuron culture conditioned medium) for primary neuron, in the absence of Cp or with functionally active purified Cp (5 μg/ml), or with inactive oxidized Cp. This latter was obtained by treatment with 5 mM hydrogen peroxide, as described above. Iron loading was also monitored through evaluation of ^{55}Fe retained in, and released by, the SH-SY5Y cells. SHSY5Y cells (2 x 10^5 cells/well, in triplicate) were iron loaded, as previously described, with FAC (95 μM) supplemented with 5 μM ^{55}Fe-citrate (PerkinElmer) as a tracer. After 20 h incubation, the cells were washed, and one aliquot was kept for iron-loading evaluation and considered as 100%, while other aliquots underwent further incubation (24 h) in 250 μl of serum-free medium containing 60 μM apo-transferrin (Sigma-Aldrich), with or without extracellular ferroxidase activity, as previously described. After 24 h of incubation, media were collected, and cells were washed and lysed. Media (50 μl) and cell lysates (10 μl) were each mixed with 0.5 ml of Ultima Gold (Packard) and counted (3 min) in a scintillation counter (Packard). Total protein content of cellular extracts was used to normalize radioactive counts both of lysates and of related media. Results were used to evaluate the differences in percentages of total iron contents.

To determine whether GPI-anchored membrane Cp as expressed by astrocytes was also susceptible to oxidation, we cultured pure rat astrocytes primary cultures either under resting conditions or upon treatment for 1 h with 0.6 mM H_2O_2. Cell lysates (30 μg) were then analyzed by 2DE and WB to reveal the Cp electrophoretic pattern.

5.1.6 Densitometric analysis

Anti-Cp reactivity was quantified by laser densitometric analysis (GE Healthcare), as normalized by protein loading and total protein staining. The distribution of the Cp isoforms was evaluated by densitometric analysis of 2D spot optical density, which in turn was normalized as a percentage of total anti-Cp antibody reactivity. Signals obtained from OxyBlot were quantified by means of densitometric analysis and normalized by total protein loading. Ferritin expression was evaluated by densitometric analysis, and normalized by β-tubulin expression for SH-SY5Y cell line, and by βIII-tubulin expression for primary neuron.

5.1.7 Statistical analysis

Gender distribution was assessed by 2 x 2 contingency table analysis, which in turn used Fisher's exact test and two-tailed *p* value. Continuous data (age distribution, CSF protein concentration, and spot/band volume) were evaluated by unpaired Student's t test, if the data passed the normality test for Gaussian distribution as assessed by the Kolmogorov-Smirnov test, or were evaluated by Mann–Whitney test; two-tailed p value was used for the comparison of two means and SE. Parametric one-way ANOVA was used to evaluate the statistical difference between three or more independent groups; postanalysis performed with Tukey's multiple-comparison tests was included. The receiver operating characteristic (ROC) curve was used to define the ability of the assay to discriminate between groups, and to define the threshold value at which optical density (OD) gave the best ratio between sensitivity and specificity. Correlation analysis was evaluated as Pearson's coefficient (r). In all analyses, $p<0.05$ was considered to be statistically significant. The analysis was performed with Prism, version 4.03, software (GraphPad).

5.1.8 Image processing and unsupervised machine learning techniques for 2DE-Western blot image analysis (performed by Eng. C. V. Cannistraci)

Denoising was executed by nonlinear spatial adaptive image filtering, and background removal

was obtained by 3D-morphological operators [398]. After preprocessing, each 2DE-WB image was aligned by raw vectorization of its pixel intensity; each pixel intensity accordingly became a feature in a vector that characterized the Cp image sample. To implement the subsequent machine learning analysis, features (pixels) with small profile variance were filtered out to reduce the number of low informative features [399]. Classification of Cp profiles was provided by the combined application of (1) unsupervised machine learning approaches designed to reduce linear dimensionality and executed by principal component analysis, and of (2) minimum curvilinear affinity propagation (MCAP) as a method for clustering analysis [400]. Said tool was applied to the two-dimensional projection space obtained as the outcome of dimensionality reduction.

5.2 Methods related to Chapter 2 results

5.2.1 Patients

For detailed description see chapter 5.1.1. The analysed groups were: Alzheimer's disease patients (AD, n= 16) and healthy controls (CN, n= 16). Table 5.2 summarizes the demographic and clinical features of the patients and control subjects enrolled on this discovery study.

5.2.2 Cell cultures and reagents

Human glioblastoma T98G, keratinocyte HaCaT and endothelial EA.hy926 cell lines (America Type Culture Collection, ATCC) were cultured (37°C in a 5% CO_2 atmosphere) in DMEM medium (ATCC) supplemented with L-glutamine, and 10% fetal bovine serum (FBS). Human integrins α5β1, αvβ3, and αvβ5 (Immunological Sciences), recombinant αvβ6 and αvβ8 (R&D System), and human plasma purified Cp (Alexis Biochemicals) were used.

5.2.3 Oxidation and asparagine accelerated aging treatments

Oxidation and accelerated Asn-aging treatments were performed by incubating purified Cp at 37°C in various buffers as described below. Oxidized Cp was prepared incubating for 16h at 37°C Cp (1 mg/ml) in PBS buffer containing 10 mM H_2O_2 solution. Deamidated Cp was prepared incubating for 16h at 37°C Cp (1 mg/ml) in 100 mM ammonium bicarbonate (AmBic) buffer, pH 8.5. This condition is known to favour Asn deamidation at the NGR site [321]. Before use in the assays Cp was dyalized against PBS using Slide-A-lyzer dialysis cassette 10K MWCO (Pierce Biotechnologies). Oxidized and deamidated Cp was obtained by combining the above treatments. Aging of Cp in CSF was performed by adding purified-Cp (20 µg/ml, final concentration) to CSF either from healthy subjects or from AD patients. CSF samples

Table 1. Demographic and clinical features of patients and controls

	CN			AD			
	Sex	Age	[C] mg/ml	Sex	Age	[C] mg/ml	MMSE
#1	M	70	0.37	F	56	0.41	22
#2	M	68	0.32	M	75	0.38	18
#3	M	71	0.38	M	71	0.39	21
#4	M	62	0.16	M	73	0.38	18
#5	M	63	0.85	M	72	0.33	7
#6	M	54	0.25	F	72	0.41	18
#7	F	72	0.40	M	69	0.29	18
#8	F	77	0.50	M	64	0.33	18
#9	M	61	0.34	F	73	0.45	13
#10	M	70	0.28	M	79	0.61	24
#11	F	72	0.41	F	78	0.33	21
#12	M	79	0.55	F	77	0.33	16
#13	M	80	0.40	M	70	0.24	25
#14	F	84	0.23	M	77	0.41	27
#15	M	81	0.29	F	79	0.53	29
#16	M	81	0.39	M	86	0.49	19
	12M/4F	71.5±8.53 m±sd	0.38±0.15 m±sd	10M/4F	73.1±6.84 m±sd	0.40±0.09 m±sd	

Table 5.2: Demographic and clinical features of patients and controls.Gender: no statistical differences among groups (Fischer's exact test). Age: no statistical differences among groups (Mann-Whitney test). Protein concentration [C]: no statistical differences among groups (Mann-Whitney test). CN= controls; AD= Alzheimer disease; [C] mg/ml= CSF total protein concentration; MMSE= Mini Mental State Examination; m= mean; sd= standard deviation.

were then left to incubate for different time (0, 3, 6, 9, and 12 days) at 37°C under nitrogen conditioned atmosphere, in order to avoid the exposure to atmospheric oxidative-environment.

5.2.4 Binding of Cp to integrins and competition with isoDGR peptide

α5β1, αvβ3, αvβ5, αvβ6 and αvβ8 integrin (1 µg/ml in PBS with Ca^{2+}/Mg^{2+}; DPBS, Cambrex), were added to 96-well polyvinylchloride plates (BD Biosciences) and incubated 12 h at 4°C. Subsequent steps were carried out at 20°C. After blocking (3% BSA-PBS) the plates were filled with: Cp solutions (2-20 ug/ml in *binding buffer*; 25 mM Tris-HCl, pH 7.4, 150 mM NaCl, 1 mM $MgCl_2$, 1 mM $MnCl_2$, 0,05% Tween, 1% BSA); or CSF samples from healthy subjects or AD patients supplemented with Cp (prepared as described above, diluted in binding buffer) and incubated for 2 h. Binding was detected using a polyclonal sheep anti-human Cp Ab (Abcam ab8813) followed by a secondary HRP-conjugate Ab (Abcam) and by o-phenylendiamine chromogenic substrate. Competitive binding assays were performed by mixing 10 µg/ml of either the acetyl-CisoDGRCGVRSSSRTPSDKY peptide (isoDGR-peptide) or the control peptide CARACGVRSSSRTPSDKY (ARA-peptide) [335] with Cp-ox/Ambic solutions (20 µg/ml) or mixing isoDGR-peptide (30 µg/ml) with CSF samples spiked with Cp (20 µg/ml). The mixtures were added to microtiter plates coated with integrin and the binding assay was carried out as described above. Cp bound to the αvβ6 coated plates was analyzed for biochemical features as follow; after the binding the plates were washed and incubated with Laemmli buffer (5 min at 100°C) to promote protein detachment, the solution was then collected and subjected to SDS-PAGE and Western blot (WB) analyses as described in 5.1.2 with a polyclonal anti-human Cp Ab (Abcam). Images were acquired using a laser densitometer (Molecular Dynamics).

5.2.5 Cell adhesion assay and protein L-isoaspartyl methyltransferase (PIMT) treatment

96-well polyvinyl chloride microtiter plates were coated with either untreated-, treated-Cp or Cp immunoprecipitated (see below) after aging in healthy or AD CSF (1-20 µg/ml in 50 mM Na_3PO_4, pH 7.3, 150 mM NaCl, 16 h at 4°C). After washing and blocking with 3% BSA-DPBS the plates were seeded with HaCaT, EA.hy926, T98G cells diluted in 0.1% BSA-DMEM (40,000 cells/well), and left to adhere for 3 h at 37°C. Adherent cells were fixed with 3% paraformaldehyde, 2% sucrose in PBS (pH 7.3), and stained with 0.5% crystal violet (Fluka Chemie, Buchs, Switzerland); adhesion evaluated as adsorbance at 570 nm. Cells spreading was evaluated comparing cell's area (pixels) automatically detected by image software analysis (Progenesis PG240, Nonlinear Dynamics) in different microscopy fields for each treatment conditions. For PIMT treatment, plates coated as described above, were washed and filled with 45 µl of 0.02 mM S-adenosyl-L-methionine in 50 mM Na_3PO_4, pH 6.8 and 5µl of PIMT solution (from IsoQuant isoaspartate detection kit; Promega), and incubated at 37°C for 16 h. Then plates were washed, and cell adhesion assay performed as described above.

5.2.6 Immunoprecipitation of Cp from CSF

After incubation either in healthy or AD CSF, spiked purified Cp was immunoprecipitated using protein-G Agarose Beads (Invitrogen) coated with an anti-Cp antibody (Abcam ab8813). The antibodies were crosslinked to the beads with 20 mM dimethyl pimelimidate (Sigma) and added to the CSF supplemented with Cp; the solution was then incubated for 24 h at 4°C under gently stirring. Beads were washed and Cp was eluted with 0.1 M glycin solution, pH 2.5; samples were immediately diafiltered with PBS using an Amicon filter device.

5.2.7 Bathophenanthroline assay

Ferroxidase activity of Cp after aging in CSF was evaluated on immunoprecipitated Cp by bathophenanthroline (Btp) assay as in 5.1.4. Briefly, immunoprecipitated Cp (1.25 µg) was incubated with 80 mM $FeSO_4$ (ferrous form) and analyzed after 1 h with a solution of 1 mM Btp in acetate buffer, pH 6.2. Decrease in Btp-Fe^{2+} complex absorbance at 535 nm derives from ferrous iron oxidation into ferric form (Fe^{3+}).

5.2.8 Mass spectrometry analysis

Samples were dialyzed against digestion buffer (50 mM Na_3PO_4 pH 7.3, 150 mM NaCl, 25 mM HEPES) and incubated 2 h at 20°C with trypsin (10 ng/µl, Roche). Digested samples were desalted (Stage tips C18, ThermoScientific) and injected in a capillary chromatographic system (EasyLC, Proxeon Biosystem). Peptide separations occurred on a 25 cm reverse phase silica capillary column, packed with 3-µm ReproSil 100Å C18 AQ. A gradient of acetonitrile

eluents was used to achieve separation (0.15 µL/min flow rate). Mass spectrometry (MS) analysis was performed by nanoLC-MS/MS using an LTQ-Orbitrap (ThermoScientific) equipped with a nanoelectrospray ion source (Proxeon Biosystems). Full scan spectra were acquired with the lock-mass option, resolution set to 60,000, and mass range from *m/z* 350 to 1700 Da. The six most intense doubly and triply charged ions were selected and fragmented in the ion trap. All MS/MS samples were analyzed using Mascot (v.2.2.07, Matrix Science) and X!Tandem (within Scaffold software, v.2_06_00, 2007, Proteome Software Inc.) search engines to search the UniProt_Human Complete Proteome_cp_hum_2012_07. Searches were performed with 3-missed cleavages allowed, N-terminus-acetylation, methionine oxidation and deamidation of asparagine/glutamine as variable modifications. Mass tolerance was set to 5 ppm and 0.6 Da for precursor and fragment ions, respectively. Scaffold was used to validate MS/MS based peptide and protein identifications. Protein thresholds were set to 99.0% and two peptides minimum while peptide thresholds were set to 95% minimum.

5.2.9 Circular dichroism and melting curves

Circular dichroism (CD) spectra were acquired for Cp and Cp after oxidative and aging treatments (at 1 µM in 50 mM PBS pH 7), on a Jasco J-815 CD spectrometer at 20°C. Each spectrum was averaged using four accumulations collected in 0.1 nm intervals with an average time of 0.5 sec. The protein spectra were corrected by subtracting the corresponding buffer spectra and then smoothed. The observed ellipticity (mdeg) was converted into molar residue ellipticity [Θ] (deg cm ^{2} dmol^{-1}), which is the circular dichroism corrected for concentration. Melting curves were calculated recording CD spectra in continuous from 20 °C to 96°C (1°C intervals) in a wavelength range from 190 to 260 nm in order to achieve the better resolution. Melting temperature (Tm) was calculated by nonlinear fitting Boltzmann sigmoidal with Prism V4.03 software (GraphPad Inc.).

5.2.10 Molecular dynamics simulations and docking calculations (performed by Dr. A. Spitaleri)

Homology modeling: I-TASSER server was used to predict the secondary and tertiary structure of αvβ6 integrin [401]. *Molecular dynamics (MD) simulations*: were performed on Cp wild type (P00450; PDB 2j5w), using the GROMACS 4.5.4 package [402] with the optimized parameters for liquid simulation (OPLS) force field. The ^{568}isoDGR-Cp and αvβ6 systems have been simulated in the same manner. Three independent 50 ns long MD simulations (150 ns production run) were performed for Cp to allow for better conformational sampling, while three independent 10 ns long MD simulations (30 ns) were performed for αvβ6 in order to get a set of structures to be used in docking calculations. All the analyses were performed using the Gromacs utilities on the last 40 ns of each simulation concatenated in a single trajectory (120 ns total). In particular, cluster analysis were performed using gromos algorithm. *Docking calculations*: Docking calculations of ^{568}isoDGR-Cp on the globular head of the extracellular part of αvβ6 have been performed using the docking program HADDOCK2.0 [403] with the OPLS force field. We have docked a bundle of 27 ^{568}isoDGR-Cp structures onto a bundle of 10 αvβ6 structures, which correspond to the centers of the clusters obtained from MD simulations. The protocol follows a three-stage docking procedure: (a) randomization of orientations and rigid body minimization, (b) simulated annealing in torsion angle space, and (c) refinement in Cartesian space with explicit water. Ambiguous interaction restraints (αvβ6: residues 150, 218, 506, 547, 548, 601, 815; ^{568}isoDGR-Cp: residues 568 to 570) were derived from the known interactions of the isoDGR motif of the cyclic-peptide with αvβ6 [355]. The best 200 solutions in terms of intermolecular energies were selected for a semiflexible simulated annealing in which the side-chains of αvβ6 and of the ^{568}isoDGR-Cp located at the binding interface were allowed to move in a semi-rigid body docking protocol to search for conformational rearrangements. The models were then subjected to a water refinement step. The single best docked solutions were analyzed according to hydrogen bonds, salt bridges contact and buried surface accessibility.

5.2.11 Statistical Analysis

Categorical data were analyzed by using Fisher's exact test and two-tailed p value. Continuous data were evaluated by unpaired student's t-test, if the data passed the normality test for Gaussian distribution as assessed by the Kolmogorov-Smirnov test, or were evaluated by Mann Whitney test; two-tailed p value was used for the comparison of two means and standard error. In all analyses, $p<0.05$ was

considered to be statistically significant. The analysis was performed with Prism V4.03 software (GraphPad Inc.).

5.2.12 Reverse phase protein array (RPPA) analysis

HaCaT cells were incubated (30 or 120 minutes) with either Cp or aged/oxidized-Cp. Cells lysates obtained with Zeptosens CLB1 Lysis Buffer™(Bayer) were spotted on arrays and analyzed using Zeptosens custom service (Bayer). A set of 40 antibodies (Abs, see Table 5.3), either specific for protein expression or for residues phosphorylation, that identify 25 pairs of phosphorylation rate for 16 different proteins belonging to the integrin signaling pathway (www.kegg.com/kegg-bin/show pathway?ko04510; and ko04810) were reacted in a standard Zeptosens profiling assay. Mean Referenced Fluorescence Intensity (RFI) obtained from Abs reactivity were used to evaluate the proportion of specific residues phosphorylation [RFI-(phos-protein-x) / RFI-(protein-x)] for each protein. Then, the phosphorylation proportion of the cell treated with aged/oxidized-Cp were compared with that of the time-related control Cp (Cp-ox/Cp 30 min; Cp-ox/Cp 120 min) as to define whether the phosphorylation rate was unaffected (value = 1), induced (value > 1) or inhibited (value<1) by Cp-ox. Phosphorylation rate was analyzed by hierarchical clustering performed with Mev4.6 v10.2 software [404]; the 25 data series of protein phosphorylation rate in the 2 different conditions (Cp-ox/Cp 30 min; Cp-ox/Cp 120 min) were clustered into groups on the basis of the distances between the data series reported as covariance correlation.

Zeptosens Ref #	Antibody Specificity	Modification	Position	Species
1-83	Akt			rabbit
1-57	Akt	phospho	Ser473	mouse
1-55	Akt	phospho	Thr308	rabbit
4-14	beta-Catenin			rabbit
4-16	beta-Catenin	phospho	Ser33/37,Thr41	rabbit
5-13	beta-Catenin	phospho	Thr41,Ser45	rabbit
3-47	c-Jun			mouse
2-55	c-Jun	phospho	Ser73	rabbit
2-52	CrkL			mouse
2-53	CrkL	phospho	Tyr207	rabbit
3-17	FAK1			rabbit
5-62	FAK1	phospho	Tyr397	rabbit
4-75	GSK-3-alpha/beta	phospho	Ser21/Ser9	rabbit
4-73	GSK-3-beta			rabbit
1-69	GSK-3-beta	phospho	Ser9	rabbit
2-75	JAK1			rabbit
2-49	JAK1	phospho	Tyr1022,Thr1023	rabbit
1-37	MEK1			mouse
2-22	MEK1/2			rabbit
4-42	MEK1/MEK2	phospho	Ser217/221,Ser221/225	rabbit
1-52	p44/42 MAPK (ERK1/2)			rabbit
1-82	p44/42 MAPK (ERK1/2)	phospho	Thr202/185,Tyr204/187)	rabbit
5-06	PDK-1			rabbit
5-07	PDK-1	phospho	Ser241	rabbit
2-62	PKC (pan)	phospho	Ser660 (beta-2)	rabbit
4-76	PKC-alpha			mouse
4-77	PKC-alpha	phospho	Thr638	rabbit
4-78	PKC-gamma			rabbit
4-79	PKC-gamma	phospho	Thr514	rabbit
4-80	PKC-gamma	phospho	Thr655	rabbit
5-09	PTEN			rabbit
5-08	PTEN	phospho	Ser380,Thr382,Thr383	rabbit
4-69	Raf	phospho	Ser259	rabbit
4-70	Raf	phospho	Ser338	rabbit
3-14	Raf1 (C-12)			rabbit
5-34	SAPK/JNK			rabbit
2-09	SAPK/JNK	phospho	Thr183,Tyr185	rabbit
5-51	Src			rabbit
5-53	Src	phospho	Tyr527	rabbit
5-52	Src (family)	phospho	Tyr416	rabbit

Table 5.3: List of antibodies used in integrins signaling pathway analysis performed by reverse phase protein array (Zeptosens™, Bayer).

5.3 Methods related to Chapter 3 results

5.3.1 Patients

For details see chapter 5.1.1. The analysed groups were: sporadic PD (n= 21), peripheral neuropathies (PN, n= 11) and healthy controls (CN, n= 16). Table 5.4 summarizes the demographic and clinical features of the patients and control subjects enrolled on this discovery study.

5.3.2 Oxidation and aging treatments of Cp and CSF

In-vitro accelerated aging under oxidative conditions was performed incubating purified Cp (Alexis biochemical) 16 h at 37°C with 10 mM H_2O_2 in 100 mM ammonium bicarbonate buffer pH 8.5 (ox-AmBic) (see 5.2.3). Aging of purified-Cp *ex-vivo* in CSF was achieved by incubating Cp (20-80 µg/ml) in CSF from healthy subjects or from patients, at 37°C (3-12 days) under nitrogen-conditioned atmosphere, to avoid the exposure to atmospheric oxidative-environment; in selected experiments, aging was performed in presence of catalase (60 µg/ml, Sigma).

5.3.3 Cp immunoprecipitation from CSF

Immunoprecipitation of Cp from CSF was performed as in 5.2.6. For mass spectrometry analysis, samples were diafiltered against *digestion buffer* (50 mM Na_3PO_4 pH 7.3, 150 mM NaCl, 25 mM HEPES) and incubated 2 h at 20°C in the presence of trypsin (10 ng/µl, Roche).

5.3.4 Mass spectrometry analysis

Cp samples after trypsin digestion were desalted (Stage tips C18, Thermo Scientific) and injected in a capillary chromatographic system (EasyLC, Proxeon Biosystem). MS analysis was performed as in 5.2.8. To quantify deamidation the raw data were loaded into the MaxQuant software v1.2.2.5. Label-free protein quantification was based on the intensities of precursors. Peptides and proteins were accepted with a FDR of 0.01, two minimum peptides per protein with one unique.

5.3.5 Cp sensitivity to limited proteolysis

Spiked Cp after aging in CSF was immunoprecipitated from CSF and 100 ng were resuspended in 25 µl of *digestion buffer* followed by incubation for 2 h at 20°C in the presence of agarose-

Table 5.4: Demographic and clinical features of patients and controls. Gender: no statistical differences among groups (Fischer's exact test); Age: no statistical differences among Cn vs. PD; CN vs. PN p=0.018; PD vs. PN p=0.0025 (Student's t-test); Protein concentration [C]: no statistical differences among groups (Student's t-test). CN= controls; PD= Parkinson's disease; PN= peripheral neuropathies. [C] mg/ml= CSF total protein concentration; UPDRS= Unified Parkinson's Disease Rating Scale; m= mean; sd= standard deviation; LBD= Lewy body dementia; Pkins= Parkinsonism; D=dementia; cve= chronic vascular encephalopathy; at-PD= atypical PD; pnp-infl= peripheral neuropathy inflammatory; pnp-idio= pnp-idiopathic; pnp-tox= pnp-toxic.

	CN			PD				PN			
	Sex	Age	[C] mg/ml	Sex	Age	[C] mg/ml	Diagnosis	Sex	Age	[C] mg/ml	Diagnosis
#1	F	70	0.34	F	78	0.16	PD+LBD	F	50	0.23	pnp-infl
#2	M	72	0.32	M	80	0.47	Pkins	F	60	0.35	pnp-infl
#3	M	76	0.36	M	65	0.38	PD	F	69	0.75	pnp-infl
#4	F	43	0.21	M	61	0.32	PD+LBD	M	46	0.45	pnp-idio
#5	M	54	0.25	M	77	0.63	PD+LBD	M	75	0.26	pnp-infl
#6	M	72	0.27	F	56	0.46	PD	M	50	0.58	pnp-infl
#7	M	46	0.47	M	56	0.30	PD	M	80	0.41	pnp-idio
#8	F	62	0.34	F	66	0.60	PD	F	39	0.41	pnp-infl
#9	M	78	0.53	M	59	0.32	Pkins+D	M	31	0.77	pnp-infl
#10	F	59	0.35	F	56	0.19	PD+D	M	35	0.51	pnp-tox
#11	M	81	0.47	M	84	0.69	Pkins+LBD	F	64	0.32	pnp-tox
#12	M	76	0.52	M	69	0.20	Pkins+cve				
#13	M	82	0.43	M	62	0.29	at-PD+LBD				
#14	F	69	0.28	M	67	0.14	at-PD+LBD				
#15	M	73	0.57	F	75	0.34	Pkins+LBD				
#16	F	78	0.77	M	83	0.29	at-PD+LBD				
#17				M	80	0.39	Pkins+LBD				
#18				F	80	0.85	PD+LBD				
#19				F	68	0.51	PD				
#20				F	64	0.37	PD+LBD				
#21				M	71	0.43	PD+LBD				
	10M	68.2	0.41	13M	69.4	0.40		6M	54.5	0.46	
	6F	±12	±0.15	8F	±9.3	±0.18		5F	±16.4	±0.18	
		m±sd	m±sd		m±sd	m±sd			m±sd	m±sd	

immobilized trypsin (0.5 U) (Sigma). Trypsin was removed by centrifugation, and samples were analysed by SDS-PAGE and WB.

5.3.6 Hydrogen peroxide assay kit

For the evaluation of the hydrogen peroxide concentration in the CSFs, *Hydrogen Peroxide Assay Kit* (BioVision) was used. The principle of the assay is based on the reaction between the hydrogen peroxide and a non-fluorescent probe, (AmplexRed®: 10-acetyl-3,7-dihydroxyphenoxazine) which, the presence of hydrogen peroxide produces the red-fluorescent compound resorufin. For each sample, three replicate were made, diluting 0.5 µl of CSF 1:100 in the assay buffer provided by the manufacturer. Samples were assayed according to the protocol, and H_2O_2 concentration was evaluated as fluorescence at 590 nm.

5.3.7 Additional methods

Cp binding to integrins, competition with peptide and mass spectrometry analysis were performed as in 5.2; Western blot, Cp-ferroxidase activity (1.25 µg of immunoprecipited protein), and Cp-carbonylation assay (300 ng of immunoprecipited protein) were performed as in 5.1 and 5.2.

5.4 Methods related to Chapter 4 results

5.4.1 Patients

For details, see chapter 5.1.1. For the proliferation assay performed in this chapter, samples from #9 to #16 (both of CN and AD patients) of Table 5.2 were used.

5.4.2 Oxidation and asparagine accelerated aging treatments

See chapter 5.2.3.

5.4.3 Cell culture and reagents

Keratinocyte HaCaT human cell lines (America Type Culture Collection, ATCC) were cultured (37°C in a 5% CO_2 atmosphere) in DMEM medium (ATCC) supplemented with L-glutamine, and 10% fetal bovine serum (FBS). Neural stem cells (NSCs) isolated from the subventircular zone of postnatal day 40 FVB mice were isolated and cultured as previously described [405], and maintained in DMEM/F12 medium supplemented with epidermal growth factor and fibroblast growth factor-2. Human primary fibroblasts (obtained from skin biopsies and made available by Dr. G. Zerbini, OSR) were grown on DMEM medium supplemented with L-glutamine and 10% fetal bovine serum (FBS). Human choroid plexus epithelial cells (HCPEpiC, ScienCell, Carlsbad CA) were cultured as indicated by the manufacturer in EpiCM (ScienCell) medium supplemented with 2% fetal bovine serum (FBS) and 5 ml of epithelial cell growth supplement (ScienCell). Cells were used within three culture passage to exclude un-differentiation to mesenchimal cells

Human plasma purified Cp was from Alexis Biochemicals. Anti-Vimentin antibody was from Sigma (V6630) and anti-CK-19 from GeneTex (GTX27755). Anti-Transthyretin antibody (AB16006) was from Abcam and anti β-Tubulin was from Sigma (T6199). The antibodies used for the signaling analysis (FAK #3528, P-FAK #3283, ERK1/2 #9102, P-ERK1/2 #9101, GSK3β #9315, P-GSK3β #9336) were from Cell Signaling Technology.

5.4.4 Cell proliferation assay, cell cycle and apoptosis

HaCaT cells were cultured on a 96-well tissue culture treated plate (10,000 cells/well) for 16 h, then medium was replaced with medium containing 0.1% FBS and further cultured for 24 h. Next, the cells were incubated for 24 or 48 h with various doses (0, 1, 5 and 20 µg/ml) of untreated- or treated-Cp diluted in medium containing 0.1% FBS, or as control the same amount of BSA-ox/AmBic; cells were treated also for 72 h with 2 µg/ml of purified Cp immunoprecipitated after aging in healthy or AD CSF. For the treatments protocols, see chapter 5.2.3. Cell proliferation was determined by 3-(4,5-dimethylthiazol-2-yl)-2,5-diphenyltetrazolium bromide assay using a calibration curve generated by plating different amounts of cells. For short-term proliferation assay, NSCs cells were plated ($8x10^3$ cells/cm^2) in mitogen-containing medium in the presence of Cp, Cp-ox/AmBic or BSA-ox/AmBic (5 and 20 µg/ml); the formed neurospheres were collected 96 h later and mechanically dissociated. The total number of viable cells was assessed by Trypan Blue exclusion. Cells treated as for the proliferation assay (for 24-72 h) were used for flow cytometry evaluation of cell cycle and apoptosis using an LSR Fortessa cell analyzer (Becton Dickinson). Cells were labeled with a thymidine analog in order to separate cells in S phase from those in G0/G1 and G2/M exploiting the Click-

iT® EdU Flow Cytometry Assay Kit (Invitrogen,) containing the Alexa Fluor® 647 detection fluorophore and the Vybrant® DyeCycle™ Violet (Invitrogen) dye for total DNA detection. Cells were also stained with the FITC Annexin V Apoptosis Detection Kit I (BD Biosciences) to detect externalization of phosphatidylserine, an early apoptotic indicator.

5.4.5 Western blot analysis

For the HCPEpiC epithelial markers and signaling experiments, cells were lysed in lysis buffer (50 mM TRIS, 150 mM NaCl, 1 mM EDTA, 1% Triton-X, 0,1% SDS and protease inhibitors cocktail P2714 from Sigma) and quantified with Bradford assay (Bio-Rad, 500-0006). Subsequently, cell lysates were resolved by 10%-acrylamide SDS-PAGE and analyzed by Western blot with specific antibodies.

5.4.6 Anti Transthyretin immunofluorescence

HCPEpi cells were seeded (250.000 cells/coverslip) on 10 Ø mm sterile round coverslips treated with poly-L-lysine (2 µg/cm^2) and let to adhere for 24 h in complete EpiCM medium (37°C in a 5% CO_2 atmosphere). Cells were then washed 3 times in PBS (5 min each) and fixed for 15 min with a 4% PFA solution at 20°C. After 3 washing in PBS, fixed cell layer was blocked for 1 h with blocking solution (5% normal goat serum, 0.3% Triton-X in PBS) at 20°C and subsequently incubated with anti-transthyretin antibody diluted 1:250 in binding solution (1% BSA, 0.3% Triton-X in PBS). Following three washes the coverslips were incubated with donkey anti-rabbit Alexa-488 antibody (Life Technologies), and, after further three washing, the coverslips were incubated in Hoechst solution (Sigma) for 10 min at 20°C. Coverslips were then washed in H_2O and mounted on microscope slides for the inspection performed on Leica DM 5500B microscope equipped with epifluorescence.

5.4.7 Cell adhesion assay and protein L-isoaspartyl methyltransferase (PIMT) treatment

Adhesion assay with HCPEpi cells and PIMT treatment were performed as in 5.2.5.

5.4.8 HCPEpi cells stimulation

HCPEpi cells were cultured on a 10 cm tissue culture plate (1.000.000 cells/plate) for 16 h, then the medium containing 10% FBS was replaced with a medium containing 0.1% FBS and further cultured for 24 h. Next, the cells were incubated for 2 h with 10 µg/ml of untreated- or ox/AmBic-Cp diluted in medium containing 0.1% FBS. Subsequently cells were lysed and analyzed by WB.

6 References

1. Bradbury, M.W.B., *Physiology and Pharmacology of the Blood-Brain Barrier*. Handbook of Experimental Pharmacology. Vol. Vol. 103. 1992: Springer.
2. Gitlin, J.D., *Aceruloplasminemia.* Pediatr Res, 1998. **44**(3): p. 271-6.
3. Johanson, C.E., E.G. Stopa, and P.N. McMillan, *The blood-cerebrospinal fluid barrier: structure and functional significance.* Methods Mol Biol, 2011. **686**: p. 101-31.
4. Zecca, L., et al., *Iron, brain ageing and neurodegenerative disorders.* Nat Rev Neurosci, 2004. **5**(11): p. 863-73.
5. Falcao, A.M., et al., *The path from the choroid plexus to the subventricular zone: go with the flow!* Front Cell Neurosci, 2012. **6**: p. 34.
6. Corti, A. and F. Curnis, *Isoaspartate-dependent molecular switches for integrin-ligand recognition.* J Cell Sci, 2011. **124**(Pt 4): p. 515-22.
7. Madsen, E. and J.D. Gitlin, *Copper and iron disorders of the brain.* Annu Rev Neurosci, 2007. **30**: p. 317-37.
8. De Domenico, I., et al., *Ferroxidase activity is required for the stability of cell surface ferroportin in cells expressing GPI-ceruloplasmin.* EMBO J, 2007. **26**(12): p. 2823-31.
9. Johanson, C., *Aging rat brain: a model for analyzing interactions among CSF dynamics, ventriculomegaly and theβ -amyloid retention of alzheimer's disease.* Cerebrospinal Fluid Research, 2005. **2(Suppl 1):S6**.
10. Welch, K. and V. Friedman, *The cerebrospinal fluid valves.* Brain, 1960. **83**: p. 454-69.
11. Jelinek, R. and T. Pexieder, *Pressure of the CSF and the morphogenesis of the CNS. I. Chick embryo.* Folia Morphol (Praha), 1970. **18**(2): p. 102-10.
12. Veening, J.G. and H.P. Barendregt, *The regulation of brain states by neuroactive substances distributed via the cerebrospinal fluid; a review.* Cerebrospinal Fluid Res, 2010. **7**: p. 1.
13. Cavanagh, M.E., et al., *Comparison of proteins in CSF of lateral and IVth ventricles during early development of fetal sheep.* Brain Res, 1983. **313**(2): p. 159-67.
14. Zappaterra, M.D., et al., *A comparative proteomic analysis of human and rat embryonic cerebrospinal fluid.* J Proteome Res, 2007. **6**(9): p. 3537-48.
15. Martin, C., et al., *FGF2 plays a key role in embryonic cerebrospinal fluid trophic properties over chick embryo neuroepithelial stem cells.* Dev Biol, 2006. **297**(2): p. 402-16.
16. Lehtinen, M.K., et al., *The cerebrospinal fluid provides a proliferative niche for neural progenitor cells.* Neuron, 2011. **69**(5): p. 893-905.
17. Mashayekhi, F., et al., *Changes in cerebrospinal fluid nerve growth factor levels during chick embryonic development.* J Clin Neurosci, 2009. **16**(10): p. 1334-7.
18. Reiter, R.J., et al., *Melatonin as a free radical scavenger: implications for aging and age-related diseases.* Ann N Y Acad Sci, 1994. **719**: p. 1-12.
19. Weber, M.M., et al., *Rat somatotroph insulin-like growth factor-II (IGF-II) signaling: role of the IGF-I receptor.* Endocrinology, 1992. **131**(5): p. 2147-53.
20. Joseph D'Ercole, A. and P. Ye, *Expanding the mind: insulin-like growth factor I and brain development.* Endocrinology, 2008. **149**(12): p. 5958-62.
21. Valentino, K.L., I. Ocrant, and R.G. Rosenfeld, *Developmental expression of insulin-like growth factor-II receptor immunoreactivity in the rat central nervous system.* Endocrinology, 1990. **126**(2): p. 914-20.
22. Walter, H.J., et al., *Distinct sites of insulin-like growth factor (IGF)-II expression and localization in lesioned rat brain: possible roles of IGF binding proteins (IGFBPs) in the mediation of IGF-II activity.* Endocrinology, 1999. **140**(1): p. 520-32.
23. Johanson, C., et al., *Traumatic brain injury and recovery mechanisms: peptide modulation of periventricular neurogenic regions by the choroid plexus-CSF nexus.* J Neural Transm, 2011. **118**(1): p. 115-33.
24. Siegenthaler, J.A., et al., *Retinoic acid from the meninges regulates cortical neuron generation.* Cell, 2009. **139**(3): p. 597-609.
25. Haskell, G.T. and A.S. LaMantia, *Retinoic acid signaling identifies a distinct precursor population in the developing and adult forebrain.* J Neurosci, 2005. **25**(33): p. 7636-47.
26. Freese, J.L., D. Pino, and S.J. Pleasure, *Wnt signaling in development and disease.* Neurobiol Dis, 2010. **38**(2): p. 148-53.

27. Kazanis, I., et al., *Alterations in IGF-I, BDNF and NT-3 levels following experimental brain trauma and the effect of IGF-I administration.* Exp Neurol, 2004. **186**(2): p. 221-34.
28. Endoh, M., W.A. Pulsinelli, and J.A. Wagner, *Transient global ischemia induces dynamic changes in the expression of bFGF and the FGF receptor.* Brain Res Mol Brain Res, 1994. **22**(1-4): p. 76-88.
29. Chiaretti, A., et al., *Nerve growth factor and doublecortin expression correlates with improved outcome in children with severe traumatic brain injury.* J Trauma, 2008. **65**(1): p. 80-5.
30. Morganti-Kossmann, M.C., et al., *TGF-beta is elevated in the CSF of patients with severe traumatic brain injuries and parallels blood-brain barrier function.* J Neurotrauma, 1999. **16**(7): p. 617-28.
31. Sun, D., et al., *Basic fibroblast growth factor-enhanced neurogenesis contributes to cognitive recovery in rats following traumatic brain injury.* Exp Neurol, 2009. **216**(1): p. 56-65.
32. Ehrlich, P., *Uber die Beziehung chemischer Constitution, Vertheilung, und pharmakologischer Wirkung.* 1904.
33. Goldmann, E., *Vitalfarbung am Zentralnervensystem.* Abh Preuss Wissensch Phys-Math, 1913. **1:1-60**.
34. Mollgard, K., et al., *Cell junctions and membrane specializations in the ventricular zone (germinal matrix) of the developing sheep brain: a CSF-brain barrier.* J Neurocytol, 1987. **16**(4): p. 433-44.
35. Bayer SA, A.J., *Atlas of human central nervous system development.* CRC Press, Boca Raton, 2007. **vol 5**.
36. Netsky M, S.S., *The choroid plexus in health and disease.* 1975, Charlottesville: University Press of Virginia
37. Keep, R.F. and H.C. Jones, *Cortical microvessels during brain development: a morphometric study in the rat.* Microvasc Res, 1990. **40**(3): p. 412-26.
38. Motti, E.D., et al., *The capillary bed in the choroid plexus of the lateral ventricles: a study of luminal casts.* Scan Electron Microsc, 1986(Pt 4): p. 1501-13.
39. Betz, A.L., F. Iannotti, and J.T. Hoff, *Brain edema: a classification based on blood-brain barrier integrity.* Cerebrovasc Brain Metab Rev, 1989. **1**(2): p. 133-54.
40. Vorbrodt, A.W. and D.H. Dobrogowska, *Molecular anatomy of intercellular junctions in brain endothelial and epithelial barriers: electron microscopist's view.* Brain Res Brain Res Rev, 2003. **42**(3): p. 221-42.
41. Cornford, E.M., et al., *Mitochondrial content of choroid plexus epithelium.* Exp Brain Res, 1997. **116**(3): p. 399-405.
42. Redzic, Z.B. and M.B. Segal, *The structure of the choroid plexus and the physiology of the choroid plexus epithelium.* Adv Drug Deliv Rev, 2004. **56**(12): p. 1695-716.
43. Engelhardt, B., K. Wolburg-Buchholz, and H. Wolburg, *Involvement of the choroid plexus in central nervous system inflammation.* Microsc Res Tech, 2001. **52**(1): p. 112-29.
44. Keep, R.F. and H.C. Jones, *A morphometric study on the development of the lateral ventricle choroid plexus, choroid plexus capillaries and ventricular ependyma in the rat.* Brain Res Dev Brain Res, 1990. **56**(1): p. 47-53.
45. Singhrao, S.K., et al., *Differential expression of individual complement regulators in the brain and choroid plexus.* Lab Invest, 1999. **79**(10): p. 1247-59.
46. Wolburg, H., et al., *Claudin-1, claudin-2 and claudin-11 are present in tight junctions of choroid plexus epithelium of the mouse.* Neurosci Lett, 2001. **307**(2): p. 77-80.
47. Praetorius, J., *Water and solute secretion by the choroid plexus.* Pflugers Arch, 2007. **454**(1): p. 1-18.
48. Johanson, C.E., et al., *Multiplicity of cerebrospinal fluid functions: New challenges in health and disease.* Cerebrospinal Fluid Res, 2008. **5**: p. 10.
49. Broadwell, R.D., et al., *Transcytosis of protein through the mammalian cerebral epithelium and endothelium. III. Receptor-mediated transcytosis through the blood-brain barrier of blood-borne transferrin and antibody against the transferrin receptor.* Exp Neurol, 1996. **142**(1): p. 47-65.
50. de Lange, E.C., *Potential role of ABC transporters as a detoxification system at the blood-CSF barrier.* Adv Drug Deliv Rev, 2004. **56**(12): p. 1793-809.
51. Marques, F., et al., *Kinetic profile of the transcriptome changes induced in the choroid plexus by peripheral inflammation.* J Cereb Blood Flow Metab, 2009. **29**(5): p. 921-32.
52. Marques, F., et al., *Transcriptome signature of the adult mouse choroid plexus.* Fluids Barriers CNS, 2011. **8**(1): p. 10.
53. Reboldi, A., et al., *C-C chemokine receptor 6-regulated entry of TH-17 cells into the CNS through the choroid plexus is required for the initiation of EAE.* Nat Immunol, 2009. **10**(5): p. 514-23.

54. Serot, J.M., et al., *Monocyte-derived IL-10-secreting dendritic cells in choroid plexus epithelium.* J Neuroimmunol, 2000. **105**(2): p. 115-9.
55. Nathanson, J.A. and L.L. Chun, *Immunological function of the blood-cerebrospinal fluid barrier.* Proc Natl Acad Sci U S A, 1989. **86**(5): p. 1684-8.
56. Ling, E.A., C. Kaur, and J. Lu, *Origin, nature, and some functional considerations of intraventricular macrophages, with special reference to the epiplexus cells.* Microsc Res Tech, 1998. **41**(1): p. 43-56.
57. Wolburg, K., et al., *Ultrastructural localization of adhesion molecules in the healthy and inflamed choroid plexus of the mouse.* Cell Tissue Res, 1999. **296**(2): p. 259-69.
58. Steffen, B.J., et al., *ICAM-1, VCAM-1, and MAdCAM-1 are expressed on choroid plexus epithelium but not endothelium and mediate binding of lymphocytes in vitro.* Am J Pathol, 1996. **148**(6): p. 1819-38.
59. Krumbholz, M., et al., *Chemokines in multiple sclerosis: CXCL12 and CXCL13 up-regulation is differentially linked to CNS immune cell recruitment.* Brain, 2006. **129**(Pt 1): p. 200-11.
60. Gao, B. and P.J. Meier, *Organic anion transport across the choroid plexus.* Microsc Res Tech, 2001. **52**(1): p. 60-4.
61. Chodobski, A. and J. Szmydynger-Chodobska, *Choroid plexus: target for polypeptides and site of their synthesis.* Microsc Res Tech, 2001. **52**(1): p. 65-82.
62. Li, Y., J. Chen, and M. Chopp, *Cell proliferation and differentiation from ependymal, subependymal and choroid plexus cells in response to stroke in rats.* J Neurol Sci, 2002. **193**(2): p. 137-46.
63. Kotani, M., et al., *Identification of neuronal cell lineage-specific molecules in the neuronal differentiation of P19 EC cells and mouse central nervous system.* J Neurosci Res, 2002. **67**(5): p. 595-606.
64. Irvin, D.K., et al., *Patterns of Jagged1, Jagged2, Delta-like 1 and Delta-like 3 expression during late embryonic and postnatal brain development suggest multiple functional roles in progenitors and differentiated cells.* J Neurosci Res, 2004. **75**(3): p. 330-43.
65. Yamamoto, M., P. McCaffery, and U.C. Drager, *Influence of the choroid plexus on cerebellar development: analysis of retinoic acid synthesis.* Brain Res Dev Brain Res, 1996. **93**(1-2): p. 182-90.
66. Peraldi-Roux, S., et al., *Choroidal ependymocytes in culture: expression of markers of polarity and function.* Int J Dev Neurosci, 1990. **8**(5): p. 575-88.
67. Whitman, M.C. and C.A. Greer, *Adult neurogenesis and the olfactory system.* Prog Neurobiol, 2009. **89**(2): p. 162-75.
68. Menn, B., et al., *Origin of oligodendrocytes in the subventricular zone of the adult brain.* J Neurosci, 2006. **26**(30): p. 7907-18.
69. Kitada, M., et al., *Differentiation of choroid plexus ependymal cells into astrocytes after grafting into the pre-lesioned spinal cord in mice.* Glia, 2001. **36**(3): p. 364-74.
70. Borlongan, C.V., et al., *CNS grafts of rat choroid plexus protect against cerebral ischemia in adult rats.* Neuroreport, 2004. **15**(10): p. 1543-7.
71. Serot, J.M., M.C. Bene, and G.C. Faure, *Choroid plexus, aging of the brain, and Alzheimer's disease.* Front Biosci, 2003. **8**: p. s515-21.
72. Preston, J.E., *Ageing choroid plexus-cerebrospinal fluid system.* Microsc Res Tech, 2001. **52**(1): p. 31-7.
73. Owen-Lynch, P.J., et al., *Defective cell cycle control underlies abnormal cortical development in the hydrocephalic Texas rat.* Brain, 2003. **126**(Pt 3): p. 623-31.
74. Redzic, Z.B., et al., *The choroid plexus-cerebrospinal fluid system: from development to aging.* Curr Top Dev Biol, 2005. **71**: p. 1-52.
75. Carro, E., et al., *Blockade of the insulin-like growth factor I receptor in the choroid plexus originates Alzheimer's-like neuropathology in rodents: new cues into the human disease?* Neurobiol Aging, 2006. **27**(11): p. 1618-31.
76. Wright, E.M., *Transport processes in the formation of the cerebrospinal fluid.* Rev Physiol Biochem Pharmacol, 1978. **83**: p. 3-34.
77. Nilsson, C., et al., *Distribution of peptidergic nerves in the choroid plexus, focusing on coexistence of neuropeptide Y, vasoactive intestinal polypeptide and peptide histidine isoleucine.* Regul Pept, 1990. **27**(1): p. 11-26.
78. Nakamura, S. and T.H. Milhorat, *Nerve endings in the choroid plexus of the fourth ventricle of the rat: electron microscopic study.* Brain Res, 1978. **153**(2): p. 285-93.
79. Davson, H. and W.H. Oldendorf, *Symposium on membrane transport. Transport in the central nervous system.* Proc R Soc Med, 1967. **60**(4): p. 326-9.
80. Mufson, E.J., et al., *Distribution and retrograde transport of trophic factors in the central nervous system: functional implications for the treatment of neurodegenerative diseases.* Prog Neurobiol, 1999. **57**(4): p. 451-84.
81. Amasheh, S., et al., *Tight junction proteins as channel formers and barrier builders.* Ann N Y Acad Sci, 2009. **1165**: p. 211-9.

82. Lindsey, A.E., et al., *Functional expression and subcellular localization of an anion exchanger cloned from choroid plexus.* Proc Natl Acad Sci U S A, 1990. **87**(14): p. 5278-82.
83. Speake, T., et al., *Mechanisms of CSF secretion by the choroid plexus.* Microsc Res Tech, 2001. **52**(1): p. 49-59.
84. Masuzawa, T. and F. Sato, *The enzyme histochemistry of the choroid plexus.* Brain, 1983. **106 (Pt 1)**: p. 55-99.
85. Nakamura, N., et al., *Inwardly rectifying K+ channel Kir7.1 is highly expressed in thyroid follicular cells, intestinal epithelial cells and choroid plexus epithelial cells: implication for a functional coupling with Na+,K+-ATPase.* Biochem J, 1999. **342 (Pt 2)**: p. 329-36.
86. Zeuthen, T. and E.M. Wright, *Epithelial potassium transport: tracer and electrophysiological studies in choroid plexus.* J Membr Biol, 1981. **60**(2): p. 105-28.
87. Zeuthen, T., *Water permeability of ventricular cell membrane in choroid plexus epithelium from Necturus maculosus.* J Physiol, 1991. **444**: p. 133-51.
88. Bradbury, M.W. and H.E. Brondsted, *Sodium-dependent transport of sugars and iodide from the cerebral venticles of the rabbit.* J Physiol, 1973. **234**(1): p. 127-43.
89. Lorenzo, A.V., *Factors governing the composition of the cerebrospinal fluid.* Exp Eye Res, 1977. **25 Suppl**: p. 205-28.
90. Lerma, J., et al., *In vivo determination of extracellular concentration of amino acids in the rat hippocampus. A method based on brain dialysis and computerized analysis.* Brain Res, 1986. **384**(1): p. 145-55.
91. Nilsson, C., M. Lindvall-Axelsson, and C. Owman, *Neuroendocrine regulatory mechanisms in the choroid plexus-cerebrospinal fluid system.* Brain Res Brain Res Rev, 1992. **17**(2): p. 109-38.
92. Rapoport, S.I. and K.D. Pettigrew, *A heterogenous, pore-vesicle membrane model for protein transfer from blood to cerebrospinal fluid at the choroid plexus.* Microvasc Res, 1979. **18**(1): p. 105-19.
93. Hurley, J.V., R.M. Anderson, and P.T. Sexton, *The fate of plasma protein which escapes from blood vessels of the choroid plexus of the rat--an electron microscope study.* J Pathol, 1981. **134**(1): p. 57-70.
94. Balamurugan, K. and W. Schaffner, *Copper homeostasis in eukaryotes: teetering on a tightrope.* Biochim Biophys Acta, 2006. **1763**(7): p. 737-46.
95. Ponka, P., *Hereditary causes of disturbed iron homeostasis in the central nervous system.* Ann N Y Acad Sci, 2004. **1012**: p. 267-81.
96. Zatta, P., et al., *Accumulation of copper and other metal ions, and metallothionein I/II expression in the bovine brain as a function of aging.* J Chem Neuroanat, 2008. **36**(1): p. 1-5.
97. Nischwitz, V., A. Berthele, and B. Michalke, *Speciation analysis of selected metals and determination of their total contents in paired serum and cerebrospinal fluid samples: An approach to investigate the permeability of the human blood-cerebrospinal fluid-barrier.* Anal Chim Acta, 2008. **627**(2): p. 258-69.
98. Pena, M.M., J. Lee, and D.J. Thiele, *A delicate balance: homeostatic control of copper uptake and distribution.* J Nutr, 1999. **129**(7): p. 1251-60.
99. Hartter, D.E. and A. Barnea, *Evidence for release of copper in the brain: depolarization-induced release of newly taken-up 67copper.* Synapse, 1988. **2**(4): p. 412-5.
100. Doreulee, N., Y. Yanovsky, and H.L. Haas, *Suppression of long-term potentiation in hippocampal slices by copper.* Hippocampus, 1997. **7**(6): p. 666-9.
101. Tao, T.Y. and J.D. Gitlin, *Hepatic copper metabolism: insights from genetic disease.* Hepatology, 2003. **37**(6): p. 1241-7.
102. Puig, S. and D.J. Thiele, *Molecular mechanisms of copper uptake and distribution.* Curr Opin Chem Biol, 2002. **6**(2): p. 171-80.
103. Lech, T. and J.K. Sadlik, *Copper concentration in body tissues and fluids in normal subjects of southern Poland.* Biol Trace Elem Res, 2007. **118**(1): p. 10-5.
104. Platonova, N.A., et al., *[In vivo expression of copper transporting proteins in rat brain sections].* Izv Akad Nauk Ser Biol, 2005(2): p. 141-54.
105. Molloy, S.A. and J.H. Kaplan, *Copper-dependent recycling of hCTR1, the human high affinity copper transporter.* J Biol Chem, 2009. **284**(43): p. 29704-13.
106. Kuo, Y.M., et al., *Copper transport protein (Ctr1) levels in mice are tissue specific and dependent on copper status.* J Nutr, 2006. **136**(1): p. 21-6.
107. Culotta, V.C., M. Yang, and T.V. O'Halloran, *Activation of superoxide dismutases: putting the metal to the pedal.* Biochim Biophys Acta, 2006. **1763**(7): p. 747-58.
108. Hamza, I. and J.D. Gitlin, *Copper chaperones for cytochrome c oxidase and human disease.* J Bioenerg Biomembr, 2002. **34**(5): p. 381-8.
109. Hung, I.H., et al., *HAH1 is a copper-binding protein with distinct amino acid residues mediating copper homeostasis and antioxidant defense.* J Biol Chem, 1998. **273**(3): p. 1749-54.

110. Hamza, I., et al., *The metallochaperone Atox1 plays a critical role in perinatal copper homeostasis.* Proc Natl Acad Sci U S A, 2001. **98**(12): p. 6848-52.
111. Niciu, M.J., et al., *Altered ATP7A expression and other compensatory responses in a murine model of Menkes disease.* Neurobiol Dis, 2007. **27**(3): p. 278-91.
112. Kelly, E.J., et al., *Metallothionein I and II protect against zinc deficiency and zinc toxicity in mice.* J Nutr, 1996. **126**(7): p. 1782-90.
113. Bronson, N.W., et al., *LOXL null mice demonstrate selective dentate structural changes but maintain dentate granule cell and CA1 pyramidal cell potentiation in the hippocampus.* Neurosci Lett, 2005. **390**(2): p. 118-22.
114. Lob, H.E., et al., *Induction of hypertension and peripheral inflammation by reduction of extracellular superoxide dismutase in the central nervous system.* Hypertension, 2010. **55**(2): p. 277-83, 6p following 283.
115. Weihl, C.C. and G. Lopate, *Motor neuron disease associated with copper deficiency.* Muscle Nerve, 2006. **34**(6): p. 789-93.
116. Jaiser, S.R. and G.P. Winston, *Copper deficiency myelopathy.* J Neurol, 2010. **257**(6): p. 869-81.
117. Bothwell, T.H. and R.W. Charlton, *Current problems of iron overload.* Recent Results Cancer Res, 1979. **69**: p. 87-95.
118. Conrad, M.E., J.N. Umbreit, and E.G. Moore, *A role for mucin in the absorption of inorganic iron and other metal cations. A study in rats.* Gastroenterology, 1991. **100**(1): p. 129-36.
119. McKie, A.T., *The role of Dcytb in iron metabolism: an update.* Biochem Soc Trans, 2008. **36**(Pt 6): p. 1239-41.
120. Mims, M.P. and J.T. Prchal, *Divalent metal transporter 1.* Hematology, 2005. **10**(4): p. 339-45.
121. Anderson, G.J. and C.D. Vulpe, *Mammalian iron transport.* Cell Mol Life Sci, 2009. **66**(20): p. 3241-61.
122. Wessling-Resnick, M., *Iron imports. III. Transfer of iron from the mucosa into circulation.* Am J Physiol Gastrointest Liver Physiol, 2006. **290**(1): p. G1-6.
123. Harris, Z.L., L.W. Klomp, and J.D. Gitlin, *Aceruloplasminemia: an inherited neurodegenerative disease with impairment of iron homeostasis.* Am J Clin Nutr, 1998. **67**(5 Suppl): p. 972S-977S.
124. Nemeth, E., et al., *Hepcidin regulates cellular iron efflux by binding to ferroportin and inducing its internalization.* Science, 2004. **306**(5704): p. 2090-3.
125. Nemeth, E. and T. Ganz, *Regulation of iron metabolism by hepcidin.* Annu Rev Nutr, 2006. **26**: p. 323-42.
126. Ohgami, R.S., et al., *The Steap proteins are metalloreductases.* Blood, 2006. **108**(4): p. 1388-94.
127. Hodgson, L.L., E.A. Quail, and E.H. Morgan, *Iron transport mechanisms in reticulocytes and mature erythrocytes.* J Cell Physiol, 1995. **162**(2): p. 181-90.
128. Baker, E., S.M. Baker, and E.H. Morgan, *Characterisation of non-transferrin-bound iron (ferric citrate) uptake by rat hepatocytes in culture.* Biochim Biophys Acta, 1998. **1380**(1): p. 21-30.
129. Conrad, M.E., et al., *Alternate iron transport pathway. Mobilferrin and integrin in K562 cells.* J Biol Chem, 1994. **269**(10): p. 7169-73.
130. Koury, M.J. and P. Ponka, *New insights into erythropoiesis: the roles of folate, vitamin B12, and iron.* Annu Rev Nutr, 2004. **24**: p. 105-31.
131. Walker, A.R., *The remedying of iron deficiency: what priority should it have?* Br J Nutr, 1998. **79**(3): p. 227-35.
132. Rouault, T.A. and S. Cooperman, *Brain iron metabolism.* Semin Pediatr Neurol, 2006. **13**(3): p. 142-8.
133. Ponka, P., *Cellular iron metabolism.* Kidney Int Suppl, 1999. **69**: p. S2-11.
134. Haacke, E.M., et al., *Imaging iron stores in the brain using magnetic resonance imaging.* Magn Reson Imaging, 2005. **23**(1): p. 1-25.
135. Moos, T., P.S. Oates, and E.H. Morgan, *Expression of the neuronal transferrin receptor is age dependent and susceptible to iron deficiency.* J Comp Neurol, 1998. **398**(3): p. 420-30.
136. Taylor, E.M., A. Crowe, and E.H. Morgan, *Transferrin and iron uptake by the brain: effects of altered iron status.* J Neurochem, 1991. **57**(5): p. 1584-92.
137. Rouault, T.A., *The role of iron regulatory proteins in mammalian iron homeostasis and disease.* Nat Chem Biol, 2006. **2**(8): p. 406-14.
138. Iacopetta, B.J. and E.H. Morgan, *The kinetics of transferrin endocytosis and iron uptake from transferrin in rabbit reticulocytes.* J Biol Chem, 1983. **258**(15): p. 9108-15.
139. Burdo, J.R., et al., *Distribution of divalent metal transporter 1 and metal transport protein 1 in the normal and Belgrade rat.* J Neurosci Res, 2001. **66**(6): p. 1198-207.
140. Burdo, J.R., et al., *Mechanisms and regulation of transferrin and iron transport in a model blood-brain barrier system.* Neuroscience, 2003. **121**(4): p. 883-90.
141. Moos, T. and E.H. Morgan, *Kinetics and distribution of [59Fe-125I]transferrin injected*

into the ventricular system of the rat. Brain Res, 1998. **790**(1-2): p. 115-28.
142. Morgan, E.H., *Iron exchange between transferrin molecules mediated by phosphate compounds and other cell metabolites.* Biochim Biophys Acta, 1977. **499**(1): p. 169-77.
143. Neary, J.T., et al., *Trophic actions of extracellular nucleotides and nucleosides on glial and neuronal cells.* Trends Neurosci, 1996. **19**(1): p. 13-8.
144. Terent, A., et al., *Lactoferrin, lysozyme, and beta 2-microglobulin in cerebrospinal fluid. Elevated levels in patients with acute cerebrovascular lesions as indices of inflammation.* Stroke, 1981. **12**(1): p. 40-6.
145. Ke, Y., et al., *Age-dependent and iron-independent expression of two mRNA isoforms of divalent metal transporter 1 in rat brain.* Neurobiol Aging, 2005. **26**(5): p. 739-48.
146. Hansen, T.M., et al., *Expression of ferritin protein and subunit mRNAs in normal and iron deficient rat brain.* Brain Res Mol Brain Res, 1999. **65**(2): p. 186-97.
147. Moos, T. and E.H. Morgan, *The metabolism of neuronal iron and its pathogenic role in neurological disease: review.* Ann N Y Acad Sci, 2004. **1012**: p. 14-26.
148. Patel, B.N. and S. David, *A novel glycosylphosphatidylinositol-anchored form of ceruloplasmin is expressed by mammalian astrocytes.* J Biol Chem, 1997. **272**(32): p. 20185-90.
149. Moos, T. and T. Rosengren Nielsen, *Ferroportin in the postnatal rat brain: implications for axonal transport and neuronal export of iron.* Semin Pediatr Neurol, 2006. **13**(3): p. 149-57.
150. Dexter, D.T., et al., *Increased nigral iron content in postmortem parkinsonian brain.* Lancet, 1987. **2**(8569): p. 1219-20.
151. Sofic, E., et al., *Increased iron (III) and total iron content in post mortem substantia nigra of parkinsonian brain.* J Neural Transm, 1988. **74**(3): p. 199-205.
152. Koschinsky, M.L., et al., *Complete cDNA sequence of human preceruloplasmin.* Proc Natl Acad Sci U S A, 1986. **83**(14): p. 5086-90.
153. Gitlin, J.D., *Transcriptional regulation of ceruloplasmin gene expression during inflammation.* J Biol Chem, 1988. **263**(13): p. 6281-7.
154. Klomp, L.W., et al., *Ceruloplasmin gene expression in the murine central nervous system.* J Clin Invest, 1996. **98**(1): p. 207-15.
155. Patel, B.N., R.J. Dunn, and S. David, *Alternative RNA splicing generates a glycosylphosphatidylinositol-anchored form of ceruloplasmin in mammalian brain.* J Biol Chem, 2000. **275**(6): p. 4305-10.
156. Ortel, T.L., N. Takahashi, and F.W. Putnam, *Structural model of human ceruloplasmin based on internal triplication, hydrophilic/hydrophobic character, and secondary structure of domains.* Proc Natl Acad Sci U S A, 1984. **81**(15): p. 4761-5.
157. Zaitsev, V.N., et al., *An X-ray crystallographic study of the binding sites of the azide inhibitor and organic substrates to ceruloplasmin, a multi-copper oxidase in the plasma.* J Biol Inorg Chem, 1999. **4**(5): p. 579-87.
158. Musci, G., G.C. Bellenchi, and L. Calabrese, *The multifunctional oxidase activity of ceruloplasmin as revealed by anion binding studies.* Eur J Biochem, 1999. **265**(2): p. 589-97.
159. Farver, O., et al., *Human ceruloplasmin. Intramolecular electron transfer kinetics and equilibration.* J Biol Chem, 1999. **274**(37): p. 26135-40.
160. Takahashi, N., T.L. Ortel, and F.W. Putnam, *Single-chain structure of human ceruloplasmin: the complete amino acid sequence of the whole molecule.* Proc Natl Acad Sci U S A, 1984. **81**(2): p. 390-4.
161. Sato, M. and J.D. Gitlin, *Mechanisms of copper incorporation during the biosynthesis of human ceruloplasmin.* J Biol Chem, 1991. **266**(8): p. 5128-34.
162. Lutsenko, S., et al., *Function and regulation of human copper-transporting ATPases.* Physiol Rev, 2007. **87**(3): p. 1011-46.
163. Hellman, N.E., et al., *Mechanisms of copper incorporation into human ceruloplasmin.* J Biol Chem, 2002. **277**(48): p. 46632-8.
164. Gitlin, J.D., et al., *Mechanisms of caeruloplasmin biosynthesis in normal and copper-deficient rats.* Biochem J, 1992. **282 (Pt 3)**: p. 835-9.
165. Portnoy, M.E., et al., *Structure-function analyses of the ATX1 metallochaperone.* J Biol Chem, 1999. **274**(21): p. 15041-5.
166. Prohaska, J.R. and A.A. Gybina, *Intracellular copper transport in mammals.* J Nutr, 2004. **134**(5): p. 1003-6.
167. De Iuliis, A., et al., *Increased dopamine peroxidation in postmortem Parkinsonian brain.* Biochim Biophys Acta, 2002. **1573**(1): p. 63-7.
168. Armendariz, A.D., et al., *Gene expression profiling in chronic copper overload reveals upregulation of Prnp and App.* Physiol Genomics, 2004. **20**(1): p. 45-54.
169. Morita, H., et al., *Hereditary ceruloplasmin deficiency with hemosiderosis: a*

clinicopathological study of a Japanese family. Ann Neurol, 1995. **37**(5): p. 646-56.
170. Halliwell, B. and J.M. Gutteridge, *Oxygen toxicity, oxygen radicals, transition metals and disease.* Biochem J, 1984. **219**(1): p. 1-14.
171. Floris, G., et al., *The physiopathological significance of ceruloplasmin. A possible therapeutic approach.* Biochem Pharmacol, 2000. **60**(12): p. 1735-41.
172. Calabrese, L., M. Carbonaro, and G. Musci, *Presence of coupled trinuclear copper cluster in mammalian ceruloplasmin is essential for efficient electron transfer to oxygen.* J Biol Chem, 1989. **264**(11): p. 6183-7.
173. Osaki, S., D.A. Johnson, and E. Frieden, *The possible significance of the ferrous oxidase activity of ceruloplasmin in normal human serum.* J Biol Chem, 1966. **241**(12): p. 2746-51.
174. Jeong, S.Y. and S. David, *Glycosylphosphatidylinositol-anchored ceruloplasmin is required for iron efflux from cells in the central nervous system.* J Biol Chem, 2003. **278**(29): p. 27144-8.
175. Frieden, E. and H.S. Hsieh, *The biological role of ceruloplasmin and its oxidase activity.* Adv Exp Med Biol, 1976. **74**: p. 505-29.
176. Lovstad, R.A., *Interaction of ceruloplasmin with L- and D-dopa.* Acta Chem Scand, 1972. **26**(7): p. 2832-6.
177. Medda, R., et al., *Effect of ceruloplasmin on 6-hydroxydopamine oxidation.* Biochem Mol Biol Int, 1996. **38**(4): p. 721-8.
178. Cha, M.K. and I.H. Kim, *Ceruloplasmin has a distinct active site for the catalyzing glutathione-dependent reduction of alkyl hydroperoxide.* Biochemistry, 1999. **38**(37): p. 12104-10.
179. Inoue, K., et al., *Nitrosothiol formation catalyzed by ceruloplasmin. Implication for cytoprotective mechanism in vivo.* J Biol Chem, 1999. **274**(38): p. 27069-75.
180. Musci, G., et al., *Interaction of nitric oxide with ceruloplasmin lacking an EPR-detectable type 2 copper.* Biochemistry, 1991. **30**(41): p. 9866-72.
181. Choi, S.Y., et al., *Fragmentation of human ceruloplasmin induced by hydrogen peroxide.* Biochimie, 2000. **82**(2): p. 175-80.
182. Kang, J.H., et al., *Oxidative modification of human ceruloplasmin by peroxyl radicals.* Biochim Biophys Acta, 2001. **1568**(1): p. 30-6.
183. Swain, J.A., V. Darley-Usmar, and J.M. Gutteridge, *Peroxynitrite releases copper from caeruloplasmin: implications for atherosclerosis.* FEBS Lett, 1994. **342**(1): p. 49-52.
184. Musci, G., et al., *Age-related changes in human ceruloplasmin. Evidence for oxidative modifications.* J Biol Chem, 1993. **268**(18): p. 13388-95.
185. Arumanayagam, M., et al., *Serum ceruloplasmin, plasma copper concentration and copper to ceruloplasmin ratio in cervical carcinoma.* Gynecol Obstet Invest, 1993. **35**(3): p. 175-8.
186. Linder, M.C., J.R. Moor, and K. Wright, *Ceruloplasmin assays in diagnosis and treatment of human lung, breast, and gastrointestinal cancers.* J Natl Cancer Inst, 1981. **67**(2): p. 263-75.
187. Raju, K.S., et al., *Ceruloplasmin, copper ions, and angiogenesis.* J Natl Cancer Inst, 1982. **69**(5): p. 1183-8.
188. Jeffery, C.J., *Moonlighting proteins.* Trends Biochem Sci, 1999. **24**(1): p. 8-11.
189. Duce, J.A., et al., *Iron-export ferroxidase activity of beta-amyloid precursor protein is inhibited by zinc in Alzheimer's disease.* Cell, 2010. **142**(6): p. 857-67.
190. Priller, C., et al., *Synapse formation and function is modulated by the amyloid precursor protein.* J Neurosci, 2006. **26**(27): p. 7212-21.
191. Hardy, J., *Has the amyloid cascade hypothesis for Alzheimer's disease been proved?* Curr Alzheimer Res, 2006. **3**(1): p. 71-3.
192. Nunomura, A., et al., *Neuronal RNA oxidation in Alzheimer's disease and Down's syndrome.* Ann N Y Acad Sci, 1999. **893**: p. 362-4.
193. Rottkamp, C.A., et al., *Redox-active iron mediates amyloid-beta toxicity.* Free Radic Biol Med, 2001. **30**(4): p. 447-50.
194. Nerelius, C., M. Fitzen, and J. Johansson, *Amino acid sequence determinants and molecular chaperones in amyloid fibril formation.* Biochem Biophys Res Commun, 2010. **396**(1): p. 2-6.
195. Younkin, S.G., *The role of A beta 42 in Alzheimer's disease.* J Physiol Paris, 1998. **92**(3-4): p. 289-92.
196. Meraz-Rios, M.A., et al., *Tau oligomers and aggregation in Alzheimer's disease.* J Neurochem, 2010. **112**(6): p. 1353-67.
197. Takashima, A., *Amyloid-beta, tau, and dementia.* J Alzheimers Dis, 2009. **17**(4): p. 729-36.
198. Hensley, K., et al., *Brain regional correspondence between Alzheimer's disease histopathology and biomarkers of protein oxidation.* J Neurochem, 1995. **65**(5): p. 2146-56.
199. Mecocci, P., U. MacGarvey, and M.F. Beal, *Oxidative damage to mitochondrial DNA is*

increased in Alzheimer's disease. Ann Neurol, 1994. **36**(5): p. 747-51.
200. Ames, B.N., *Oxygen radicals and 8-hydroxyguanine in DNA.* Jpn J Cancer Res, 1991. **82**(12): p. 1460-1.
201. Cooper, A.J. and B.S. Kristal, *Multiple roles of glutathione in the central nervous system.* Biol Chem, 1997. **378**(8): p. 793-802.
202. Hazel, J.R. and E.E. Williams, *The role of alterations in membrane lipid composition in enabling physiological adaptation of organisms to their physical environment.* Prog Lipid Res, 1990. **29**(3): p. 167-227.
203. Casadesus, G., et al., *Alzheimer disease: evidence for a central pathogenic role of iron-mediated reactive oxygen species.* J Alzheimers Dis, 2004. **6**(2): p. 165-9.
204. Loeffler, D.A., et al., *Transferrin and iron in normal, Alzheimer's disease, and Parkinson's disease brain regions.* J Neurochem, 1995. **65**(2): p. 710-24.
205. Bodovitz, S., et al., *Iron levels modulate alpha-secretase cleavage of amyloid precursor protein.* J Neurochem, 1995. **64**(1): p. 307-15.
206. Mezzetti, A., et al., *Copper/zinc ratio and systemic oxidant load: effect of aging and aging-related degenerative diseases.* Free Radic Biol Med, 1998. **25**(6): p. 676-81.
207. Multhaup, G., et al., *The amyloid precursor protein of Alzheimer's disease in the reduction of copper(II) to copper(I).* Science, 1996. **271**(5254): p. 1406-9.
208. Linder, M.C. and M. Hazegh-Azam, *Copper biochemistry and molecular biology.* Am J Clin Nutr, 1996. **63**(5): p. 797S-811S.
209. Takeuchi, M. and S. Yamagishi, *Possible involvement of advanced glycation end-products (AGEs) in the pathogenesis of Alzheimer's disease.* Curr Pharm Des, 2008. **14**(10): p. 973-8.
210. Harrington, C.R. and C.A. Colaco, *Alzheimer's disease. A glycation connection.* Nature, 1994. **370**(6487): p. 247-8.
211. Munch, G., et al., *Advanced glycation endproducts in ageing and Alzheimer's disease.* Brain Res Brain Res Rev, 1997. **23**(1-2): p. 134-43.
212. Vitek, M.P., et al., *Advanced glycation end products contribute to amyloidosis in Alzheimer disease.* Proc Natl Acad Sci U S A, 1994. **91**(11): p. 4766-70.
213. Yan, S.D., et al., *Glycated tau protein in Alzheimer disease: a mechanism for induction of oxidant stress.* Proc Natl Acad Sci U S A, 1994. **91**(16): p. 7787-91.
214. Eikelenboom, P. and R. Veerhuis, *The role of complement and activated microglia in the pathogenesis of Alzheimer's disease.* Neurobiol Aging, 1996. **17**(5): p. 673-80.
215. Klegeris, A. and P.L. McGeer, *beta-amyloid protein enhances macrophage production of oxygen free radicals and glutamate.* J Neurosci Res, 1997. **49**(2): p. 229-35.
216. Akiyama, H., et al., *Cell mediators of inflammation in the Alzheimer disease brain.* Alzheimer Dis Assoc Disord, 2000. **14 Suppl 1**: p. S47-53.
217. Good, P.F., et al., *Evidence of neuronal oxidative damage in Alzheimer's disease.* Am J Pathol, 1996. **149**(1): p. 21-8.
218. Keller, J.N., K.B. Hanni, and W.R. Markesbery, *Impaired proteasome function in Alzheimer's disease.* J Neurochem, 2000. **75**(1): p. 436-9.
219. Brunk, U.T., J. Neuzil, and J.W. Eaton, *Lysosomal involvement in apoptosis.* Redox Rep, 2001. **6**(2): p. 91-7.
220. Zhao, M., et al., *Lysosomal enzymes promote mitochondrial oxidant production, cytochrome c release and apoptosis.* Eur J Biochem, 2003. **270**(18): p. 3778-86.
221. Castellani, R., et al., *Role of mitochondrial dysfunction in Alzheimer's disease.* J Neurosci Res, 2002. **70**(3): p. 357-60.
222. Blass, J.P., *The mitochondrial spiral. An adequate cause of dementia in the Alzheimer's syndrome.* Ann N Y Acad Sci, 2000. **924**: p. 170-83.
223. Mutisya, E.M., A.C. Bowling, and M.F. Beal, *Cortical cytochrome oxidase activity is reduced in Alzheimer's disease.* J Neurochem, 1994. **63**(6): p. 2179-84.
224. Parker, W.D., Jr. and J.K. Parks, *Cytochrome c oxidase in Alzheimer's disease brain: purification and characterization.* Neurology, 1995. **45**(3 Pt 1): p. 482-6.
225. Davis, R.E., et al., *Mutations in mitochondrial cytochrome c oxidase genes segregate with late-onset Alzheimer disease.* Proc Natl Acad Sci U S A, 1997. **94**(9): p. 4526-31.
226. Seripa, D., et al., *The genetics of the human APOE polymorphism.* Rejuvenation Res, 2011. **14**(5): p. 491-500.
227. Hogh, P., et al., *The apolipoprotein E epsilon4-allele and antihypertensive treatment are associated with increased risk of cerebral MRI white matter hyperintensities.* Acta Neurol Scand, 2007. **115**(4): p. 248-53.
228. Hansson, O., et al., *Association between CSF biomarkers and incipient Alzheimer's disease in patients with mild cognitive impairment: a follow-up study.* Lancet Neurol, 2006. **5**(3): p. 228-34.
229. Gauthier, S., H. Loft, and J. Cummings, *Improvement in behavioural symptoms in patients with moderate to severe Alzheimer's*

disease by memantine: a pooled data analysis. Int J Geriatr Psychiatry, 2008. **23**(5): p. 537-45.
230. Wilcock, G.K., et al., *Memantine for agitation/aggression and psychosis in moderately severe to severe Alzheimer's disease: a pooled analysis of 3 studies.* J Clin Psychiatry, 2008. **69**(3): p. 341-8.
231. Birks, J. and R.J. Harvey, *Donepezil for dementia due to Alzheimer's disease.* Cochrane Database Syst Rev, 2006(1): p. CD001190.
232. Schenk, D., et al., *Immunization with amyloid-beta attenuates Alzheimer-disease-like pathology in the PDAPP mouse.* Nature, 1999. **400**(6740): p. 173-7.
233. de Lau, L.M. and M.M. Breteler, *Epidemiology of Parkinson's disease.* Lancet Neurol, 2006. **5**(6): p. 525-35.
234. Bower, J.H., et al., *Incidence and distribution of parkinsonism in Olmsted County, Minnesota, 1976-1990.* Neurology, 1999. **52**(6): p. 1214-20.
235. Zaccai, J., et al., *Patterns and stages of alpha-synucleinopathy: Relevance in a population-based cohort.* Neurology, 2008. **70**(13): p. 1042-8.
236. Apaydin, H., et al., *Parkinson disease neuropathology: later-developing dementia and loss of the levodopa response.* Arch Neurol, 2002. **59**(1): p. 102-12.
237. Halliday, G., et al., *The progression of pathology in longitudinally followed patients with Parkinson's disease.* Acta Neuropathol, 2008. **115**(4): p. 409-15.
238. Dickson, D.W., et al., *Evidence that incidental Lewy body disease is pre-symptomatic Parkinson's disease.* Acta Neuropathol, 2008. **115**(4): p. 437-44.
239. Braak, H., et al., *Stages in the development of Parkinson's disease-related pathology.* Cell Tissue Res, 2004. **318**(1): p. 121-34.
240. George, J.M., *The synucleins.* Genome Biol, 2002. **3**(1): p. REVIEWS3002.
241. Vekrellis, K., et al., *Pathological roles of alpha-synuclein in neurological disorders.* Lancet Neurol, 2011. **10**(11): p. 1015-25.
242. Theuns, J. and C. Van Broeckhoven, *alpha-Synuclein gene duplications in sporadic Parkinson disease.* Neurology, 2008. **70**(1): p. 7-9.
243. Nussbaum, R.L. and M.H. Polymeropoulos, *Genetics of Parkinson's disease.* Hum Mol Genet, 1997. **6**(10): p. 1687-91.
244. Seet, R.C., et al., *Oxidative damage in Parkinson disease: Measurement using accurate biomarkers.* Free Radic Biol Med, 2010. **48**(4): p. 560-6.
245. Lotharius, J. and P. Brundin, *Impaired dopamine storage resulting from alpha-synuclein mutations may contribute to the pathogenesis of Parkinson's disease.* Hum Mol Genet, 2002. **11**(20): p. 2395-407.
246. Hastings, T.G., *The role of dopamine oxidation in mitochondrial dysfunction: implications for Parkinson's disease.* J Bioenerg Biomembr, 2009. **41**(6): p. 469-72.
247. Conway, K.A., et al., *Kinetic stabilization of the alpha-synuclein protofibril by a dopamine-alpha-synuclein adduct.* Science, 2001. **294**(5545): p. 1346-9.
248. Berman, S.B. and T.G. Hastings, *Dopamine oxidation alters mitochondrial respiration and induces permeability transition in brain mitochondria: implications for Parkinson's disease.* J Neurochem, 1999. **73**(3): p. 1127-37.
249. Zafar, K.S., S.H. Inayat-Hussain, and D. Ross, *A comparative study of proteasomal inhibition and apoptosis induced in N27 mesencephalic cells by dopamine and MG132.* J Neurochem, 2007. **102**(3): p. 913-21.
250. Halliwell, B. and J.M. Gutteridge, *Biologically relevant metal ion-dependent hydroxyl radical generation. An update.* FEBS Lett, 1992. **307**(1): p. 108-12.
251. Sofic, E., et al., *Selective increase of iron in substantia nigra zona compacta of parkinsonian brains.* J Neurochem, 1991. **56**(3): p. 978-82.
252. Jellinger, K., et al., *Brain iron and ferritin in Parkinson's and Alzheimer's diseases.* J Neural Transm Park Dis Dement Sect, 1990. **2**(4): p. 327-40.
253. Zeevalk, G.D., R. Razmpour, and L.P. Bernard, *Glutathione and Parkinson's disease: is this the elephant in the room?* Biomed Pharmacother, 2008. **62**(4): p. 236-49.
254. Pearce, R.K., et al., *Alterations in the distribution of glutathione in the substantia nigra in Parkinson's disease.* J Neural Transm, 1997. **104**(6-7): p. 661-77.
255. Bosco, D.A., et al., *Elevated levels of oxidized cholesterol metabolites in Lewy body disease brains accelerate alpha-synuclein fibrilization.* Nat Chem Biol, 2006. **2**(5): p. 249-53.
256. Zecca, L., et al., *The neuromelanin of human substantia nigra: structure, synthesis and molecular behaviour.* J Neural Transm Suppl, 2003(65): p. 145-55.
257. Zecca, L., et al., *Neuromelanin can protect against iron-mediated oxidative damage in system modeling iron overload of brain aging and Parkinson's disease.* J Neurochem, 2008. **106**(4): p. 1866-75.

258. Devi, L., et al., *Mitochondrial import and accumulation of alpha-synuclein impair complex I in human dopaminergic neuronal cultures and Parkinson disease brain.* J Biol Chem, 2008. **283**(14): p. 9089-100.
259. Bender, A., et al., *High levels of mitochondrial DNA deletions in substantia nigra neurons in aging and Parkinson disease.* Nat Genet, 2006. **38**(5): p. 515-7.
260. Gallagher, D.A. and A.H. Schapira, *Etiopathogenesis and treatment of Parkinson's disease.* Curr Top Med Chem, 2009. **9**(10): p. 860-8.
261. Gandhi, S., et al., *PINK1 protein in normal human brain and Parkinson's disease.* Brain, 2006. **129**(Pt 7): p. 1720-31.
262. Nagakubo, D., et al., *DJ-1, a novel oncogene which transforms mouse NIH3T3 cells in cooperation with ras.* Biochem Biophys Res Commun, 1997. **231**(2): p. 509-13.
263. Zhang, L., et al., *Mitochondrial localization of the Parkinson's disease related protein DJ-1: implications for pathogenesis.* Hum Mol Genet, 2005. **14**(14): p. 2063-73.
264. Lucking, C.B., et al., *Coding polymorphisms in the parkin gene and susceptibility to Parkinson disease.* Arch Neurol, 2003. **60**(9): p. 1253-6.
265. Corti, O., S. Lesage, and A. Brice, *What genetics tells us about the causes and mechanisms of Parkinson's disease.* Physiol Rev, 2011. **91**(4): p. 1161-218.
266. West, A.B., et al., *Parkinson's disease-associated mutations in leucine-rich repeat kinase 2 augment kinase activity.* Proc Natl Acad Sci U S A, 2005. **102**(46): p. 16842-7.
267. McGeer, P.L., et al., *Reactive microglia are positive for HLA-DR in the substantia nigra of Parkinson's and Alzheimer's disease brains.* Neurology, 1988. **38**(8): p. 1285-91.
268. Akiyama, H., et al., *Expression of intercellular adhesion molecule (ICAM)-1 by a subset of astrocytes in Alzheimer disease and some other degenerative neurological disorders.* Acta Neuropathol, 1993. **85**(6): p. 628-34.
269. Qian, L., P.M. Flood, and J.S. Hong, *Neuroinflammation is a key player in Parkinson's disease and a prime target for therapy.* J Neural Transm, 2010. **117**(8): p. 971-9.
270. Lee, H.J., S. Patel, and S.J. Lee, *Intravesicular localization and exocytosis of alpha-synuclein and its aggregates.* J Neurosci, 2005. **25**(25): p. 6016-24.
271. Farina, C., F. Aloisi, and E. Meinl, *Astrocytes are active players in cerebral innate immunity.* Trends Immunol, 2007. **28**(3): p. 138-45.
272. Harris, Z.L., et al., *Aceruloplasminemia: molecular characterization of this disorder of iron metabolism.* Proc Natl Acad Sci U S A, 1995. **92**(7): p. 2539-43.
273. Yoshida, K., et al., *A mutation in the ceruloplasmin gene is associated with systemic hemosiderosis in humans.* Nat Genet, 1995. **9**(3): p. 267-72.
274. Okamoto, N., et al., *Hereditary ceruloplasmin deficiency with hemosiderosis.* Hum Genet, 1996. **97**(6): p. 755-8.
275. Takeuchi, Y., et al., *A case of aceruloplasminaemia: abnormal serum ceruloplasmin protein without ferroxidase activity.* J Neurol Neurosurg Psychiatry, 2002. **72**(4): p. 543-5.
276. Miyajima, H., *Aceruloplasminemia, an iron metabolic disorder.* Neuropathology, 2003. **23**(4): p. 345-50.
277. Nittis, T. and J.D. Gitlin, *The copper-iron connection: hereditary aceruloplasminemia.* Semin Hematol, 2002. **39**(4): p. 282-9.
278. Miyajima, H., et al., *Familial apoceruloplasmin deficiency associated with blepharospasm and retinal degeneration.* Neurology, 1987. **37**(5): p. 761-7.
279. McNeill, A., et al., *The neurological presentation of ceruloplasmin gene mutations.* Eur Neurol, 2008. **60**(4): p. 200-5.
280. Kaneko, K., et al., *Astrocytic deformity and globular structures are characteristic of the brains of patients with aceruloplasminemia.* J Neuropathol Exp Neurol, 2002. **61**(12): p. 1069-77.
281. Oide, T., et al., *Iron overload and antioxidative role of perivascular astrocytes in aceruloplasminemia.* Neuropathol Appl Neurobiol, 2006. **32**(2): p. 170-6.
282. Harris, Z.L., et al., *Targeted gene disruption reveals an essential role for ceruloplasmin in cellular iron efflux.* Proc Natl Acad Sci U S A, 1999. **96**(19): p. 10812-7.
283. Kono, S. and H. Miyajima, *Molecular and pathological basis of aceruloplasminemia.* Biol Res, 2006. **39**(1): p. 15-23.
284. di Patti, M.C., et al., *Dominant mutants of ceruloplasmin impair the copper loading machinery in aceruloplasminemia.* J Biol Chem, 2009. **284**(7): p. 4545-54.
285. Chelly, J. and A.P. Monaco, *Cloning the Wilson disease gene.* Nat Genet, 1993. **5**(4): p. 317-8.
286. Leventer, R.J., et al., *Early magnetic resonance imaging findings in Menkes' disease.* J Child Neurol, 1997. **12**(3): p. 222-4.
287. Barnard, R.O., P.V. Best, and M. Erdohazi, *Neuropathology of Menkes' disease.* Dev Med Child Neurol, 1978. **20**(5): p. 586-97.
288. Bull, P.C., et al., *The Wilson disease gene is a putative copper transporting P-type ATPase*

similar to the Menkes gene. Nat Genet, 1993. **5**(4): p. 327-37.
289. Tanzi, R.E., et al., *The Wilson disease gene is a copper transporting ATPase with homology to the Menkes disease gene.* Nat Genet, 1993. **5**(4): p. 344-50.
290. Petrukhin, K., et al., *Mapping, cloning and genetic characterization of the region containing the Wilson disease gene.* Nat Genet, 1993. **5**(4): p. 338-43.
291. Gitlin, J.D., *Wilson disease.* Gastroenterology, 2003. **125**(6): p. 1868-77.
292. Lutsenko, S., R. Tsivkovskii, and J.M. Walker, *Functional properties of the human copper-transporting ATPase ATP7B (the Wilson's disease protein) and regulation by metallochaperone Atox1.* Ann N Y Acad Sci, 2003. **986**: p. 204-11.
293. Tao, T.Y., et al., *The copper toxicosis gene product Murr1 directly interacts with the Wilson disease protein.* J Biol Chem, 2003. **278**(43): p. 41593-6.
294. Oder, W., et al., *Neurological and neuropsychiatric spectrum of Wilson's disease: a prospective study of 45 cases.* J Neurol, 1991. **238**(5): p. 281-7.
295. Gollan, J.L. and T.J. Gollan, *Wilson disease in 1998: genetic, diagnostic and therapeutic aspects.* J Hepatol, 1998. **28 Suppl 1**: p. 28-36.
296. Loeffler, D.A., et al., *Increased regional brain concentrations of ceruloplasmin in neurodegenerative disorders.* Brain Res, 1996. **738**(2): p. 265-74.
297. Capo, C.R., et al., *Features of ceruloplasmin in the cerebrospinal fluid of Alzheimer's disease patients.* Biometals, 2008. **21**(3): p. 367-72.
298. Snaedal, J., et al., *Copper, ceruloplasmin and superoxide dismutase in patients with Alzheimer's disease . a case-control study.* Dement Geriatr Cogn Disord, 1998. **9**(5): p. 239-42.
299. Arnal, N., et al., *Clinical utility of copper, ceruloplasmin, and metallothionein plasma determinations in human neurodegenerative patients and their first-degree relatives.* Brain Res, 2010. **1319**: p. 118-30.
300. Schrag, M., et al., *Iron, zinc and copper in the Alzheimer's disease brain: a quantitative meta-analysis. Some insight on the influence of citation bias on scientific opinion.* Prog Neurobiol, 2011. **94**(3): p. 296-306.
301. Torsdottir, G., et al., *Ceruloplasmin and superoxide dismutase (SOD1) in heterozygotes for Wilson disease: A case control study.* Neuropsychiatr Dis Treat, 2009. **5**: p. 55-9.
302. Martinez-Hernandez, R., et al., *Plasma ceruloplasmin ferroxidase activity correlates with the nigral sonographic area in Parkinson's disease patients: a pilot study.* Neurochem Res, 2011. **36**(11): p. 2111-5.
303. Torsdottir, G., et al., *Copper, ceruloplasmin and superoxide dismutase (SOD1) in patients with Down's syndrome.* Pharmacol Toxicol, 2001. **89**(6): p. 320-5.
304. Hochstrasser, H., et al., *Ceruloplasmin gene variations and substantia nigra hyperechogenicity in Parkinson disease.* Neurology, 2004. **63**(10): p. 1912-7.
305. Lee, K.H., et al., *Activation of microglial cells by ceruloplasmin.* Brain Res, 2007. **1171**: p. 1-8.
306. Uversky, V.N., *Neurotoxicant-induced animal models of Parkinson's disease: understanding the role of rotenone, maneb and paraquat in neurodegeneration.* Cell Tissue Res, 2004. **318**(1): p. 225-41.
307. Robinson, N.E., et al., *Structure-dependent nonenzymatic deamidation of glutaminyl and asparaginyl pentapeptides.* J Pept Res, 2004. **63**(5): p. 426-36.
308. Johnson, B.A., E.L. Langmack, and D.W. Aswad, *Partial repair of deamidation-damaged calmodulin by protein carboxyl methyltransferase.* J Biol Chem, 1987. **262**(25): p. 12283-7.
309. Clarke, S., *Aging as war between chemical and biochemical processes: protein methylation and the recognition of age-damaged proteins for repair.* Ageing Res Rev, 2003. **2**(3): p. 263-85.
310. Geiger, T. and S. Clarke, *Deamidation, isomerization, and racemization at asparaginyl and aspartyl residues in peptides. Succinimide-linked reactions that contribute to protein degradation.* J Biol Chem, 1987. **262**(2): p. 785-94.
311. Brennan, T.V. and S. Clarke, *Effect of adjacent histidine and cysteine residues on the spontaneous degradation of asparaginyl- and aspartyl-containing peptides.* Int J Pept Protein Res, 1995. **45**(6): p. 547-53.
312. Reissner, K.J. and D.W. Aswad, *Deamidation and isoaspartate formation in proteins: unwanted alterations or surreptitious signals?* Cell Mol Life Sci, 2003. **60**(7): p. 1281-95.
313. Ingrosso, D., et al., *Increased methyl esterification of altered aspartyl residues in erythrocyte membrane proteins in response to oxidative stress.* Eur J Biochem, 2000. **267**(14): p. 4397-405.
314. Wright, H.T., *Sequence and structure determinants of the nonenzymatic deamidation of asparagine and glutamine residues in proteins.* Protein Eng, 1991. **4**(3): p. 283-94.

315. Xie, M. and R.L. Schowen, *Secondary structure and protein deamidation.* J Pharm Sci, 1999. **88**(1): p. 8-13.
316. Flatmark, T. and K. Sletten, *Multiple forms of cytochrome c in the rat. Precursor-product relationship between the main component Cy I and the minor components Cy II and Cy 3 in vivo.* J Biol Chem, 1968. **243**(7): p. 1623-9.
317. Robinson, A.B., *Evolution and the distribution of glutaminyl and asparaginyl residues in proteins.* Proc Natl Acad Sci U S A, 1974. **71**(3): p. 885-8.
318. Robinson, A.B. and L.R. Robinson, *Distribution of glutamine and asparagine residues and their near neighbors in peptides and proteins.* Proc Natl Acad Sci U S A, 1991. **88**(20): p. 8880-4.
319. Rogers, S.W. and M. Rechsteiner, *Degradation of structurally characterized proteins injected into HeLa cells. Basic measurements.* J Biol Chem, 1988. **263**(36): p. 19833-42.
320. Mould, A.P., L. Burrows, and M.J. Humphries, *Identification of amino acid residues that form part of the ligand-binding pocket of integrin alpha5 beta1.* J Biol Chem, 1998. **273**(40): p. 25664-72.
321. Curnis, F., et al., *Spontaneous formation of L-isoaspartate and gain of function in fibronectin.* J Biol Chem, 2006. **281**(47): p. 36466-76.
322. Johnson, B.A., et al., *Protein carboxyl methyltransferase facilitates conversion of atypical L-isoaspartyl peptides to normal L-aspartyl peptides.* J Biol Chem, 1987. **262**(12): p. 5622-9.
323. Galletti, P., et al., *Mechanism of protein carboxyl methyl transfer reactions: structural requirements of methyl accepting substrates.* Adv Exp Med Biol, 1988. **231**: p. 229-45.
324. Diliberto, E.J., Jr. and J. Axelrod, *Regional and subcellular distribution of protein carboxymethylase in brain and other tissues.* J Neurochem, 1976. **26**(6): p. 1159-65.
325. Sandmeier, E., et al., *Spontaneous deamidation and isomerization of Asn108 in prion peptide 106-126 and in full-length prion protein.* Biochem Biophys Res Commun, 1999. **261**(3): p. 578-83.
326. Watanabe, A., K. Takio, and Y. Ihara, *Deamidation and isoaspartate formation in smeared tau in paired helical filaments. Unusual properties of the microtubule-binding domain of tau.* J Biol Chem, 1999. **274**(11): p. 7368-78.
327. Pasqualini, R., et al., *Aminopeptidase N is a receptor for tumor-homing peptides and a target for inhibiting angiogenesis.* Cancer Res, 2000. **60**(3): p. 722-7.
328. Luan, Y. and W. Xu, *The structure and main functions of aminopeptidase N.* Curr Med Chem, 2007. **14**(6): p. 639-47.
329. Riemann, D., A. Kehlen, and J. Langner, *CD13--not just a marker in leukemia typing.* Immunol Today, 1999. **20**(2): p. 83-8.
330. Curnis, F., et al., *Differential binding of drugs containing the NGR motif to CD13 isoforms in tumor vessels, epithelia, and myeloid cells.* Cancer Res, 2002. **62**(3): p. 867-74.
331. Dixon, J., et al., *Expression of aminopeptidase-n (CD 13) in normal tissues and malignant neoplasms of epithelial and lymphoid origin.* J Clin Pathol, 1994. **47**(1): p. 43-7.
332. Curnis, F., et al., *Enhancement of tumor necrosis factor alpha antitumor immunotherapeutic properties by targeted delivery to aminopeptidase N (CD13).* Nat Biotechnol, 2000. **18**(11): p. 1185-90.
333. Curnis, F., et al., *Targeted delivery of IFNgamma to tumor vessels uncouples antitumor from counterregulatory mechanisms.* Cancer Res, 2005. **65**(7): p. 2906-13.
334. Curnis, F., et al., *Coupling tumor necrosis factor-alpha with alphaV integrin ligands improves its antineoplastic activity.* Cancer Res, 2004. **64**(2): p. 565-71.
335. Curnis, F., et al., *Critical role of flanking residues in NGR-to-isoDGR transition and CD13/integrin receptor switching.* J Biol Chem, 2010. **285**(12): p. 9114-23.
336. Gao, R. and D.R. Brigstock, *A novel integrin alpha5beta1 binding domain in module 4 of connective tissue growth factor (CCN2/CTGF) promotes adhesion and migration of activated pancreatic stellate cells.* Gut, 2006. **55**(6): p. 856-62.
337. Rusnati, M., et al., *alphavbeta3 integrin mediates the cell-adhesive capacity and biological activity of basic fibroblast growth factor (FGF-2) in cultured endothelial cells.* Mol Biol Cell, 1997. **8**(12): p. 2449-61.
338. Corti, A., et al., *The neovasculature homing motif NGR: more than meets the eye.* Blood, 2008. **112**(7): p. 2628-35.
339. Lanthier, J. and R.R. Desrosiers, *Protein L-isoaspartyl methyltransferase repairs abnormal aspartyl residues accumulated in vivo in type-I collagen and restores cell migration.* Exp Cell Res, 2004. **293**(1): p. 96-105.
340. Eliceiri, B.P. and D.A. Cheresh, *Role of alpha v integrins during angiogenesis.* Cancer J, 2000. **6 Suppl 3**: p. S245-9.
341. Loeffler, D.A., et al., *Ceruloplasmin is increased in cerebrospinal fluid in Alzheimer's disease but*

not Parkinson's disease. Alzheimer Dis Assoc Disord, 1994. **8**(3): p. 190-7.
342. Hellman, N.E. and J.D. Gitlin, *Ceruloplasmin metabolism and function.* Annu Rev Nutr, 2002. **22**: p. 439-58.
343. Cozzi, A., et al., *Oxidative stress and cell death in cells expressing L-ferritin variants causing neuroferritinopathy.* Neurobiol Dis, 2010. **37**(1): p. 77-85.
344. Dalle-Donne, I., et al., *Protein carbonylation in human diseases.* Trends Mol Med, 2003. **9**(4): p. 169-76.
345. Boll, M.C., et al., *Reduced ferroxidase activity in the cerebrospinal fluid from patients with Parkinson's disease.* Neurosci Lett, 1999. **265**(3): p. 155-8.
346. Boll, M.C., et al., *Free copper, ferroxidase and SOD1 activities, lipid peroxidation and NO(x) content in the CSF. A different marker profile in four neurodegenerative diseases.* Neurochem Res, 2008. **33**(9): p. 1717-23.
347. Vassiliev, V., Z.L. Harris, and P. Zatta, *Ceruloplasmin in neurodegenerative diseases.* Brain Res Brain Res Rev, 2005. **49**(3): p. 633-40.
348. Baraj B, C.J., Sastre A, Granados M Fresenius, *Copper interference on spectrophotometric determination of iron and their simultaneous determination using bathophenantroline-disulfonic acid disodium salt.* . J Anal Chem, 1998. **360**: p. 263–265.
349. Pelizzoni, I., et al., *Iron handling in hippocampal neurons: activity-dependent iron entry and mitochondria-mediated neurotoxicity.* Aging Cell, 2011. **10**(1): p. 172-83.
350. Conti, A., et al., *Differential expression of ceruloplasmin isoforms in the cerebrospinal fluid of amyotrophic lateral sclerosis patients.* Proteomics Clin Appl, 2008. **2**(12): p. 1628-37.
351. Bento, I., et al., *Ceruloplasmin revisited: structural and functional roles of various metal cation-binding sites.* Acta Crystallogr D Biol Crystallogr, 2007. **63**(Pt 2): p. 240-8.
352. Olivieri, S., et al., *Ceruloplasmin oxidation, a feature of Parkinson's disease CSF, inhibits ferroxidase activity and promotes cellular iron retention.* J Neurosci, 2011. **31**(50): p. 18568-77.
353. Sedlak, E., G. Zoldak, and P. Wittung-Stafshede, *Role of copper in thermal stability of human ceruloplasmin.* Biophys J, 2008. **94**(4): p. 1384-91.
354. Dehart, M.P. and B.D. Anderson, *A mechanism-based kinetic analysis of succinimide-mediated deamidation, racemization, and covalent adduct formation in a model peptide in amorphous lyophiles.* J Pharm Sci, 2012. **101**(9): p. 3096-109.
355. Spitaleri, A., et al., *Structural basis for the interaction of isoDGR with the RGD-binding site of alphavbeta3 integrin.* J Biol Chem, 2008. **283**(28): p. 19757-68.
356. Zhu, J.X., et al., *Protein repair in the brain, proteomic analysis of endogenous substrates for protein L-isoaspartyl methyltransferase in mouse brain.* J Biol Chem, 2006. **281**(44): p. 33802-13.
357. Barbariga, M., et al., *Oxidation-induced structural changes of ceruloplasmin foster NGR-motifs deamidation that promote integrin binding and signalling.* J Biol Chem, 2013.
358. Redzic, Z.B., *Studies on the human choroid plexus in vitro.* Fluids Barriers CNS, 2013. **10**(1): p. 10.
359. Bharucha, K.J., et al., *Lower serum ceruloplasmin levels correlate with younger age of onset in Parkinson's disease.* J Neurol, 2008. **255**(12): p. 1957-62.
360. Jin, L., et al., *Decreased serum ceruloplasmin levels characteristically aggravate nigral iron deposition in Parkinson's disease.* Brain, 2011. **134**(Pt 1): p. 50-8.
361. Torsdottir, G., et al., *Ceruloplasmin and superoxide dismutase (SOD1) in Parkinson's disease: a follow-up study.* J Neurol Sci, 2006. **241**(1-2): p. 53-8.
362. Youdim, M.B., G. Stephenson, and D. Ben Shachar, *Ironing iron out in Parkinson's disease and other neurodegenerative diseases with iron chelators: a lesson from 6-hydroxydopamine and iron chelators, desferal and VK-28.* Ann N Y Acad Sci, 2004. **1012**: p. 306-25.
363. Gotz, M.E., et al., *The relevance of iron in the pathogenesis of Parkinson's disease.* Ann N Y Acad Sci, 2004. **1012**: p. 193-208.
364. Brewer, G.J., et al., *Copper and ceruloplasmin abnormalities in Alzheimer's disease.* Am J Alzheimers Dis Other Demen, 2010. **25**(6): p. 490-7.
365. Kuznetsov, A.V., et al., *Changes in mitochondrial redox state, membrane potential and calcium precede mitochondrial dysfunction in doxorubicin-induced cell death.* Biochim Biophys Acta, 2011. **1813**(6): p. 1144-52.
366. Patel, B.N., et al., *Ceruloplasmin regulates iron levels in the CNS and prevents free radical injury.* J Neurosci, 2002. **22**(15): p. 6578-86.
367. Oakley, A.E., et al., *Individual dopaminergic neurons show raised iron levels in Parkinson disease.* Neurology, 2007. **68**(21): p. 1820-5.

368. Tapryal, N., et al., *Reactive oxygen species regulate ceruloplasmin by a novel mRNA decay mechanism involving its 3'-untranslated region: implications in neurodegenerative diseases.* J Biol Chem, 2009. **284**(3): p. 1873-83.
369. Shimizu, T., Y. Matsuoka, and T. Shirasawa, *Biological significance of isoaspartate and its repair system.* Biol Pharm Bull, 2005. **28**(9): p. 1590-6.
370. Weintraub, S.J. and B.E. Deverman, *Chronoregulation by asparagine deamidation.* Sci STKE, 2007. **2007**(409): p. re7.
371. Tabner, B.J., et al., *Hydrogen peroxide is generated during the very early stages of aggregation of the amyloid peptides implicated in Alzheimer disease and familial British dementia.* J Biol Chem, 2005. **280**(43): p. 35789-92.
372. Ayton, S., et al., *Ceruloplasmin dysfunction and therapeutic potential for parkinson disease.* Ann Neurol, 2012.
373. Texel, S.J., X. Xu, and Z.L. Harris, *Ceruloplasmin in neurodegenerative diseases.* Biochem Soc Trans, 2008. **36**(Pt 6): p. 1277-81.
374. Eskici, G. and P.H. Axelsen, *Copper and oxidative stress in the pathogenesis of Alzheimer's disease.* Biochemistry, 2012. **51**(32): p. 6289-311.
375. Loeffler, D.A., A.A. Sima, and P.A. LeWitt, *Ceruloplasmin immunoreactivity in neurodegenerative disorders.* Free Radic Res, 2001. **35**(2): p. 111-8.
376. Hwang, I.K., et al., *Ischemia-related change of ceruloplasmin immunoreactivity in neurons and astrocytes in the gerbil hippocampus and dentate gyrus.* Neurochem Int, 2004. **44**(8): p. 601-7.
377. Aouffen, M., et al., *Oxidative aggregation of ceruloplasmin induced by hydrogen peroxide is prevented by pyruvate.* Free Radic Res, 2004. **38**(1): p. 19-26.
378. Kim, K.S., et al., *The ceruloplasmin and hydrogen peroxide system induces alpha-synuclein aggregation in vitro.* Biochimie, 2002. **84**(7): p. 625-31.
379. Luo, B.H., C.V. Carman, and T.A. Springer, *Structural basis of integrin regulation and signaling.* Annu Rev Immunol, 2007. **25**: p. 619-47.
380. Grace, E.A. and J. Busciglio, *Aberrant activation of focal adhesion proteins mediates fibrillar amyloid beta-induced neuronal dystrophy.* J Neurosci, 2003. **23**(2): p. 493-502.
381. Caltagarone, J., Z. Jing, and R. Bowser, *Focal adhesions regulate Abeta signaling and cell death in Alzheimer's disease.* Biochim Biophys Acta, 2007. **1772**(4): p. 438-45.
382. Svineng, G., et al., *The role of reactive oxygen species in integrin and matrix metalloproteinase expression and function.* Connect Tissue Res, 2008. **49**(3): p. 197-202.
383. Glass, C.K., et al., *Mechanisms underlying inflammation in neurodegeneration.* Cell, 2010. **140**(6): p. 918-34.
384. Fuentealba, L.C., K. Obernier, and A. Alvarez-Buylla, *Adult neural stem cells bridge their niche.* Cell Stem Cell, 2012. **10**(6): p. 698-708.
385. Winner, B., Z. Kohl, and F.H. Gage, *Neurodegenerative disease and adult neurogenesis.* Eur J Neurosci, 2011. **33**(6): p. 1139-51.
386. Wang, Y., et al., *The promotion of neural progenitor cells proliferation by aligned and randomly oriented collagen nanofibers through beta1 integrin/MAPK signaling pathway.* Biomaterials, 2011. **32**(28): p. 6737-44.
387. Krzyzanowska, A. and E. Carro, *Pathological alteration in the choroid plexus of Alzheimer's disease: implication for new therapy approaches.* Front Pharmacol, 2012. **3**: p. 75.
388. Perez-Gracia, E., et al., *Oxidative stress damage and oxidative stress responses in the choroid plexus in Alzheimer's disease.* Acta Neuropathol, 2009. **118**(4): p. 497-504.
389. *The diagnosis of Parkinson's disease.* Neurol Sci, 2003. **24 Suppl 3**: p. S157-64.
390. Brooks, B.R., *El Escorial World Federation of Neurology criteria for the diagnosis of amyotrophic lateral sclerosis. Subcommittee on Motor Neuron Diseases/Amyotrophic Lateral Sclerosis of the World Federation of Neurology Research Group on Neuromuscular Diseases and the El Escorial "Clinical limits of amyotrophic lateral sclerosis" workshop contributors.* J Neurol Sci, 1994. **124 Suppl**: p. 96-107.
391. McKhann, G., et al., *Clinical diagnosis of Alzheimer's disease: report of the NINCDS-ADRDA Work Group under the auspices of Department of Health and Human Services Task Force on Alzheimer's Disease.* Neurology, 1984. **34**(7): p. 939-44.
392. Conti, A., et al., *Pigment epithelium-derived factor is differentially expressed in peripheral neuropathies.* Proteomics, 2005. **5**(17): p. 4558-67.
393. Hoehn, M.M. and M.D. Yahr, *Parkinsonism: onset, progression and mortality.* Neurology, 1967. **17**(5): p. 427-42.
394. Fahn, S., *Systemic therapy of dystonia.* Can J Neurol Sci, 1987. **14**(3 Suppl): p. 528-32.

395. Codazzi, F., et al., *Synergistic control of protein kinase Cgamma activity by ionotropic and metabotropic glutamate receptor inputs in hippocampal neurons.* J Neurosci, 2006. **26**(13): p. 3404-11.
396. Bettegazzi, B., et al., *beta-Secretase activity in rat astrocytes: translational block of BACE1 and modulation of BACE2 expression.* Eur J Neurosci, 2011. **33**(2): p. 236-43.
397. Ruggeri, G., et al., *Antibodies for denatured human H-ferritin stain only reticuloendothelial cells within the bone marrow.* Br J Haematol, 1992. **81**(1): p. 118-24.
398. Cannistraci, C.V., F.M. Montevecchi, and M. Alessio, *Median-modified Wiener filter provides efficient denoising, preserving spot edge and morphology in 2-DE image processing.* Proteomics, 2009. **9**(21): p. 4908-19.
399. Kohane IS, K.A., Butte AJ, *Microarrays for an integrative genomics.*
. 2003 Cambridge: MA: MIT.
400. Cannistraci, C.V., et al., *Nonlinear dimension reduction and clustering by Minimum Curvilinearity unfold neuropathic pain and tissue embryological classes.* Bioinformatics, 2010. **26**(18): p. i531-9.
401. Zhang, Y., *I-TASSER server for protein 3D structure prediction.* BMC Bioinformatics, 2008. **9**: p. 40.
402. Hess, B., et al., *GROMACS 4: Algorithms for Highly Efficient, Load-Balanced, and Scalable Molecular Simulation.* J Chem Theory Comput, 2008. **4**: p. 435-47.
403. de Vries, S.J., et al., *HADDOCK versus HADDOCK: new features and performance of HADDOCK2.0 on the CAPRI targets.* Proteins, 2007. **69**(4): p. 726-33.
404. Saeed, A.I., et al., *TM4: a free, open-source system for microarray data management and analysis.* Biotechniques, 2003. **34**(2): p. 374-8.
405. Gritti, A., et al., *Multipotential stem cells from the adult mouse brain proliferate and self-renew in response to basic fibroblast growth factor.* J Neurosci, 1996. **16**(3): p. 1091-100.